

Design of Non-Isolated DC-DC Converters for Maximum Power Point Tracking in Stand-Alone Photovoltaic System

Project Report Submitted in Partial Fulfilment of the Requirements for the Degree of

Bachelor of Technology

in

Electrical and Electronics Engineering

Submitted by

Mr. Vishal Kevat (18EEE1029)

Mr. Burri Sai Bhargav (18EEE1007)

Under the Supervision of

**Dr. Suresh Mikkili
Associate Professor**



Department of Electrical and Electronics Engineering
National Institute of Technology Goa

May, 2022



Department of Electrical and Electronics Engineering
National Institute of Technology Goa
Farmagudi, Goa, India - 403401

CERTIFICATE

This is to certify that the work contained in this report entitled "**Design of Non-Isolated DC-DC Converters for Maximum Power Point Tracking in Stand-Alone Photovoltaic System**" is submitted by the group members Mr. Vishal Kevat (Roll No: 18EEE1029) and Mr. Burri Sai Bhargav (Roll No: 18EEE1007) to the Department of Electrical and Electronics Engineering, National Institute of Technology Goa, for the partial fulfilment of the requirements for the degree of **Bachelor of Technology** in **Electrical and Electronics Engineering**.

They have carried out their work under my supervision. This work has not been submitted else-where for the award of any other degree or diploma.

The project work in our opinion, has reached the standard fulfilling of the requirements for the degree of Bachelor of Technology in Electrical and Electronics Engineering in accordance with the regulations of the Institute.

Dr. Suresh Mikkili
Associate Professor, Department of EEE
National Institute of Technology Goa
(Supervisor)

Dr. Soumitra Das
HoD, Department of EEE
National Institute of Technology Goa

ACKNOWLEDGMENT

It gives us great pleasure and satisfaction to express our heartfelt gratitude to those who helped us complete this project.

First and foremost, we would want to express our gratitude to our supervisor, **Dr. Suresh Mikkili**, for providing us with advice and continual supervision as we worked on the project. Working with him has been a fantastic experience that has given us a unique perspective on the world of research. His traits of determination, passion, inventiveness, ingenuity, and discipline have inspired us to achieve this project. His constant encouragement, constant monitoring, and commitment to excellence have always encouraged us to enhance our job and employ our full potential. We have gained many experiences outside of study as a result of his blessing, which will benefit us throughout our lives.

We would like to thank our Major Project Committee members **Dr. Amol D Rahulkar** and **Dr. Soumitra Das** for providing us valuable comments and suggestions for the betterment of our project work. We also thank to **Dr. Sree Raj E S**, **Dr. C. Vyjayanthi**, **Dr. B. Venugopal Reddy**, and non-teaching staff **Mr. Digambar**, **Mrs. Suvida Naik**, **Mr. Pinaki Chatterje**, and **Mr. Rohit Gawas** of Electrical and Electronics Engineering Department for extending all possible help during the course of our project work.

We would like to thank **Mr. Praveen Kumar Bonthagorla**, our senior Ph. D. student, who assisted us like a big brother. Life would have been dull without our pals in and out of NIT Goa. We owe them all our gratitude for their unwavering support, invaluable contributions, and ongoing encouragement.

Last but not least, we want to thank our parents and family for their continuous support and for creating such a fantastic atmosphere for us to grow up in.

Finally, we are grateful to the Almighty for their blessings in assisting us in raising our academic level to this point. We ask for their blessing on all of our future endeavours. Their blessings may be bestowed onto us for future strength, knowledge, and determination.

TABLE OF CONTENTS

	Title	Page No.
	LIST OF FIGURES	iv
	LIST OF TABLES	viii
	ABBREVIATIONS	ix
	ABSTRACT	x
CHAPTER - 1		
INTRODUCTION		
CHAPTER - 1	1.1 Renewable Solar Photovoltaic System	1
	1.2 Scope of Photovoltaic Power Generation in India	4
	1.3 Motivation of the Thesis	5
	1.4 Objective of the Thesis	6
	1.5 Outline of the Thesis	6
CHAPTER - 2		
FUNDAMENTALS OF PV SYSTEM		
CHAPTER - 2	2.1 Introduction	8
	2.2 Principle of PV Energy Conversion	8
	2.3 Classification of PV Systems	10
	2.3.1 <i>Stand-Alone PV System</i>	10
	2.3.2 <i>Grid-Connected PV System</i>	11
	2.3.3 <i>Hybrid PV System</i>	12
	2.4 Partial Shading Conditions and its Effects	13
	CHAPTER - 3	
MATHEMATICAL MODELLING OF PV SYSTEM		
CHAPTER - 3	3.1 Introduction	15
	3.2 Modelling of PV Cell and Module	15
	3.3 Modelling of PV Array	17
	3.4 Effect of Insolation on PV Characteristics	17

CHAPTER - 4		
PV ARRAY CONFIGURATIONS		
CHAPTER - 4	4.1 Introduction	20
	4.2 Conventional PV Array Configurations	20
	4.2.1 <i>Series (S) Configuration</i>	20
	4.2.2 <i>Series-Parallel (SP) Configuration</i>	22
	4.2.3 <i>Total-Cross-Tied Configuration</i>	23
	4.3 Partial Shading Scenarios for TCT Configuration	25
	4.3.1 <i>Center shading scenario</i>	25
	4.3.2 <i>Corner shading scenario</i>	25
	4.3.3 <i>Diagonal shading scenario</i>	26
	4.3.4 <i>Frame shading scenario</i>	26
	4.3.5 <i>Random shading scenario</i>	26
	4.3.6 <i>Right side end shading scenario</i>	26
	4.4 Factors affecting the Performance of PV Array	28
	4.4.1 <i>Mismatching Power Loss (MPL)</i>	28
	4.4.2 <i>Fill Factor (FF)</i>	28
4.4.3 <i>Efficiency</i>	28	
4.5 Results and Discussions	29	

CHAPTER - 5		
MAXIMUM POWER POINT TRACKING TECHNIQUE		
CHAPTER - 5	5.1 Introduction	32
	5.2 Perturbation and Observation MPPT Technique	33
	5.3 Flowchart of P&O MPPT Algorithm	34
	5.4 Implementation of P&O MPPT Technique	35

CHAPTER - 6		
TOPOLOGIES OF DC-DC CONVERTERS		
	6.1 Introduction	36
	6.2 Classification of DC-DC Converters	36
	6.3 Non-Isolated DC-DC Converters	37

CHAPTER - 6	6.3.1	<i>Boost Converter</i>	37
	6.3.2	<i>Buck-Boost Converter</i>	38
	6.3.3	<i>Cuk Converter</i>	39
	6.3.4	<i>SEPIC Converter</i>	40
	6.3.5	<i>Zeta Converter</i>	40
	6.3.6	<i>Super-Lift Luo Converter</i>	41
	6.3.7	<i>Ultra-Lift Luo Converter</i>	42
	6.4	Comparison of Gains of Non-Isolated Converters	43
6.5	Designing of Boost Converter	44	
CHAPTER - 7			
SIMULATION IN MATLAB/SIMULINK			
CHAPTER - 7	7.1	Introduction	46
	7.2	Simulink Model of Stand-Alone PV System	47
	7.3	Simulation Results and Discussions	48
	7.3.1	<i>Boost Converter Waveforms</i>	48
	7.3.2	<i>Buck-Boost Converter Waveforms</i>	56
	7.3.3	<i>Cuk Converter Waveforms</i>	64
	7.3.4	<i>SEPIC Converter Waveforms</i>	72
	7.3.5	<i>Zeta Converter Waveforms</i>	80
	7.3.6	<i>Super-Lift Luo Converter Waveforms</i>	88
	7.3.7	<i>Ultra-Lift Luo Converter Waveforms</i>	96
CHAPTER – 8			
CONCLUSION AND FUTURE SCOPE			
CHAPTER - 8	8.1	Conclusion	104
	8.2	Future Scope	105
	REFERENCES		106

LIST OF FIGURES

Fig. No.	Title	Page No.
CHAPTER - 1		
1.1	Global Cumulative PV installed Capacity	2
1.2	Global Annual PV Installed Capacity	3
1.3	Annual India's growth in Conventional Power Generation	4
1.4	Annual India's growth in Renewable Power Generation	5
CHAPTER - 2		
2.1	Conversion mechanism of solar light energy to electricity	9
2.2	Representation of PV cell, PV module, and PV Array	9
2.3	Stand-Alone PV system architectures	10
2.4	Grid-connected PV system architecture	11
2.5	Hybrid PV system architecture	12
2.6	Partial shading scenarios due to: (a) moving clouds, (b) water droplets, (c) shadow of trees and (d) snow covering	13
2.7	Partial shading effect on PV array: (a) Shaded PV array, and (b) P-V Curves of shaded PV array.	14
CHAPTER - 3		
3.1	(a) Equivalent circuit of PV cell, (b) Equivalent circuit of PV array	15
3.2	(a) I-V Characteristics and (b) P-V Characteristics of PV Module under different solar insolation	18
CHAPTER - 4		
4.1	Schematic of 7×7 Series (S) PV array configuration	21
4.2	Schematic of 7×7 Series-Parallel (SP) PV array configuration	22
4.3	Schematic of 7×7 Total-Cross-Tied (TCT) PV array configuration	24
4.4	Representation of different partial shading scenarios	27
4.5	(a) I-V and (b) P-V Characteristics of TCT PV array under PSCs	29

4.6	Global Maximum Power of TCT PV array under different partial shadings	30
4.7	Number of Local Maximum Power Points under PSCs	31
CHAPTER - 5		
5.1	Classification of PV MPPT techniques.	32
5.2	Perturbation and Observation on PV Curve	33
5.3	Flowchart of P&O MPPT Algorithm	34
5.4	P&O MPPT controller implementation.	35
5.5	MATLAB/Simulink model of the P&O MPPT algorithm	35
CHAPTER - 6		
6.1	Classification of DC-DC Converters	36
6.2	Boost converter for PV Application	37
6.3	Buck–Boost converter for PV application	38
6.4	Cuk converter for PV application	39
6.5	SEPIC converter for PV application	40
6.6	Zeta converter for PV application	41
6.7	Super-Lift Luo converter for PV application	42
6.8	Ultra-Lift Luo converter for PV application	42
CHAPTER - 7		
7.1	Block diagram of MPPT Stand-Slone PV system with load resistor	46
7.2	Simulink Model of Boost Converter with center shading on TCT PV Array	47
7.3	Boost converter waveforms under center shading condition	48
7.4	Boost converter waveforms under corner shading condition	49
7.5	Boost converter waveforms under diagonal shading condition	50
7.6	Boost converter waveforms under frame shading condition	51
7.7	Boost converter waveforms under random shading condition	52
7.8	Boost converter waveforms under right side end shading condition	53

7.9	Boost converter waveforms under uniform shading condition	54
7.10	Buck-Boost converter waveforms under center shading condition	56
7.11	Buck-Boost converter waveforms under corner shading condition	57
7.12	Buck-Boost converter waveforms under diagonal shading condition	58
7.13	Buck-Boost converter waveforms under frame shading condition	59
7.14	Buck-Boost converter waveforms under random shading condition	60
7.15	Buck-Boost converter waveforms under right side end shading condition	61
7.16	Buck-Boost converter waveforms under uniform shading condition	62
7.17	Cuk converter waveforms under center shading condition	63
7.18	Cuk converter waveforms under corner shading condition	65
7.19	Cuk converter waveforms under diagonal shading condition	66
7.20	Cuk converter waveforms under frame shading condition	67
7.21	Cuk converter waveforms under random shading condition	68
7.22	Cuk converter waveforms under right side end shading condition	69
7.23	Cuk converter waveforms under uniform shading condition	70
7.24	SEPIC converter waveforms under center shading condition	72
7.25	SEPIC converter waveforms under corner shading condition	73
7.26	SEPIC converter waveforms under diagonal shading condition	74
7.27	SEPIC converter waveforms under frame shading condition	75
7.28	SEPIC converter waveforms under random shading condition	76
7.29	SEPIC converter waveforms under right side end shading condition	77
7.30	SEPIC converter waveforms under uniform shading condition	78
7.31	Zeta converter waveforms under center shading condition	80
7.32	Zeta converter waveforms under corner shading condition	81
7.33	Zeta converter waveforms under diagonal shading condition	82
7.34	Zeta converter waveforms under frame shading condition	83
7.35	Zeta converter waveforms under random shading condition	84

7.36	Zeta converter waveforms under right side end shading condition	85
7.37	Zeta converter waveforms under uniform shading condition	86
7.38	Super-Lift Luo converter waveforms under center shading condition	88
7.39	Super-Lift Luo converter waveforms under corner shading condition	89
7.40	Super-Lift Luo converter waveforms under diagonal shading condition	90
7.41	Super-Lift Luo converter waveforms under frame shading condition	91
7.42	Super-Lift Luo converter waveforms under random shading condition	92
7.43	Super-Lift Luo converter waveforms under right side shading condition	93
7.44	Super-Lift Luo converter waveforms under uniform shading condition	94
7.45	Ultra-Lift Luo converter waveforms under center shading condition	96
7.46	Ultra-Lift Luo converter waveforms under corner shading condition	97
7.47	Ultra-Lift Luo converter waveforms under diagonal shading condition	98
7.48	Ultra-Lift Luo converter waveforms under frame shading condition	99
7.49	Ultra-Lift Luo converter waveforms under random shading condition	100
7.50	Ultra-Lift Luo converter waveforms under right side end shading condition	101
7.51	Ultra-Lift Luo converter waveforms under uniform shading condition	102

LIST OF TABLES

Table No.	Title	Page No.
CHAPTER - 3		
3.1	Technical parameters of the Kyocera Solar KC200GT PV Module	19
CHAPTER - 4		
4.1	Performance of TCT PV Array under PSCs	30
CHAPTER - 6		
6.1	Converter's Gain comparison for different duty cycle (D)	43
6.2	Design Specification of DC-DC Converters	45
CHAPTER - 7		
7.1	Boost Converter Observations	55
7.2	Buck-Boost Converter Observations	63
7.3	Cuk Converter Observations	71
7.4	SEPIC Converter Observations	79
7.5	Zeta Converter Observations	87
7.6	Super-Lift Luo Converter Observations	95
7.7	Ultra-Lift Luo Converter Observations	103

ABBREVIATIONS

PV	Photovoltaic
RES	Renewable Energy Sources
SPV	Solar Photovoltaic
CO ₂	Carbon Dioxide
MNRE	Ministry of New and Renewable Energy
PSC	Partial Shading Condition
MPPT	Maximum Power Point Tracking
GMPP	Global Maximum Power Point
LMPP	Local Maximum Power Point
MPPT	Maximum Power Point Tracking
DC	Direct Current
AC	Alternate Current
BD	Bypass Diode
SP	Series Parallel
TCT	Total Cross Tied
BL	Bridge-Linked
HC	Honey-Comb
MPL	Mismatching Power loss
FF	Fill Factor
SEPIC	Single-Ended Primary Inductance Converter
P&O	Perturbation and Observation
SAPV	Stand-Alone Photovoltaic
PWM	Pulse Width Modulation

ABSTRACT

In recent years, the rapid expansion of solar Photovoltaic (PV) power generation has injected new hope into worldwide efforts to reduce greenhouse gas emissions and mitigate the most serious effects of climate change. Solar PV power generation systems are generally divided into two types: stand-alone and grid-connected. The main problem in solar PV systems nowadays is to make them energy efficient. Partial shadowing condition (PSC) is one of the primary elements that might affect the efficiency of a PV system, and it can be caused by clouds, buildings, trees, bird waste, dust, and other reasons. PSCs significantly limit the power output of PV systems, increasing mismatch power losses and forming hotspots in PV modules. With the addition of bypass diodes, the severity of PSCs increases to the point that several peaks appear in the power-voltage (P-V) characteristics, complicating the tracking of the global maximum power point (GMPP). PSCs and their negative impact on PV system performance have received a lot of attention in the last decade.

A DC-DC boost converter is used to match the impedance between the PV panel and the load in order to get the most out of the solar panel. Solar panels, converters, and MPPT controllers are the three main components of a PV system. In order to get the most power out of the PV plant, the converter plays a crucial role. The DC-DC converter is used to connect a PV system to a grid load or a stand-alone system by balancing the power between both.

Selection of the appropriate DC-DC converter is essential because it plays an important role in the overall performance of the PV system. In this project, various non-isolated conventional DC-DC converter are compared and P&O MPPT technique is used to extract maximum power from the PV module. We designed and simulated the DC-DC converter in MATLAB/Simulink and the results were compared to extract maximum power from the PV array under partial shading conditions.

Chapter - 1

INTRODUCTION

- **Renewable Solar Photovoltaic System**
- **Scope of Photovoltaic Power Generation in India**
- **Motivation of the Thesis**
- **Objective of the Thesis**
- **Outline of the Thesis**

Chapter - 1

Introduction

This chapter provides a brief overview of the research conducted in the project, including the current state of solar photovoltaic (PV) power generation around the world, different types of PV systems, causes and effects of partial shading, and partial shading mitigation approaches for PV systems. Finally, the motivation, objectives, and outline of the project are presented.

1.1. Renewable Solar Photovoltaic System

Developing countries are leading the way in the growth of global demand for electrical energy as the economy expands, population increases, urbanization and greater access to power are all contributing factors [1]-[2]. As a result of severe environmental, economic, and social consequences of relying on fossil fuels, governments are looking for better alternatives that are more sustainable to meet the energy demand [3]. Rapid technological advancement and continuous government assistance has resulted in renewable energy sources (RESs) such as solar, hydro, wind, geo-thermal, and bio-fuels becoming more feasible and cost-effective solutions [4]-[5]. Among the various RESs, solar photovoltaic (SPV) power generation has a significant potential to meet the global energy demand due to its numerous advantages in terms of environmental and economic considerations [6]. The benefits of SPV power generation are as follows:

- It is abundant in nature, freely available and generates clean and green energy.
- It does not emit any green-house gases and is eco-friendly.
- The cost for operational and maintenance of PV panels is very low compared to other renewable energy sources.
- It requires bare minimum maintenance and hence less requirement in manpower.
- It offers easy installation and noise-less power generation suitable for residential and urban applications.
- It shows versatility. i.e., PV panels can generate electricity anywhere where the sun is available.
- It does not have any moving parts, so losses are very less.

- It has almost no material depletion.

It is evident that from the last two decades, solar PV power generation has grown at an annual rate of 20 percent to 25 percent. It is due to dropping prices of PV modules, incentives provided by the government, and innovative models for standalone and grid-connected and PV systems [7]-[8]. Many countries have reached grid parity with solar PV systems, and many plans are proposed to reach 100 percent utilization of green energy sources by 2050. Furthermore, in the next ten years, the cost of renewables is projected to undercut the price of fossil fuels [9].

Nevertheless, PV system is one of the preferable solutions for future energy demand. The factors for increasing the tendency of PV markets are: demand for energy increases, government policies towards renewable energy sources, concerns related to environment, rapid development in PV technologies, increase in PV installations globally etc., The global cumulative PV installed capacity at the end of 2020 is at least about 760.4 GW. Fig. 1.1 shows the global PV cumulative capacity of top 10 countries. China Leads the market with 253.4 GW, over one third of overall installed capacity. India is in the Top 10 Countries with 47.4 GW of PV Cumulative Capacity [10].

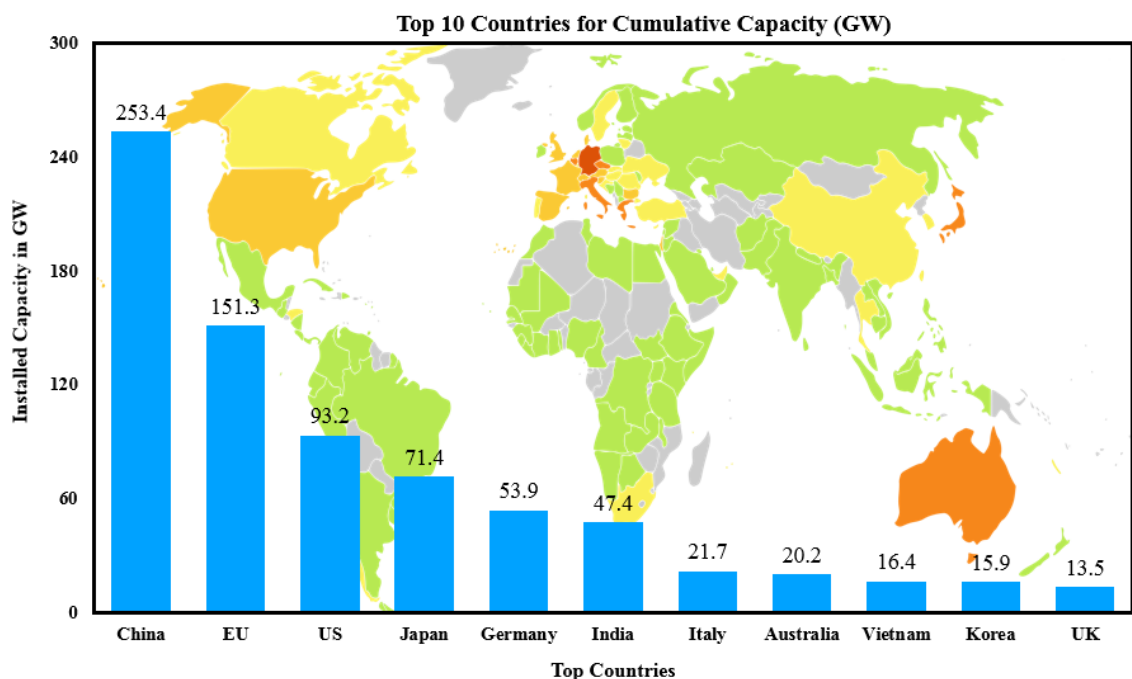


Figure 1.1: Global Cumulative PV installed Capacity

About 139.4 GW of PV systems have been commissioned and installed worldwide at the end of 2020. Fig. 1.2 shows the global annual PV installed capacity of top 10 countries. China is at 1st position with 48.2 GW, followed by EU, 19.6 GW and USA, 19.2 GW. In the European Union, Germany (4.9 GW), Netherlands (3.0 GW) reported with highest installations in the year 2020 followed by Spain, Poland, Belgium and France. The US records with 73 % new utility scale installations in the year 2020. In the top ten countries, six from Asia, two from EU and two from America.

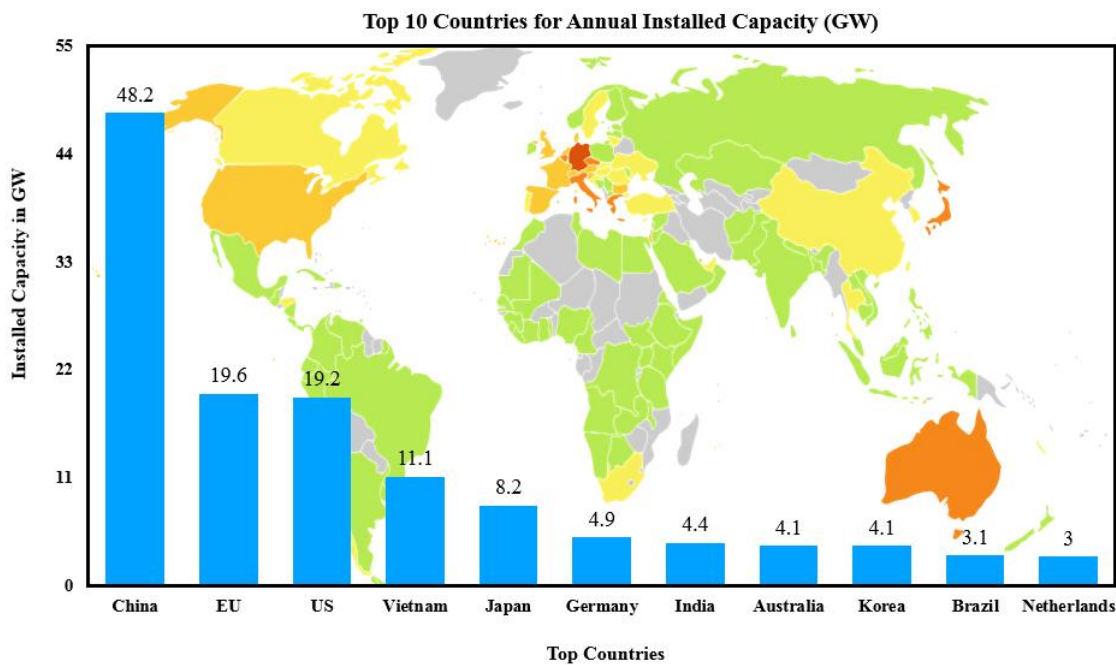


Figure 1.2: Global Annual PV Installed Capacity

The Highlights of PV Market in 2021 are given below:

- PV systems generate 3.7 % of global electricity.
- Total CO₂ emissions reduced by 877 Mt.
- At least 20 countries installed 1 GW of PV systems.
- At least 14 countries installed 10 GW of cumulative capacity.
- Solar PV per capita 2020 lead by Australia followed by Germany and Japan.

The above statistics clearly shows that photovoltaic generation systems have a significant demand and share in today's electricity market.

1.2. Scope of PV Power Generation in India

Today's India is looking towards renewable energy sources for its power demands. According to the Ministry of New and Renewable Energy (MNRE) [11]. The atmospheric conditions in India can harness enormous solar energy. Annually about 5000 trillion kWh energy is incident on the surface area in India. Almost every component receives 4-7 kWh per sq. m per day. Due to this, conversion of solar radiation to electricity are successfully utilized in India. Photovoltaic generations are available in both grid connected mode and islanded mode. It is generously available and meets the energy demands such as power, heating, cooling, etc. in both urban and rural areas of India. Photovoltaic generation is the most secure power and green energy generation of all renewable resources in India. If we harness solar energy efficiently, it meets the whole countries demands. Still, many un-electrified areas are there in India. Ministry of Power, India [12] states that there has been a significant growth in renewable power generation from the past four years. Annual India's growth in power generation with the conventional energy sources during recent years is shown in the Fig. 1.3.

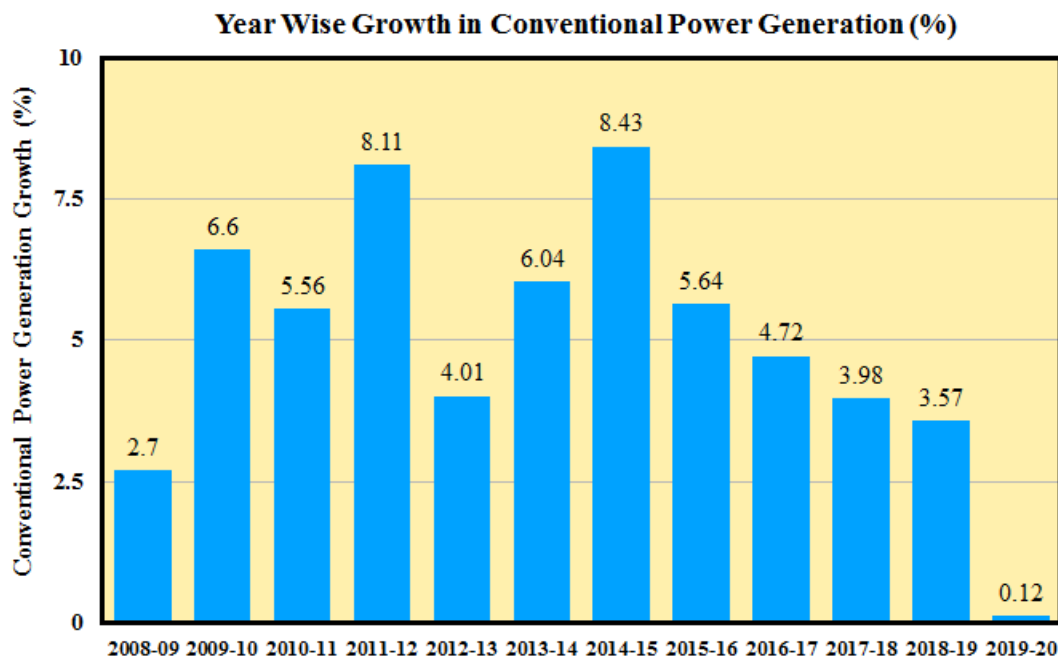


Figure 1.3: Annual India's growth in Conventional Power Generation

The government of India brings many policies for the development of renewable energy sources. From the Fig. 1.4 statistics, renewable energy sources' scope has

numerously increased in the past four years. The Ministry of New and Renewable Energy (MNRE) website reports that renewable energy installed capacity has increased about 226 % in the past 5 years. Solar energy is increased from 2.6 GW to more than 34 GW. Solar power tariff reduced day by day in India and a new record of low solar tariff i.e. Rs: 2.44 /- per unit is recorded in Bhadla, Rajasthan. By 2022 India will become the world's largest renewable energy, i.e., 175 GW of capacity.

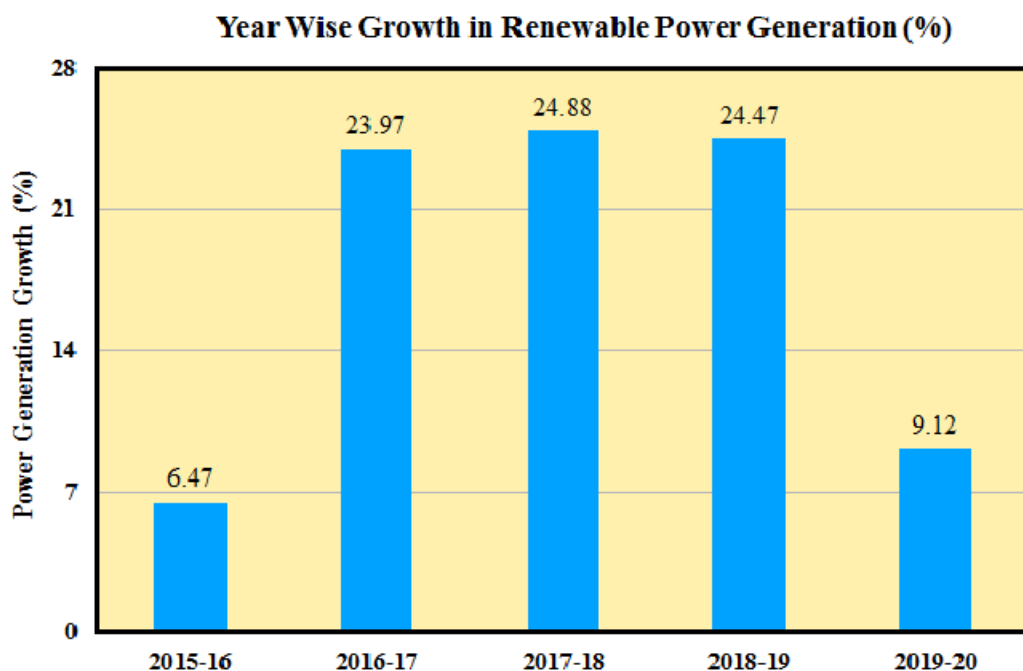


Figure 1.4: Annual India's growth in Renewable Power Generation

1.3. Motivation of the Thesis

Now a days, the use of PV systems has become a prevalent technique of power generation because of its environmental friendliness, development of semiconductor technologies, improvement in efficiency, requires little maintenance, and suitable for supplying electrical energy where conventional power-grid is absent. Basically, PV system generates non-liner I-V and P-V characteristics, since they vary with irradiance and temperature. However, the PV system has following drawbacks:

- The conversion efficiency is very low. i.e. (approximately 9% - 20%)
- The output power of the PV system is reduced drastically under PSCs which are caused by moving clouds, shadows of buildings, trees, poles, chimneys etc.,

Also, under PSCs the P-V characteristic exhibits multiple maximum power points (MPPs) out of which one is global maximum power point (GMPP) and rest are local maximum power points (LMPPs). Which in turn affects the performance of the controller, resulting in a reduction in the complete output power of the system. To overcome the above-mentioned drawbacks, there is a need to develop new schemes to enhance the maximum power from the PV system under PSCs.

1.4. Objective of the Thesis

This project focuses on using different non-isolated DC-DC Converters to enhance the maximum power from the PV system and for fast convergence speed. It tracks the GMPP of PV system accurately under PSCs. The main objectives of this project work are briefly summarized as:

- Modelling and performance investigation of conventional PV array configurations under partial shading conditions (PSCs).
- Developing different non-isolated DC-DC converters to extract the maximum power from the PV under partial shading conditions (PSCs).
- Selecting the best non-isolated DC-DC converter for the MPPT.

1.5. Outline of the Thesis

The research work presented in this thesis is organized into eight chapters.

Chapter 2: In this chapter, various fundaments of PV Systems are described. It explains about the energy conversion in PV cell in detail. Various classification of PV systems such as Stand-Alone PV system, Grid-Connected PV system, etc. is available in this chapter. The chapter ends explaining causes of Partial shading on PV array and its effect on the PV curve.

Chapter 3: This chapter models the PV Systems, that is it formulates mathematical modelling of the PV Cell, PV Module and finally PV Array. At the end of this chapter, Effect of various Insulation levels on PV Module is shown using I-V and P-V characteristics of the Kyocera KC-200GT PV Module.

Chapter 4: This chapter is all about PV Array configurations and Partial shading conditions on the TCT PV Array configurations. Various PSCs such as center, corner, diagonal, frame, etc. are discussed in this chapter. The simulation of TCT PV array configuration is made for its performance investigation. The chapter ends with the results and discussion of the performance of TCT PV array configuration.

Chapter 5: This chapter talks about the different types of MPPT available at present. It explains in detail about the Perturb and Observe MPPT algorithm to obtain the maximum power point under partial shading conditions. It shows the implementation method of PnO algorithm in Matlab/Simulink which we will be using for the simulations in this project.

Chapter 6: This chapter sums up all the non-isolated DC-DC converters which we are going to use for the simulation to obtain the MPP under PSC. Various converters and their classification are available here. The gain comparison of non-isolated DC-DC converter's is made in this chapter followed by designing of Boost converter for the Stand-Alone PV system.

Chapter 7: This chapter contains the simulation model of the Stand-Alone PV system for MPP tracking. The MPP is tracked using PnO Technique for different converters as mentioned in the previous chapter. The simulation is done for various shading conditions on the TCT PV Array.

Chapter 8: This chapter summarizes the work done in this thesis and presents the future scope of the thesis.

Chapter - 2

FUNDAMENTALS OF PV SYSTEM

- **Introduction**
- **Principle of PV Energy Conversion**
- **Classification of PV Systems**
- **Partial Shading Conditions and its Effects**

Chapter - 2

2.1 Introduction

The word ‘photovoltaic’ comes from the Greek words ‘Phos’ (meaning light) and ‘voltaic’ (electrical), which means the generation of electricity. Among English speakers, the term "photovoltaic" has been in widespread usage since 1849. Bequerel discovered PV effects in 1839, but it was not until the late 1950s that commercial PV applications were found. The prices of generating PV power have historically been greater than for comparable forms of traditional power sources [13]-[15]. Due to a significant drop in pricing, the development of new semiconductor technologies, and government subsidies depending on the market and system location PV power generation has gained a lot of importance in these days.

2.2 Principle of PV Energy Conversion

The PV cell is the most important part of the PV energy conversion system. The PV cell's principal function is to convert incident solar light energy into electricity via the photovoltaic effect [16]. A solar PV cell is essentially a P-N junction device made up of two layers of silicon doped with a small amount of impurity atoms. Atoms with one more valence electron are known as donors in the n-layer, whereas atoms with one less valence electron are known as acceptors in the p-layer. Because there are more electrons in the first layer, it is negatively charged. Because there are more holes in the P-type layer, it is positively charged. P-N junctions are generated when these two layers come into touch with each other. When photons of light energy strike the solar PV cell's surface, electron-hole pairs form in the depletion layer.

Due to the junction field, the produced electrons and holes travel in the opposite direction [17]. The electron migrates to the N-side, whereas the hole migrates to the P-side. When an external load is attached to the PV cell, this movement of charge carriers in a certain direction result in a current flow [18], as seen in Fig. 2.1. The quantity of current generated by a PV cell is proportional to the amount of solar insolation it receives.

A typical PV cell produces only 0.5V, therefore to fulfil output power needs, multiple PV cells are coupled in series and parallel.

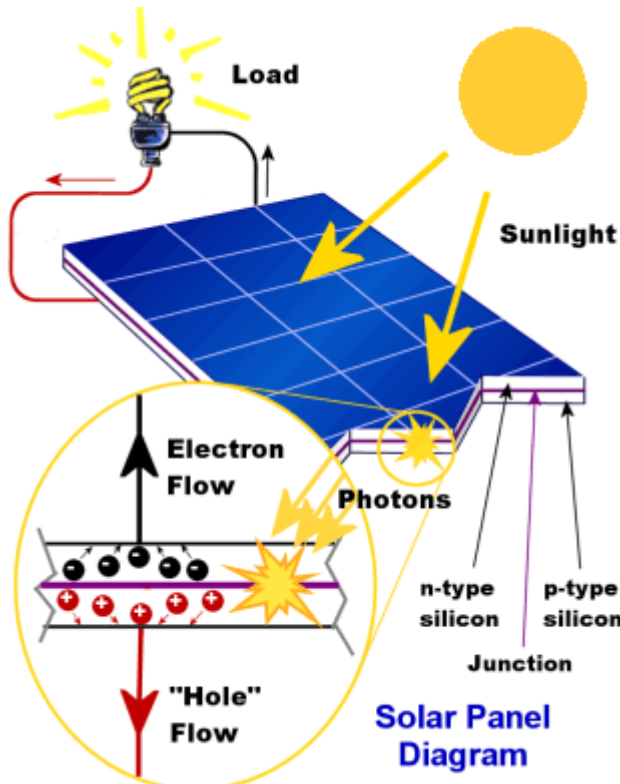


Figure 2.1: Conversion mechanism of solar light energy to electricity

The PV module can be formed by connecting several PV cells in series to achieve the required voltage level. PV array is formed by connecting several numbers of PV modules either in series or parallel to achieve the required power level [19]. The structure of PV cell, PV module, and PV Array is shown in Fig. 2.2.



Figure 2.2: Representation of PV cell, PV module, and PV Array

2.3 Classification of PV Systems

The scope of solar PV systems has expanded tremendously in recent years, with the possibility for further expansion. Semiconducting materials are utilised in PV systems to convert sunlight into electrical energy. PV systems are becoming more popular for solar applications as a result of this fact. The modular nature of the solar PV system is one of its main advantages. When power demands vary, a modular system design provides for easy expansion. PV systems are classified as standalone, grid-connected, or hybrid PV systems based on operational and functional requirements, component configurations, and how the equipment is connected to other power sources and electrical loads [20]-[21].

2.3.1 Stand-Alone PV System

Off-grid PV systems, often known as stand-alone PV systems, are solar-only systems. For rural areas where connecting to the grid is problematic, stand-alone PV systems might be beneficial. PV modules can directly connect to loads without energy storage, referred to as direct-coupled stand-alone PV system, and PV modules can directly connect to loads with energy storage, referred to as stand-alone PV system with battery storage supplying DC and AC loads, as shown in Fig. 2.3. Water pumps, ventilation fans, and solar thermal heating systems can all be powered by PV systems of this type.

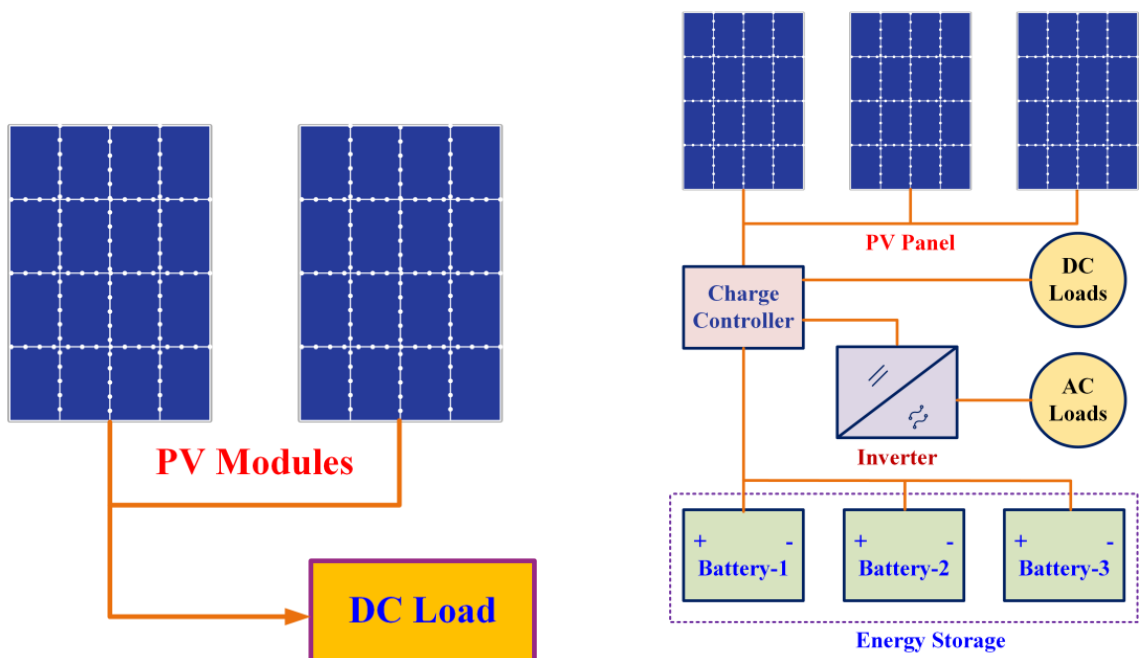


Figure 2.3: Stand-Alone PV system architectures

2.3.2 Grid-Connected PV System

For building integrated PV applications, grid-connected solar PV systems are becoming more prevalent. Solar panels absorb solar energy, which is then converted into direct electricity in a grid-connected PV system (DC). The DC energy is subsequently converted to alternating current via the solar system's inverter (AC). The AC can then be used by household devices in the same manner that a grid system is used. Figure 2.4 depicts the schematic layout of a grid-connected PV system.

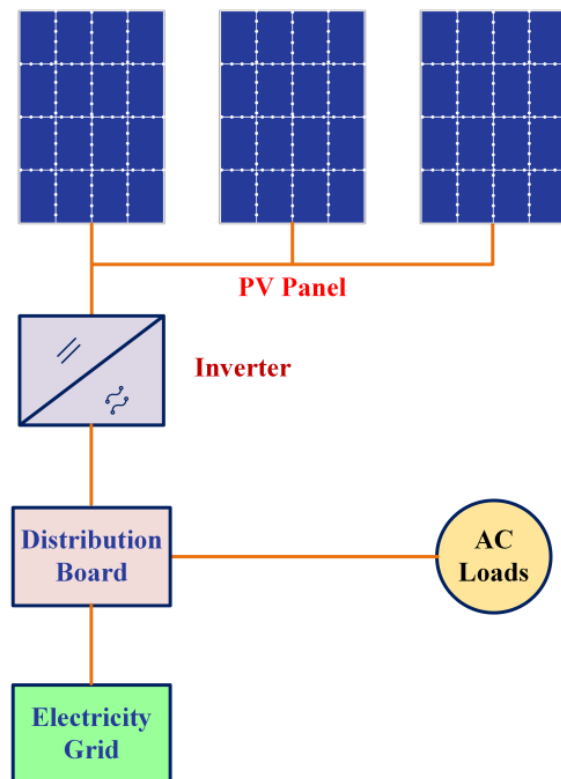


Figure 2.4: Grid-Connected PV system architecture

The inverter is connected to the distribution board in a small system, such as in a residential home, where the PV-generated power is sent to the electricity grid or to AC appliances in the house. Because these systems are connected to the grid, which functions as a buffer, an excess of PV electricity is transferred while the grid also provides electricity to the house when PV power generation is insufficient.

2.3.3 Hybrid PV System

A hybrid PV system combines different power sources to improve power availability and utilisation. A system like this can use energy from the wind, the sun, or even hydrocarbons. In addition, to enhance the system's efficiency, hybrid PV systems are frequently backed up with a battery. Figure 2.5 depicts the schematic layout of a hybrid PV system.

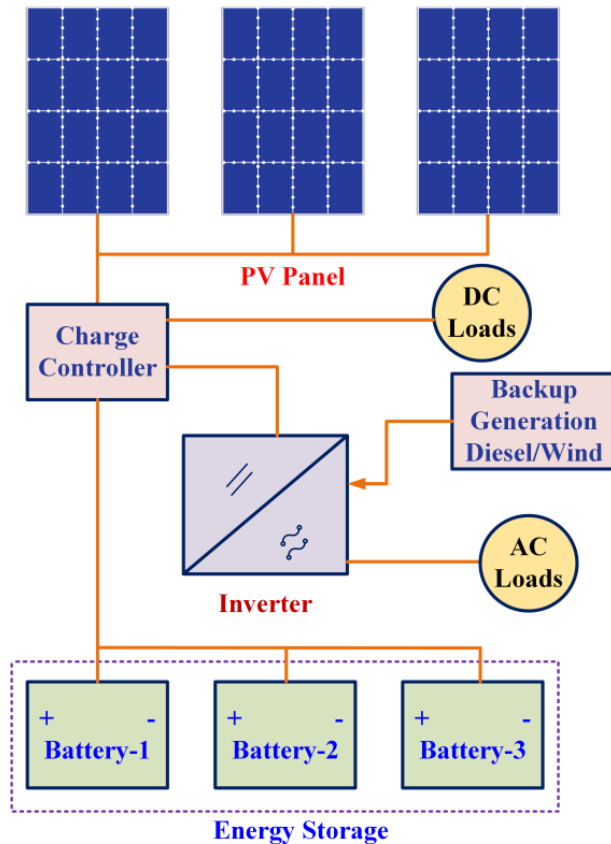


Figure 2.5: Hybrid PV system architecture

Using a hybrid system has a number of benefits. The presence of multiple energy sources indicates that the system is not reliant on a single source of energy. If the weather is suitable for generating enough solar energy, the PV array can, for example, charge the battery. In the same way, if the weather is windy or cloudy, a wind turbine can meet the battery's charging needs. Hybrid PV systems are best for remote locations with limited grid access. In comparison to standalone or grid-connected PV systems, hybrid PV systems often require more sophisticated controls.

2.4 Partial Shading Conditions and its Effects

When some PV cells and/or modules are shaded for various reasons, partial shading condition (PSC) arises. It could happen for a variety of causes connected to the site itself, which can be addressed early on during the PV system installation. For example, choosing the best and most suitable sites for PV system installation based on site factors (temperature and irradiance) and the absence of neighbouring buildings and towers can considerably increase the PV system's output power and overall efficiency. On the other hand, it may happen for a variety of causes, including proximity to neighbouring buildings, towers, trees, dust, ageing and moving clouds, or other things [22]. Shaded PV cells/modules are forced to carry large currents through unshaded cells/modules, using energy rather than creating it.



(a)



(b)



(c)



(d)

Figure 2.6: Partial shading scenarios due to: (a) moving clouds, (b) water droplets, (c) shadow of trees and (d) snow covering

The power losses grow as the percentage of the shaded area increases, and the output power falls. The partially shaded photovoltaic environment limits generated power and contributes to hot spot issues, which could lead to shaded PV module thermal failure. As a result, shaded PV cells/modules/arrays reduce the output power captured and the

overall efficiency of a partially shaded solar system. PV system power losses owing to partial shade or faulty global maximum power tracking are quite large, perhaps exceeding 70% of total power generated. In order to achieve high power efficiency, low power losses, and high output power, tracking the global maximum power is of relevance [23] - [25]. Fig. 2.6 depicts partial shading conditions that have occurred in nature.

In the uniform condition, the P-V curve will produce a single peak. Partial shadowing conditions (PSCs), on the other hand, cause variable radiation on each PV array to generate different power from one PV module/array to the next, as shown in Fig. 2.7. PV system topologies [26]-[27], PV module configurations [28]-[29], MPPT algorithms [30]-[33], converter topologies [34]-[38], inverter topologies [39]-[41], grid-integration strategies [42]-[44], and so on all affect the operation and performance of PV systems.

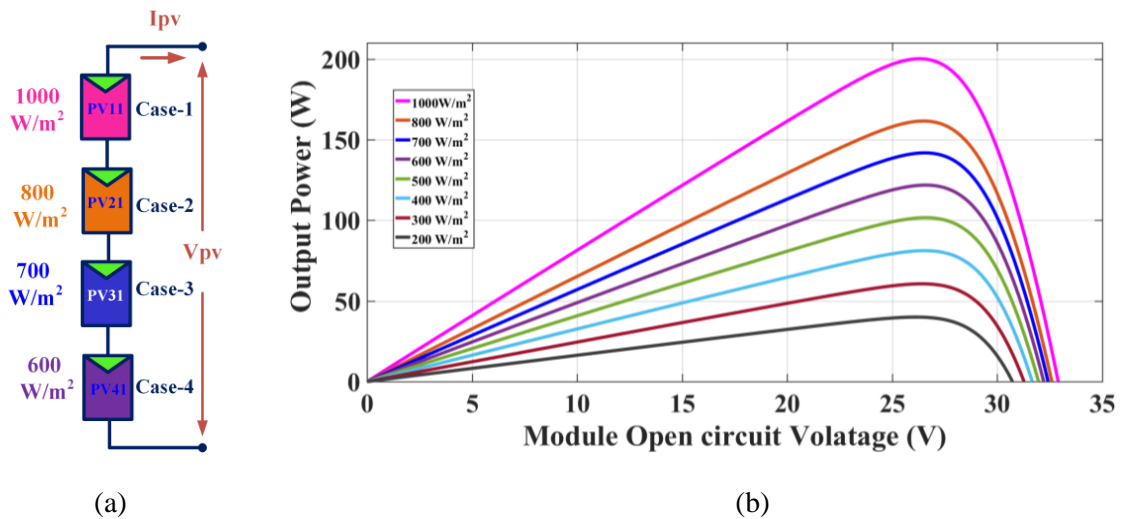


Figure 2.7: Partial shading effect on PV array: (a) Shaded PV array, and (b) P-V Curves of shaded PV array.

Chapter - 3

MATHEMATICAL MODELLING OF PV SYSTEM

- Introduction
- Modelling of PV Cell and Module
- Modelling of PV Array
- Effect of Insolation on PV Characteristics

Chapter - 3

3.1 Introduction

The PV cell is the most important part of a PV system. The PV cell's primary function is to convert solar insolation into electricity. PV cells are designed using polycrystalline and mono-crystalline semi-conducting materials during the production process. A typical PV cell produces 1.5 to 2 W of maximum power. PV cell performance is primarily influenced by solar insolation (G) and temperature (T). The output voltage and power are a function of incident solar insolation, and the PV cell performance parameters (I-V and P-V) are non-linear. Before we can analyse the behaviour of PV cells, we must first model them. For the operation of a PV cell at an optimum point during various solar insolation levels and temperatures, good and precise mathematical modelling is required. In the literature, several mathematical models have been published, with a single diode and two diode mathematical models being the most widely utilised [45]-[46]. A single diode model is favoured due to the additional computational work necessary to solve the nonlinear equations of a two-diode model, but the output characteristics of the two-diode model PV cell are extremely close to the practical behaviour of the PV cell. As a result, in this thesis [45], a single diode model of a practical PV cell is adopted.

3.2 Modelling of PV Cell and Module

A controlled current source, a single diode, a series and shunt resistance, and a controlled current source are all part of the practical equivalent circuit of a single diode PV cell model depicted in Fig. 3.1 (a).

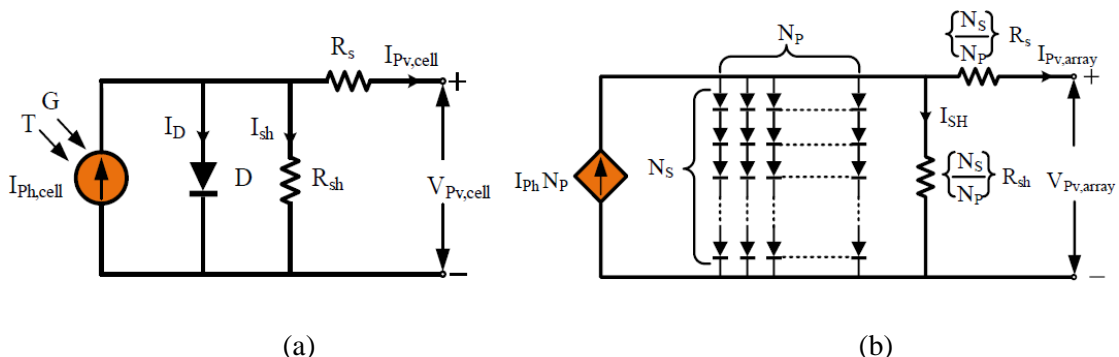


Figure 3.1: (a) Equivalent model of PV cell, (b) Equivalent model of PV array

Eq. (3.1) represents the mathematical expression for the PV cell's electrical Current-Voltage (I-V) behaviour.

$$I_{Pv,cell} = I_{Ph,cell} - I_r \left[\exp \left(\frac{V_{Pv,cell} + R_{sh} I_{Pv,cell}}{V_{T,cell} a} \right) - 1 \right] - \frac{V_{Pv,cell} + R_s I_{Pv,cell}}{R_{sh}} \quad (3.1)$$

$$\text{where, } V_{T,cell} = \frac{KT}{q}$$

Where $I_{Pv,cell}$ is the output current [A] of PV cell, $I_{Ph,cell}$ is the current generated by photon due to incidence of solar irradiance, I_r is the termed as reverse saturation current of diode, $V_{Pv,cell}$ is the output voltage of PV cell, $V_{T,cell}$ is named as thermal voltage of the PV cell, T is the operating temperature of PV cell, 'K' is the Boltzmann constant [$1.3806503 \times 10^{-23} \text{ J/K}$], 'q' is the charge of electron [$1.602 \times 10^{-19} \text{ C}$], R_s and R_{sh} are the series and shunt resistance of PV cell in [Ω], 'a' is the called the ideality factor of the diode and the value is unity for the ideal diode. The value of 'a' is varied if temperature and diode current are varied.

The photon current which is generated in the PV cell mainly depends on the solar irradiance level and the operating temperature. The expression for the photon current in a PV cell is expressed by Eq. (3.2).

$$I_{Ph,cell} = [I_{SC,cell} + K_{I,cell}(T - T_{ref})] \frac{G}{G_n} \quad (3.2)$$

Where $I_{SC,cell}$ is the short circuit current of the cell at standard test conditions (25°C and 1000 W/m^2), $K_{I,cell}$ is the temperature coefficient of short circuit current of the cell, T and T_{ref} are the operating temperature and reference temperature of the cell, G and G_n are the operating, and nominal solar insolation in W/m^2 . The reverse saturation current of the diode is varying with the cell temperature, and it can be expressed by Eq. (3.3).

$$I_r = I_{r,n} \left(\frac{T_{ref}}{T} \right)^3 \exp \left[\frac{qE_g}{aK} \left(\frac{1}{T_{ref}} - \frac{1}{T} \right) \right] \quad (3.3)$$

Where $I_{r,n}$ is the nominal reverse saturation current, E_g is the energy bandgap of the semiconductor. Typically, a single PV cell produces 0.5 V of output power, which is insufficient for nearly all applications. Several cells are connected in series or parallel to form a photovoltaic module, which increases the output power of the system.

Eq. (3.4) represents the mathematical expression for the PV module's electrical Current-Voltage (I-V) behaviour.

$$I_{Pv,m} = I_{Ph} - I_r \left[\exp \left(\frac{(qV_{Pv,m} + R_s I_{Pv,m})}{n_s K T_a} \right) - 1 \right] - \frac{V_{Pv,m} + R_s I_{Pv,m}}{R_{sh}} \quad (3.4)$$

Where, $I_{Pv,m}$ and $V_{Pv,m}$ are the module's current and voltage.

3.3 Modelling of PV Array

In order to achieve the higher voltage and current levels, several PV modules are connected either in series or in parallel referred to as PV array and its equivalent circuit is shown in Fig. 3.1 (b). Eq. (3.5) represents the mathematical expression for the PV array's electrical Current-Voltage (I-V) behaviour.

$$I_{Pv,ar} = I_{Ph} N_p - I_r N_p \left[\exp \left(\frac{q \left(V_{Pv,ar} + R_s \left(\frac{N_s}{N_p} \right) I_{Pv,ar} \right)}{n_s K T_a} \right) - 1 \right] + \frac{V_{Pv,ar} + R_s \left(\frac{N_s}{N_p} \right) I_{Pv,ar}}{R_{sh} \left(\frac{N_s}{N_p} \right)} \quad (3.5)$$

Where N_s is the number of PV modules connected in series, N_p is the number of PV modules connected in parallel, $I_{Pv,ar}$ and $V_{Pv,ar}$ is the output current and output voltage of the PV array.

3.4 Effect of Insolation on PV Characteristics

When PV panels are exposed to partial shading, they exhibit reverse polarity and PV panels absorb the power instead of generating. Due to absorption of power, heat is generated, a condition known as hot spot might occur and cause damage to the cells. With the help of a bypass diode (BD), it is possible to prevent a hotspot situation [47]. The power output from the module depends mainly on the solar insolation level and temperature. As the solar insolation varies, the short circuit current is also varied, and these are proportionally related in nature. According to Eq. (3.2), the photon current is directly proportional to short circuit current, and hence indirectly the short circuit current is directly proportional to solar insolation. Therefore, the power output from the PV module is directly proportional to incident solar insolation. As the solar insolation changes, the power output from the PV module is also changing.

The technical parameters of the Kyocera Solar KC200GT PV Module are available in the Table 3.1. The I-V and P-V characteristics of this PV module (*Kyocera Solar KC200GT*) at constant temperature and different insolation levels are shown in Fig. 3.2 (a) and (b) respectively. It shows how the maximum power rises with the irradiance level while the cell temperatures remain constant. The variations in insolation level indicate the presence of current and voltage fluctuations, most notably MPP. As a result, each increase in solar radiation causes an increase in the optimal power.

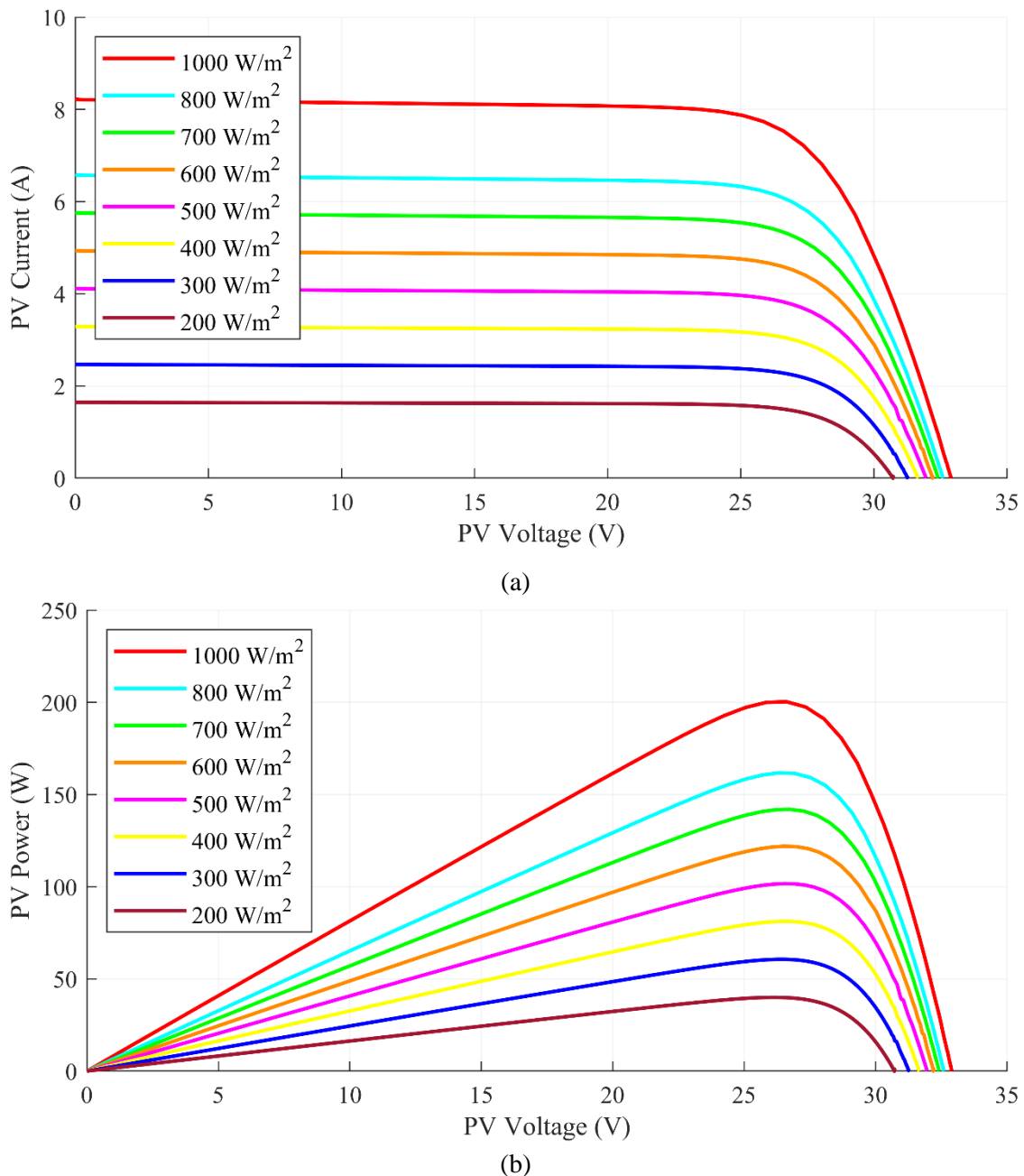


Figure 3.2: (a) I-V Characteristics and (b) P-V Characteristics of PV Module under different solar insolation

Table 3.1: Technical parameters of the Kyocera Solar KC200GT PV Module

Parameters	Value
Peak Power, P_{max}	200.143 W
Peak Power Voltage, V_{MP}	26.3 V
Peak Power Current, I_{MP}	7.61 A
Open Circuit Voltage, V_{OC}	32.9 V
Short Circuit Current, I_{SC}	8.21 A
Temperature co-efficient of V_{OC} , K_V	-0.123 V/K
Temperature co-efficient of I_{SC} , K_I	0.0032 A/K
Number of series connected cells, n_s	54

Table 3.1 describes the technical parameters of Kyocera Sola KC200GT PV Module. The maximum power of the above PV Module at 1000 W/m² is obtained at 200.143 W with voltage and current at 26.3 V and 7.61 A respectively at the maximum power point (MPP). The open circuit voltage of PV module is at 32.9 V and short circuit current is at 8.21 A.

Chapter - 4

PV ARRAY CONFIGURATIONS

- **Introduction**
- **Conventional PV Array Configurations**
- **Partial Shading Scenarios for TCT Configuration**
- **Factors affecting the Performance of PV Array Configuration**
- **Results and Discussions**

Chapter - 4

4.1 Introduction

Different PV module layouts can be used to reduce partial shading effects. Several PV array configurations, such as Series, Parallel, Series–Parallel (SP), Total-Cross-Tied (TCT), Bridge-Linked (BL), and honeycomb (HC), have been given in recent developments [48] – [51]. SP, TCT, BL, and HC are the most well-known PV array configurations. Kaushika et al. [52] compared the performance of three distinct PV array topologies (SP, TCT, and BL) to see which was more resistant to the PSC problem and electrical mismatch. TCT's superiority in terms of maximum power and fill factor was demonstrated in all circumstances of fresh cells, unclean cells, and even shadowed cells.

4.2 Conventional PV Array Configurations

4.2.1 Series (S) Configuration

The series PV array layout shown in Figure 4.1 is a very basic and straightforward setup. This arrangement is represented by serially connecting all of the modules. Because of the series connection, the same current runs through all PV modules, resulting in the PV module current matching the PV array output current and the PV array output voltage equaling the sum of the individual module voltages. Let i be the total number of PV modules in PV array, V_M (V_1, V_2, \dots, V_{49}) are the voltages of the module, V_{RW} represents voltage of the row, and I_M and I_{Str} are the termed respectively as module currents and string currents.

The total current at the output (I_{PV}), voltage at the output (V_{PV}) and the power at the output (P_{PV}) of the series PV array configuration is identified by set of Eq. (4.1).

$$\begin{aligned}
 I_{PV} &= I_{M1} = I_{M2} = I_{M3} \dots \dots = I_{M49} = I_M \\
 V_{PV} &= V_{M1} + V_{M2} + V_{M3} \dots \dots + V_{M49} = \sum_{i=1}^{i=49} V_{Mi} = 49 \times V_M \\
 P_{PV} &= V_{PV} \times I_{PV}
 \end{aligned} \tag{4.1}$$

The value of the output current of a PV array is determined by the lowest insolation received by the associated module, which is mostly affected by partial shading situations. Due to the minor mismatch between the shadowed and un-shadowed modules caused by the difference in module currents, shadowed modules are operated in reverse bias to keep the short circuit current the same as the shaded module current.

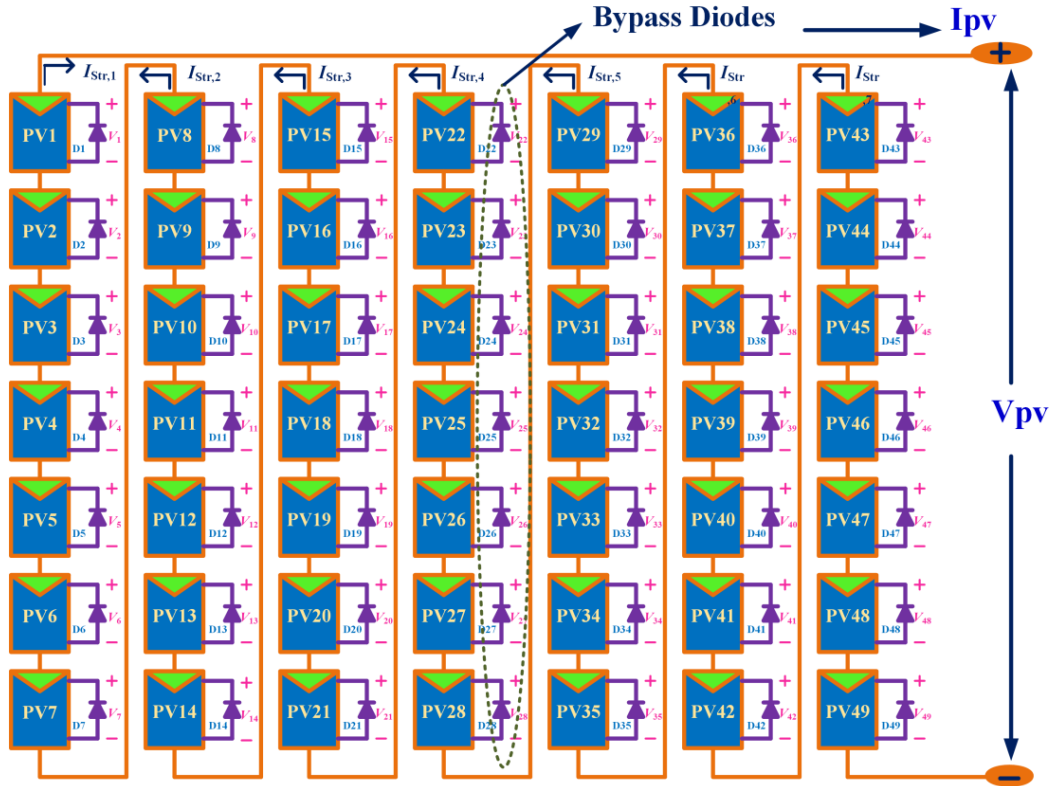


Figure 4.1: Schematic of 7×7 Series (S) PV array configuration

When shadowed modules are operated in reverse bias mode, they receive power from un-shadowed modules rather than giving it, and dissipate energy in the form of heat, resulting in the formation of local hotspots. PV modules are permanently damaged as a result of this. The bypass diodes are linked in antiparallel to each PV module to solve this problem. The P-V curve has many peaks as a result of the connecting of bypass diodes. To prevent the reverse current from flowing via shading modules, bypass diodes are connected across one or more PV modules, while the blocking diode is connected in series with the PV array. The bypass diode will be in reverse bias under uniform conditions, but it will be in conduction mode under non-uniform conditions.

4.2.2 Series-Parallel (SP) Configuration

Because there are no redundant connections between modules, no cross-ties between modules, and it is straightforward to design, the SP configuration is commonly utilised in PV system applications. As shown in Fig. 4.2, the SP PV array layout uses blocking diodes and bypass diodes to protect each string from critical short circuit currents or PSCs.

The total current at the output (I_{Pv}), voltage at the output (V_{Pv}) and the power at the output (P_{Pv}) of the SP PV array configuration is identified by set of Eq. (4.2).

$$\begin{aligned} I_{Pv} &= I_{Str1} + I_{Str2} + I_{Str3} \dots \dots + I_{Str7} \\ V_{Pv} &= V_{M1} + V_{M2} + V_{M3} \dots \dots + V_{M7} = \sum_{M=1}^{M=7} V_M = 7 \times V_M \\ P_{Pv} &= V_{Pv} \times I_{Pv} \end{aligned} \quad (4.2)$$

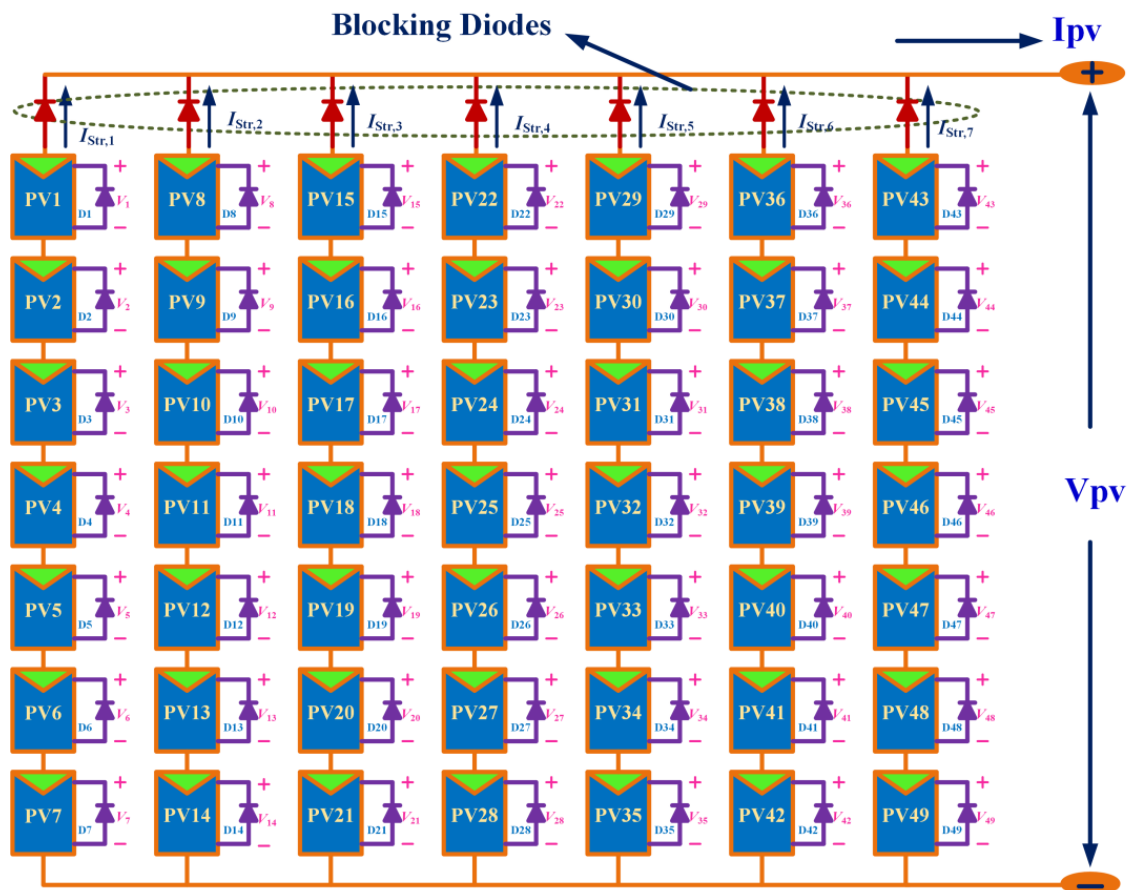


Figure 4.2: Schematic of 7×7 Series-Parallel (SP) PV array configuration

Each PV module is connected in series to form strings in the SP configuration, and then all strings are connected in parallel to achieve the PV array's required output voltage and current. This PV arrangement is broken down into seven strings, each with seven series-connected modules. The SP PV array's output voltage is equal to the voltage across each string, or the sum of seven individual PV module voltages, and the PV array's output current is equal to the total of seven individual string currents. It has the advantages of both parallel and series PV setups. Easy construction, reduced cabling, and cost-effective operations are all advantages of the SP architecture. However, due to the increased number of series connections among the modules, this arrangement is extremely sensitive to mismatch loss under PSCs.

4.2.3 Total-Cross-Tied (TCT) Configuration

TCT PV configuration is offered to overcome the influence of PSCs in SP PV system. As shown in Fig. 4.3 [60], the TCT configuration is modelled as follows: first, all PV modules in strings are stacked parallel as rows, and then each row is arranged in series with the next rows. The voltage across each row is the same as the voltage across each module in this design, and the PV array's output voltage equals the total of the individual row voltages. The output current of a PV array is equal to the sum of the individual module currents in a row.

The total current at the output (I_{Pv}), voltage at the output (V_{Pv}) and the power at the output (P_{Pv}) of the TCT PV array configuration is identified by set of Eq. (4.2).

$$\begin{aligned}
 I_{Pv} &= I_{M1} + I_{M8} + I_{M15} + I_{M22} + I_{M29} + I_{M36} + I_{M43} = 7 \times I_M \\
 V_{RW1} &= V_{RW2} = V_{RW3} = \dots \dots \dots V_{RW7} = V_M \\
 V_{Pv} &= V_{RW1} + V_{RW2} + V_{RW3} + \dots \dots \dots + V_{RW7} \\
 P_{Pv} &= V_{Pv} \times I_{Pv}
 \end{aligned} \tag{4.3}$$

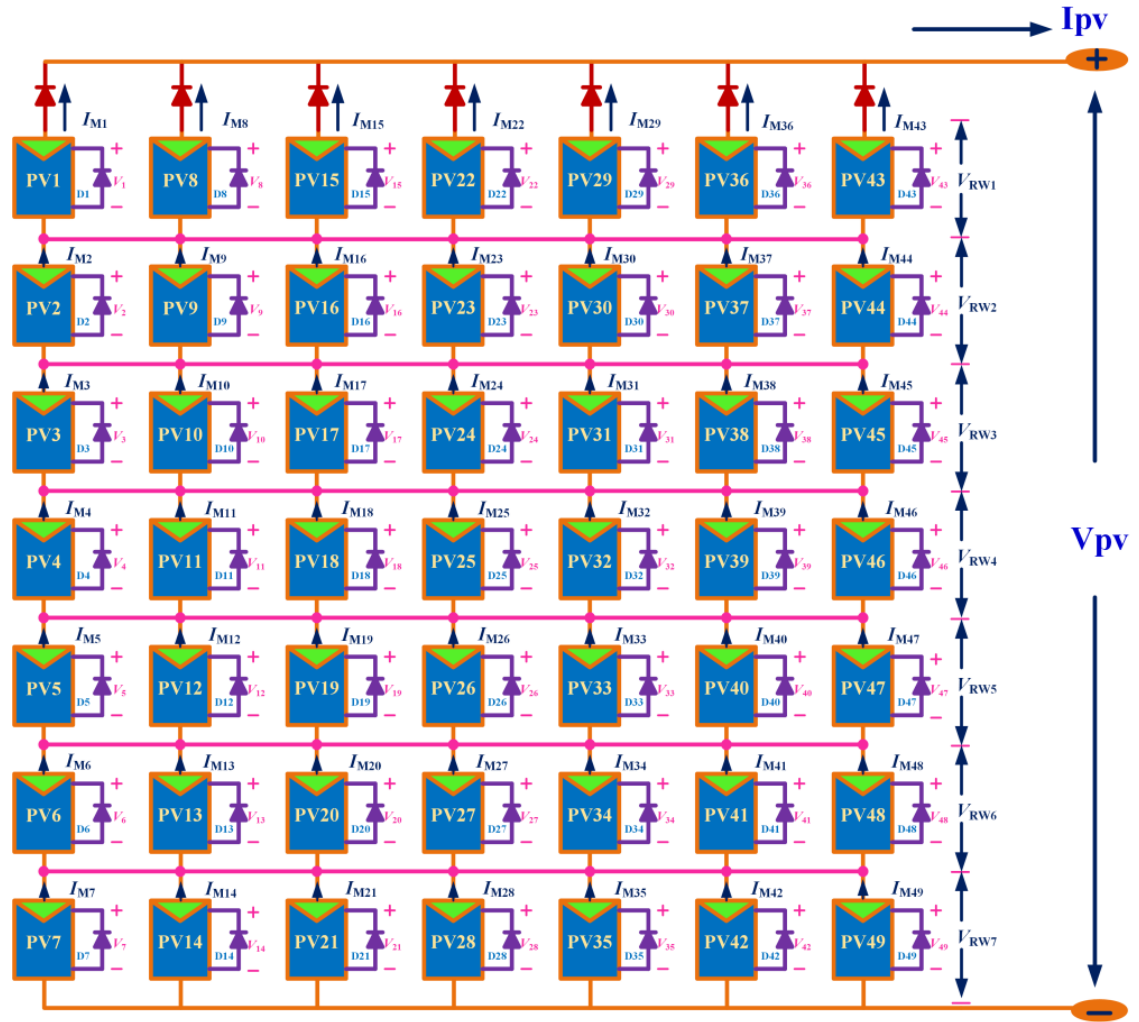


Figure 4.3: Schematic of 7×7 Total-Cross-Tied (TCT) PV array configuration

The TCT configuration offers the advantages such as higher power generation capability, longer operational life-time, good fault tolerance, and less multi-peak effect. But, the drawbacks of TCT configuration are complexity in operation, more wiring cost, and high-power losses even though it is generating more power compared to other configurations.

4.3 Partial Shading Scenarios for TCT Configuration

PSCs have a big impact on PV array performance, and the power output varies depending on the shading environment. This section examines the performance of various shading conditions that are subjected to traditional and proposed 7/7 PV array layouts. As shown in Fig. 4.4, shading patterns are classified as centre, corner, diagonal, frame, random, and right-side end shading patterns based on the level of solar intensity on PV modules in an array, and the number of rows, columns, and solar intensity on the PV module are represented along the X, Y, and Z-axis. The following is a description of all shading conditions:

4.3.1 Center shading scenario

The PV modules are shaded with varying solar insulations at the centre of the 7x7 PV array in this shading scenario, as shown in Fig. 4.4 (a), and so it is called centre shading. The modules that are center shaded are: In the second row, from the third to fifth modules (PV16, PV23 and PV30) are insulated individually at 200 W/m²; In the third row, from the third to fifth modules (PV17, PV24 and PV31) are insulated individually at 300 W/m²; In the fourth row, from the third to fifth modules (PV18, PV25 and PV32) are insulated individually at 400 W/m²; In the fifth row, from the third to fifth modules (PV19, PV26 and PV33) are insulated individually at 600 W/m²; In the sixth row, from the third to fifth modules (PV20, PV27 and PV34) are insulated individually at 800 W/m²; The remaining PV modules are insulated at 1000 W/m² respectively.

4.3.2 Corner shading scenario

The PV modules are shaded with varying solar insulations at the left corner of the 7x7 PV array in this shading scenario, as shown in Fig. 4.4 (b), and so it is called centre shading. The shaded left corner modules are: the first row up to the first three modules (PV1, PV8 and PV15) is insulated at 200 W/m², second row up to the first three modules (PV2, PV9 and PV16) is insulated at 400 W/m², third row up to the first three modules (PV3, PV10 and PV17) is insulated at 500 W/m² and fourth row up to first three modules (PV4, PV11 and PV18) is insulated at 700 W/m², and the rest of the PV modules are insulated at 1000 W/m² respectively.

4.3.3 Diagonal shading scenario

In this shading condition, the diagonally placed PV modules in array of 7x7 PV are shaded with various solar insolation levels as depicted in Fig. 4.4 (c) and hence it is named as diagonal shading. The modules numbered PV1 and PV2 are insolated at 200 W/m²; PV9 and PV10 are insolated at 300 W/m²; PV17 and PV18 are insolated at 400 W/m²; PV25 and PV26 are insolated at 500 W/m²; PV33 and PV34 are insolated at 600 W/m²; PV41 and PV42 are insolated at 700 W/m²; PV49 is insolated at 800 W/m² and the rest of the PV modules are insolated at 1000 W/m² respectively.

4.3.4 Frame shading scenario

In this shading scenario, the PV modules in a 7×7 PV array are shaded in a frame-like structure with various levels of solar insolation, as shown in Fig. 4.4 (d) and hence it is named as frame shading. The shaded modules in frame manner are: The modules numbered PV1, PV9, PV41 and PV49 are insolated at 200 W/m²; PV2, PV8, PV10, PV16, PV34, PV40, PV42 and PV48 are insolated at 300 W/m²; PV3, PV15, PV11, PV23, PV27, PV39, PV35 and PV47 are insolated at 400 W/m²; PV4, PV22, PV12, PV30, PV20, PV38, PV28 and PV46 are insolated at 500 W/m²; PV5, PV29, PV13, PV37, PV21 and PV45 are insolated at 600 W/m²; PV6, PV14, PV36 and PV44 are insolated at 700 W/m²; PV7 and PV 43 are insolated at 800 W/m², and the remaining PV modules are insolated at 1000 W/m² respectively.

4.3.5 Random shading scenario

In this shading scenario, the PV modules in a 7×7 PV are randomly shaded with different levels of solar insolation, as shown in Fig. 4.4 (e) and hence it is named as random shading. The modules numbered PV11, and PV32 are insolated at 200 W/m²; PV3, PV28, PV42 and PV45 are insolated at 300 W/m²; PV14 and PV37 are insolated at 400 W/m²; PV16, PV29 and PV48 are insolated at 500 W/m²; PV 5 is insolated at 600 W/m²; PV7 and PV20 are insolated at 700 W/m²; PV8 is insolated at 800 W/m², and the rest of the PV modules are insolated at 1000 W/m² respectively.

4.3.6 Right-side end shading scenario

In this shading scenario, as shown in Fig. 4.4 (f), the PV modules located at the right-side end of the 7×7 PV array and are shaded with different solar insolation levels

and is referred to as right-side end shading. The modules which are shaded on the right-side end are: The fifth (PV29, PV30, PV31, PV32, PV33, PV34 and PV35), sixth (PV36, PV37, PV38, PV39, PV40, PV41 and PV42) and seventh (PV43, PV44, PV45, PV46, PV47, PV48 and PV49) strings (columns) are completely shaded from top to bottom with different insolation levels of 200 W/m^2 , 300 W/m^2 , 400 W/m^2 , 500 W/m^2 , 600 W/m^2 , 700 W/m^2 and 800 W/m^2 and the rest of the PV modules are insolated at 1000 W/m^2 respectively.

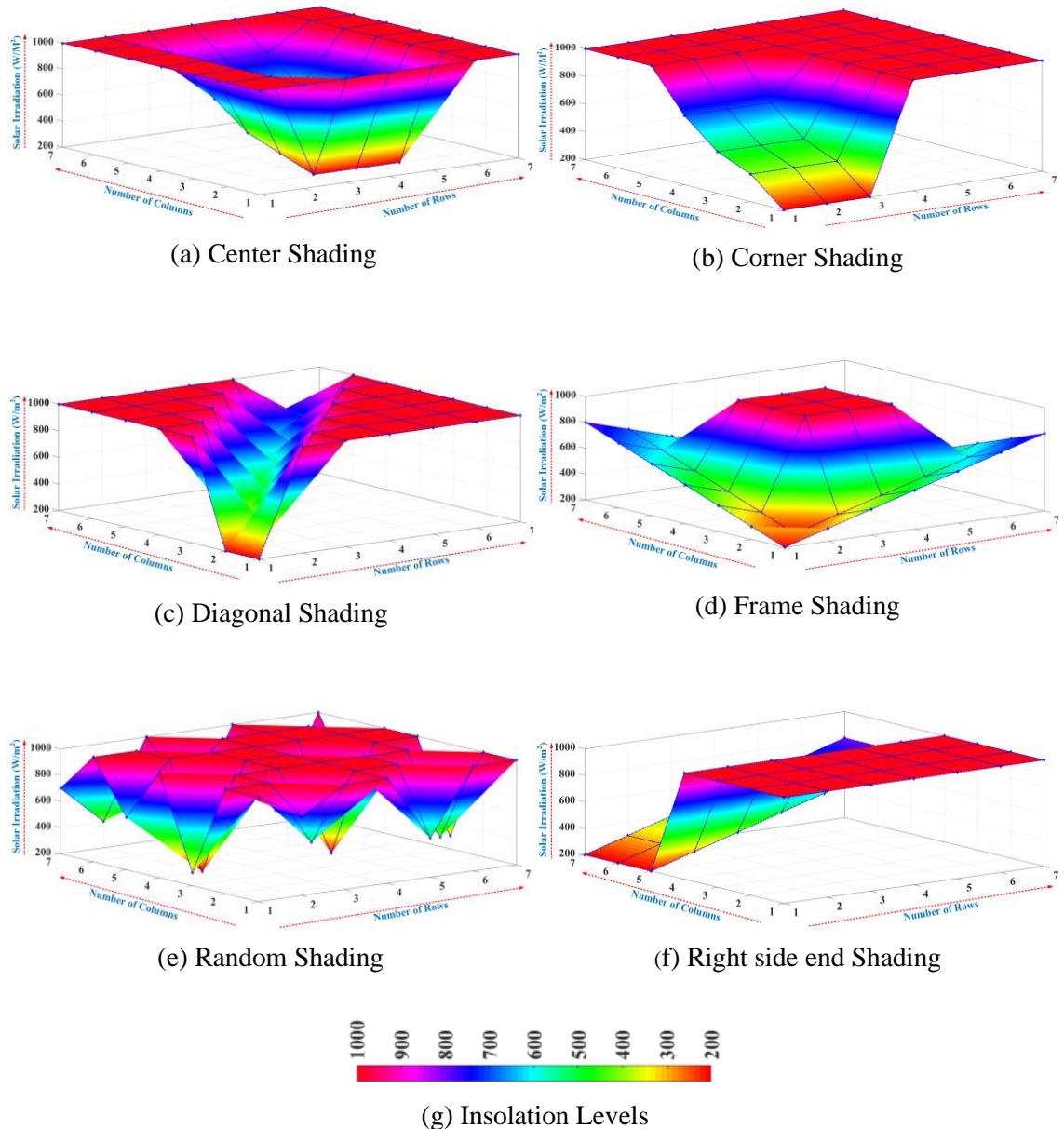


Figure 4.4: Representation of different partial shading scenarios

4.4 Factors affecting the Performance of PV Array Configuration

4.4.1 Mismatching Power Loss (MPL)

The ratio of change in peak power during uniform irradiance to partial shade situation divided by peak power generated during uniform insolation is known as mismatching power loss. Eq. (4.4) is used to calculate the mismatching power loss, which is given as a percentage.

$$MPL(\% \Delta P_{MPL}) = \frac{P_{GMP,UIC} - \Delta P_{GMP,PSC}}{P_{GMP,UIC}} \times 100 \quad (4.4)$$

Where ΔP_{MPL} is known as mismatched power loss, $P_{GMP,UIC}$ is the max power obtained under uniform shading and $P_{GMP,PSC}$ is the max power obtained under PSC.

4.4.2 Fill Factor (FF)

The ratio of global peak power to the product of open circuit voltage and short circuit current is known as Fill Factor. In the field of PV design, this is a fascinating figure. Eq. (4.5) calculates FF, which is a real indicator of PV configuration goodness. If the FF is closer to unity, the PV system has a greater performance.

$$FF = \frac{V_{MP} \times I_{MP}}{V_{OC} \times I_{SC}} \quad (4.5)$$

Where V_{MP} and I_{MP} are the voltage and currents at peak power points, and V_{OC} and I_{SC} are the open circuit voltage and short circuit current of the PV array.

4.4.3 Efficiency

It is calculated using Eq. (4.6) as the ratio of maximum peak output power to input solar power.

$$\eta = \frac{V_{MP} \times I_{MP}}{L \times A} \quad (4.6)$$

Where ' η ' is the efficiency, 'L' is the intensity level of solar fall on the PV panel per ' m^2 ', and 'A' is PV panel area.

4.5 Results and Discussion

This section discusses the performance of TCT PV array configurations by simulating it in Matlab/Simulink environment under uniform shading and six other shading conditions (center, corner, diagonal, frame, random and right-side). For simulation of PV array configuration under PSCs, KYOCERA-KC200GT PV module parameters have been used as discussed in Table 3.1.

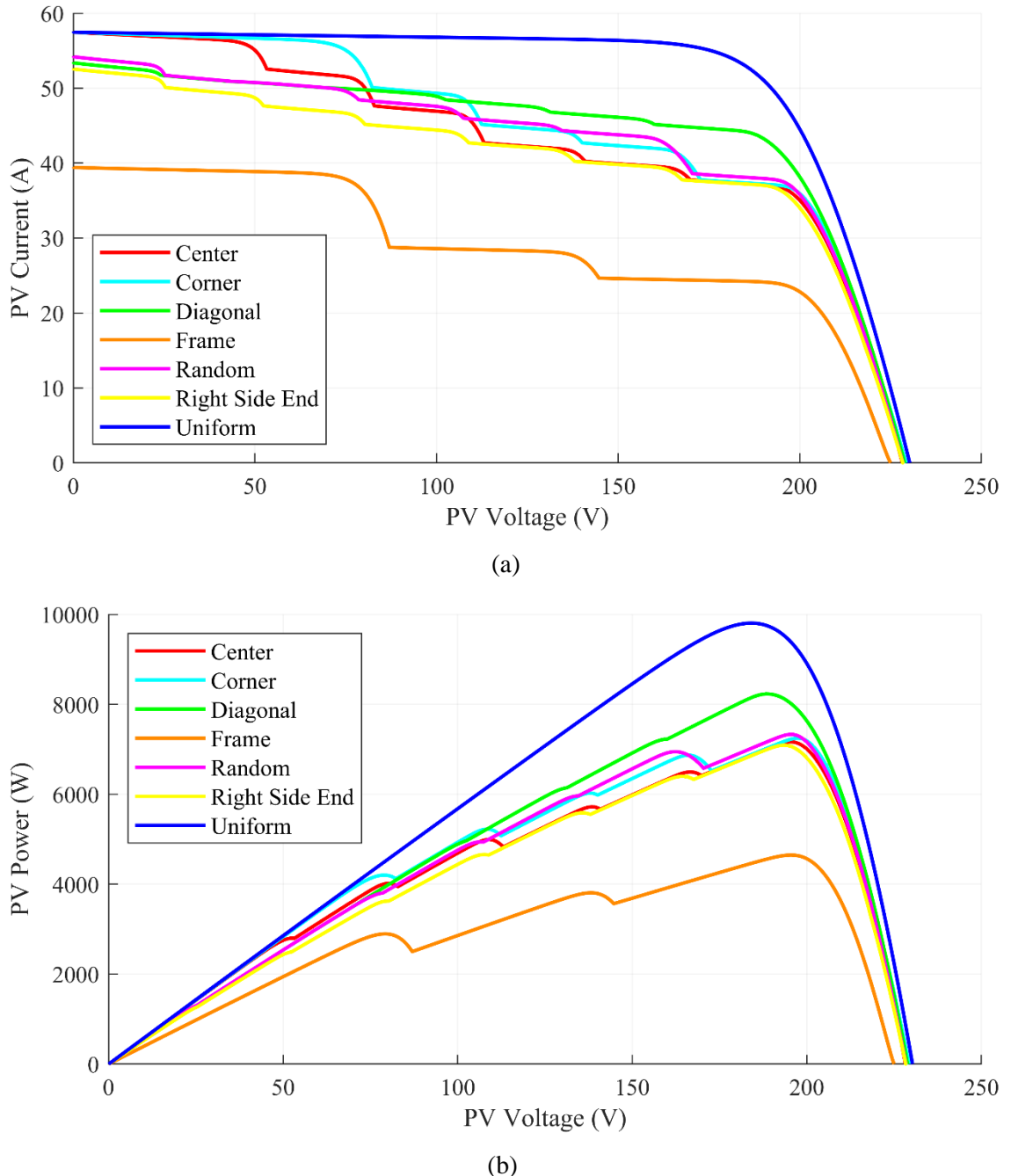


Figure 4.5: (a) I-V and (b) P-V Characteristics of TCT PV array under PSCs

Table 4.1: Performance of TCT PV Array under PSCs

Parameters Shading Conditions	V_{oc} (V)	I_{sc} (A)	V_{mp} (V)	I_{mp} (A)	P_{gmp} (W)	ΔP_{MPL} (%)	FF (%)
Centre	228.3	57.59	195.2	36.71	7166	26.92	54.50
Corner	229.3	57.59	197.5	36.67	7249	26.08	54.84
Diagonal	228.9	53.48	188.3	43.74	8234	16.03	67.28
Frame	225.0	39.49	195.4	23.79	4648	52.60	52.34
Random	228.4	54.30	195.5	37.51	7333	25.22	59.19
Right side end	228.4	52.66	193.3	36.68	7091	27.69	58.95
Uniform	230.3	57.59	184.2	53.24	9806	--	73.94

The global maximum powers (P_{GMP}), obtained under different shading conditions is compared in the below bar graph (Fig. 4.6). The number of local maximum power point peaks that can be seen from the P-V Characteristics in Fig. 4.5 (b) is summarised in the Fig. 4.7.

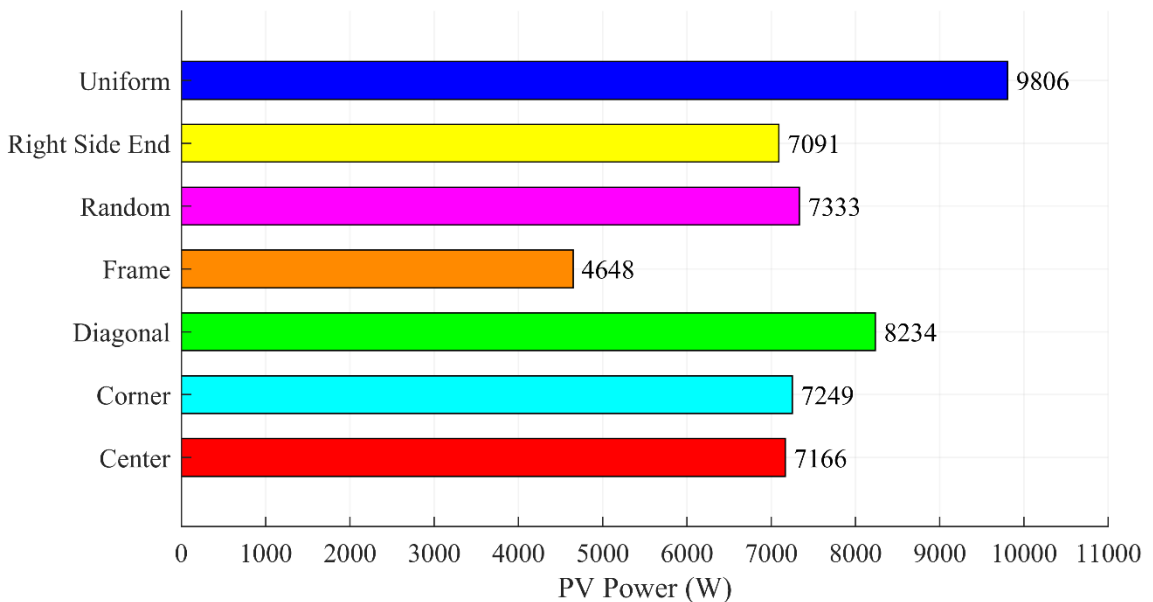


Figure 4.6: Global Maximum Power of TCT PV array under different partial shadings

As expected from the above graph, the uniform shading will give maximum power compared to all other shading conditions. Under Uniform shading, a 9806 W maximum power is obtained followed by Diagonal shading which gives max power of 8234 W. Least power among the PSCs is obtained for the Frame shading which is about 4648 W.

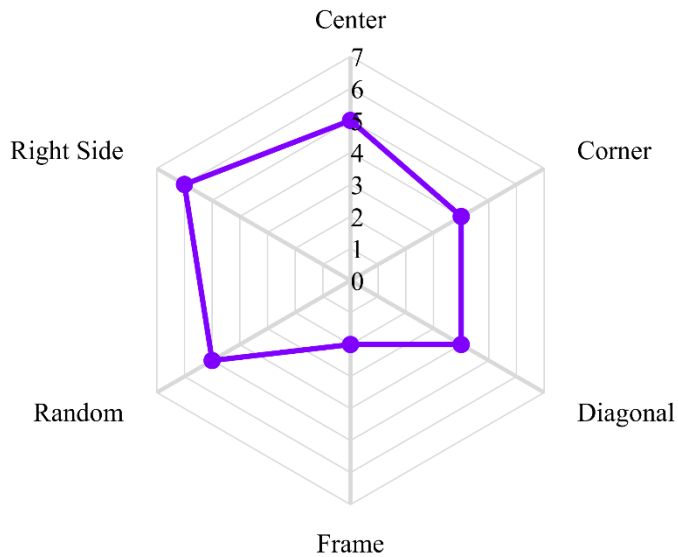


Figure 4.7: Number of Local Maximum Power Points under PSCs

Due to the partial shading conditions, a various number of local peaks is obtained in the P-V characteristics. For example, in the corner shading conditions, we can see from the Fig. 4.5 (b) that the total number of local maximum power point peaks are 4 and there is one global maximum power point which need to be extracted from the PV array. To summarise the total number of local power point peaks, a spider chart is made in Fig. 4.7 which depicts the LMPPs for all partial shading scenarios.

Chapter - 5

MAXIMUM POWER POINT TRACKING TECHNIQUES

- **Introduction**
- **Perturbation and Observation MPPT Technique**
- **Flowchart of P&O MPPT Algorithm**
- **Implementation of P&O MPPT Technique**

Chapter - 5

5.1 Introduction

Variations in the output power of the PV system are caused by changes in external factors such as temperature and solar irradiation. Partial shading refers to the occurrence of non-uniform irradiation, as we described earlier. In the uniform situation, the P-V curve has only one point (P_{max}) where the module produces maximum power. Partial shadowing circumstances (PSCs), on the other hand, cause varying radiation on each PV array to generate different power from one PV array to the next. Furthermore, by utilising bypass diodes to shield shaded PV modules/arrays from hot spots, many peaks, one GMPP, and many local maximum power points (LMPP) would be formed, reducing power generation. As a result of the aforementioned reasons, a gap exists between installed energy capacity and actual energy generation.

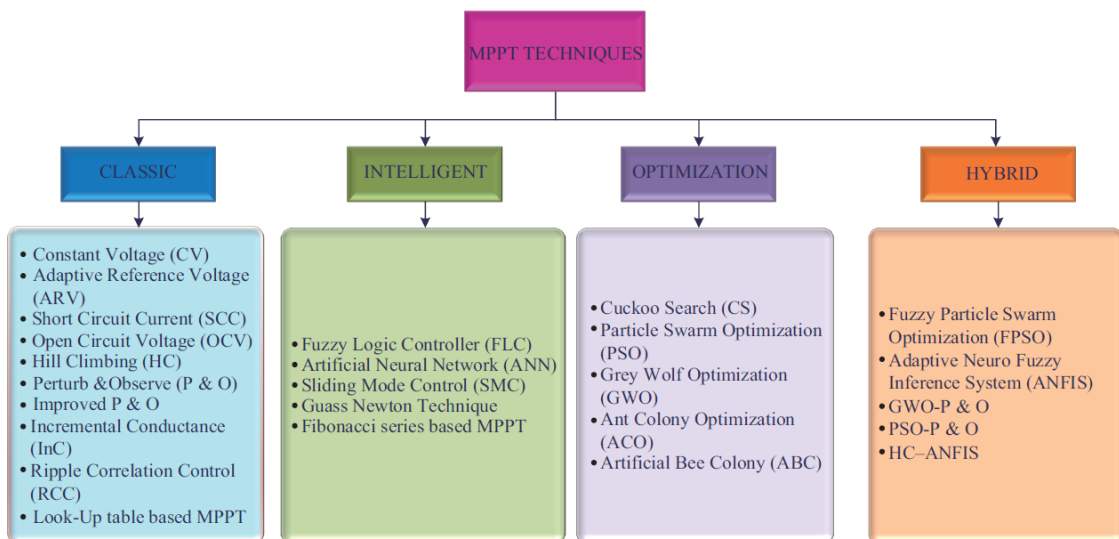


Figure 5.1: Classification of PV MPPT techniques.

Researchers have concentrated on developing maximum power point tracking systems to overcome the impacts of PSCs and increase the quantity of power generated (MPPT). Various MPPT strategies for operating PV modules at maximum power have been documented in the literature [73]-[74]. However, the effectiveness of the approach is determined by its capacity to track changes in meteorological conditions. The PV MPPT technique's implementation methods are classed as Classical PV MPPT, Intelligent

PV MPPT, Optimization PV MPPT, and Hybrid PV MPPT, as illustrated in Fig. 5.1, depending on the tracking nature.

5.2 Perturbation and Observation MPPT Technique

The traditional P&O algorithm is the simplest, most cost-effective, most widely used in practise, with an efficiency of up to 96.5 percent. The algorithm gets its data from the PV module or array's actual operational point (i.e., voltage, V_{PV} , and current, I_{PV}) to scan the P-V curve and calculate MPP, as shown in Fig. 5.2. The scanning of the P-V curve is accomplished by perturbing the operational point (V_{PV} or I_{PV}) and then measuring the change in PV power (ΔP), which is known as the observation step. The following is the change in PV power as a result of this:

- If ΔP and ΔV is positive, the perturbation of voltage should be increased from point "green region" towards MPP as shown at the left side of Fig. 5.2.
- If ΔP is negative and ΔV is positive, the perturbation of voltage should be decreased from point "blue region" towards MPP as shown at the right side.

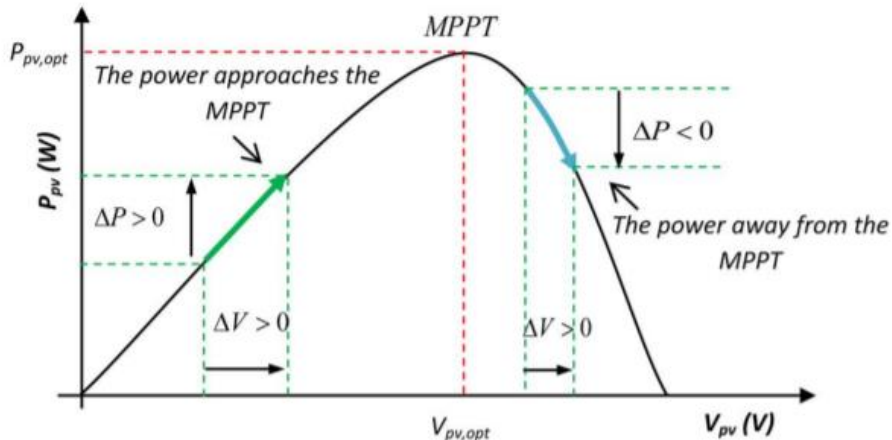


Figure 5.2: Perturbation and Observation on PV Curve

The above procedure is repeated until maximum power point is reached, at which point $\Delta P/\Delta V$ is near to zero. This satisfied condition is referred to as steady state. The P&O continues to affect the system in order to detect a change in the maximum power point (due to changes in environmental conditions or load), which initiates a new scan. Normally, this process causes the PV system's operating point to oscillate about MPP.

5.3 Flowchart of P&O MPPT Algorithm

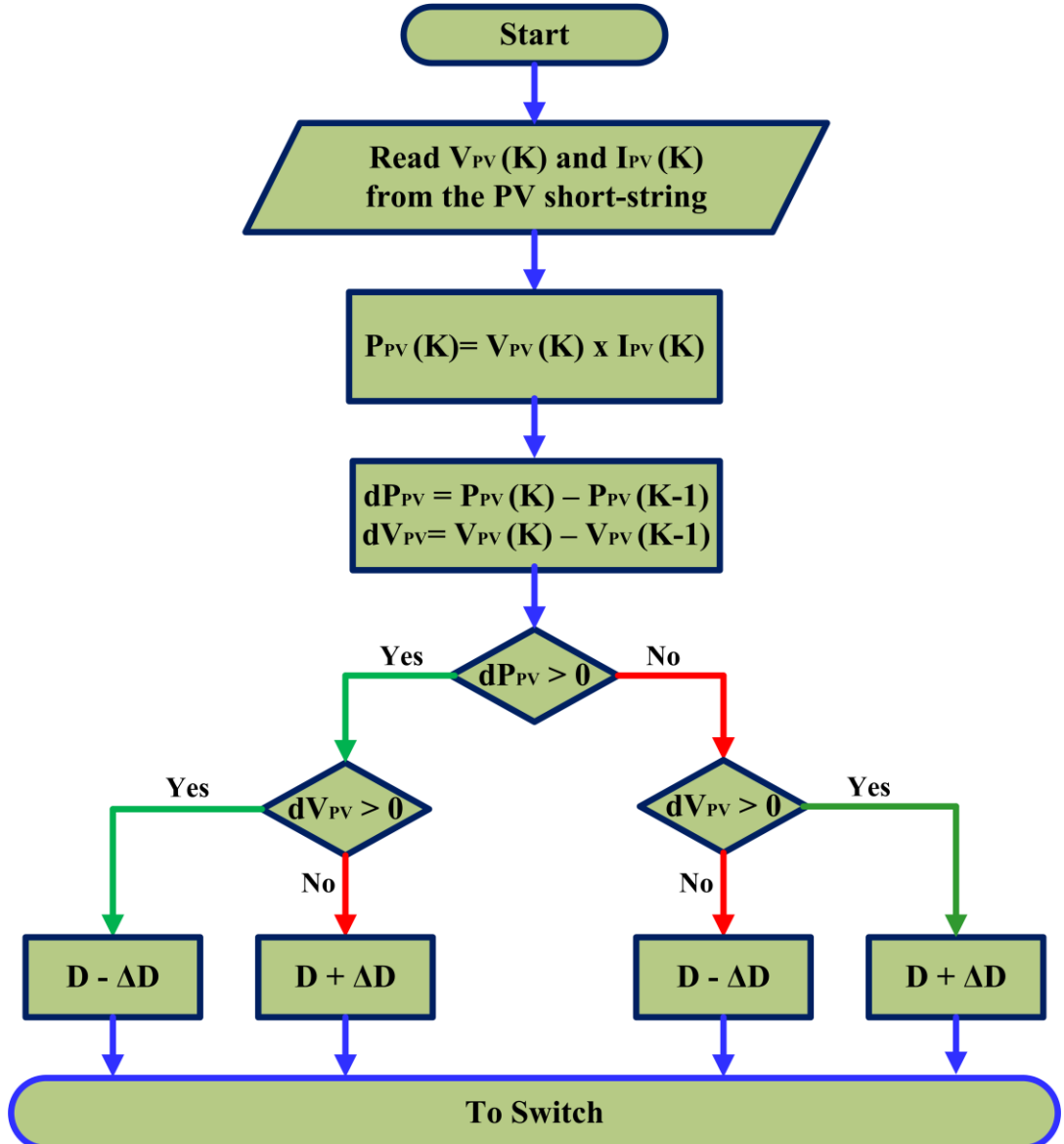


Figure 5.3: Flowchart of P&O MPPT Algorithm

The flowchart of conventional P&O algorithm is shown in Fig. 5.3. The algorithm is explained in better way using a flow chart. When product of dP_{PV} and dV_{PV} is greater than zero, then decrease the duty ratio 'D' by ΔD , if product of dP_{PV} and dV_{PV} is less than zero, then increase the duty ratio 'D' by ΔD .

5.3 Implementation of P&O MPPT Technique

The P&O MPPT method is the simplest and most common method of obtaining full power. The PV fed functional block diagram, as well as the P&O MPPT algorithm, are shown in Fig. 5.4. The variables V_{pv} and I_{pv} are detected from the PV module and sent to the MPPT controller (microcontroller) as input variables, as shown in Fig. 5.4. On the microcontroller, the P&O MPPT algorithm is implemented, and a control signal is created at the output. To generate a PWM signal, the control signal is correlated with the 10 kHz frequency saw-tooth signal.

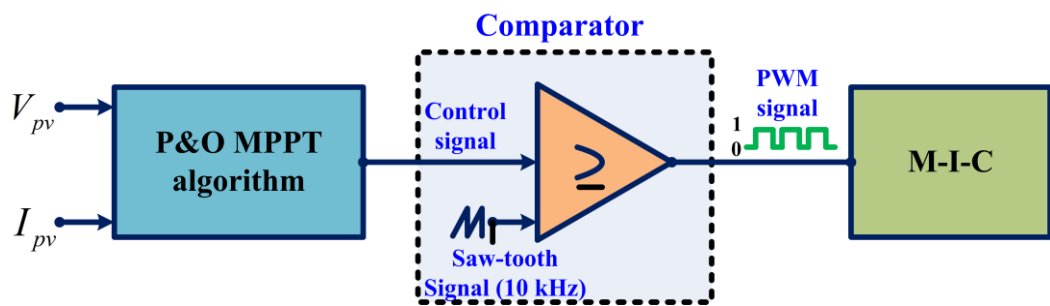


Figure 5.4: P&O MPPT controller implementation.

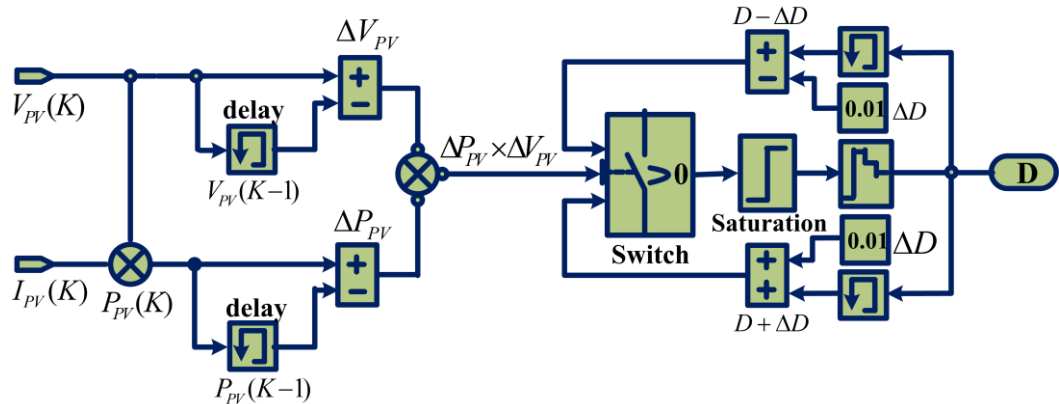


Figure 5.5: MATLAB/Simulink model of the P&O MPPT algorithm

The Fig. 5.5 shows the MATLAB/Simulink implementation of the P&O MPPT technique. The inputs V_{PV} and I_{PV} are current sensed values from the PV Module. Finally, the output of the block gives the required duty cycle ‘D’ needed for the maximum power point tracking.

Chapter - 6

TOPOLOGIES OF DC-DC CONVERTERS

- **Introduction**
- **Classification of DC-DC Converters**
- **Non-Isolated DC-DC Converters**
- **Comparison of Gains of Non-Isolated Converters**
- **Designing of Boost Converter**

Chapter - 6

6.1 Introduction

The introduction of power converters signalled a dramatic shift in the development of various electrical innovations. Furthermore, traditional power converters have long had a leadership position due to their applications and distinguishing characteristics. In the following part, we'll look at how converters are classified and how they're used in PV systems.

6.2 Classification of DC-DC Converters

DC-DC converters are separated into two categories, as shown in Fig. 6.1: isolated and non-isolated converters. The presence of an electrical barrier between the converter's inputs and outputs is referred to as "isolation." A high-frequency transformer could be used as a barrier. This barrier's main advantage is that it can be employed in high-voltage applications. These isolated converters can also be adjusted to be either positive or negative. This barrier does not exist in non-isolated converters. Flyback, forward, resonant, push-pull, and bridge converters are examples of isolated converters. Cuk, SEPIC, boost, buck-boost, positive-output super-lift Luo, and Ultra-lift Luo converters are the most often used non-isolated converters.

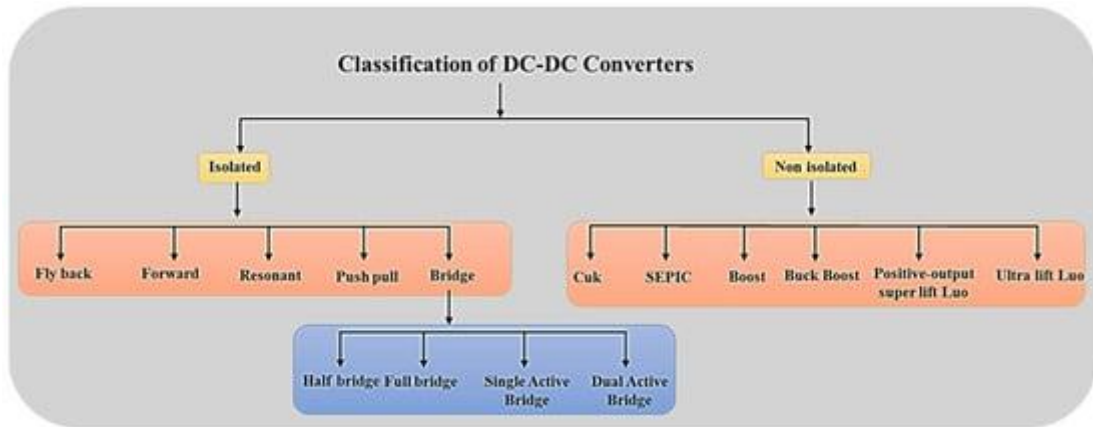


Figure 6.1: Classification of DC-DC Converters

In a PV system, the PV array can be directly connected to the load or through a converter. The greatest power obtainable at a given irradiance and temperature for an operational point on the PV array's non-linear I-V characteristic will be smaller than the power absorbed by the load in a direct connection. A DC-DC converter can be connected between the PV array and the load to allow the PV array to operate at its maximum power under fluctuating solar radiation and temperatures. The DC-DC converter can increase or decrease the voltage of the PV system depending on the load requirements.

In this project, we are going to deal with only non-isolated converters like Boost, Buck-Boost, Cuk, SEPIC, Zeta, Positive output Super-lift Luo and Ultra-lift Luo converters along with Perturbation and Observation technique to obtain the Maximum power point.

6.3 Non-Isolated DC-DC Converters

6.3.1 Boost Converter

The boost converter is displayed. The duty cycle is utilised to raise the input voltage according to the needed output voltage, as shown in Fig. 6.2. Using switches, the configuration of a boost converter for ON and OFF states is detailed below. The boost converter output voltage equation [55] based on duty cycle is as follows:

$$V_{\text{out}} = \frac{1}{1 - D} V_{\text{in}}$$

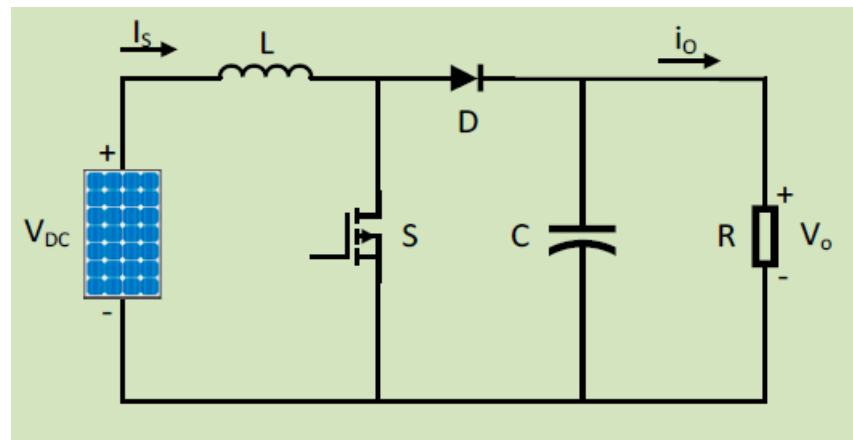


Figure 6.2: Boost converter for PV Application

When the switch is turned on, the current flowing through the inductor increases. When the circuit is short-circuited, the energy flowing through the inductor increases, whereas when the switch is open, the current is reduced due to the higher impedance. When the current through the inductor never falls to zero, it is said to be in continuous mode. When the current across the inductor reaches zero, the mode is said to be discontinuous. The input voltage appears across the inductor when the switch is turned on, and the current through the load is zero. The input current travels through the load when the switch is turned off. The input current is the same as the current in the inductor. The ripples are filtered for output voltage by the capacitor on the load side.

6.3.2 Buck-Boost Converter

The Buck-Boost converter is used to convert the higher voltage value from the solar panel to the lower voltage and vice versa. The configuration of a buck-boost converter for ON and OFF states, as shown in Fig. 6.3, is detailed below utilising switches. Based on the duty cycle, the output voltage equation for a buck-boost converter is [56],

$$V_{\text{out}} = \frac{D}{1-D} V_{\text{in}}$$

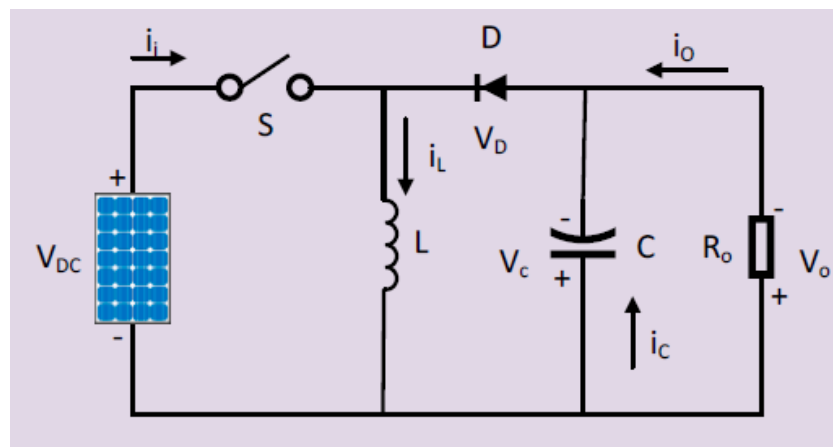


Figure 6.3: Buck-Boost converter for PV application

The input voltage is directly linked to the inductor when the switch is turned on. As a result of the inductor, energy is increased. The load receives energy from the capacitor on the output side. The voltage across the output is in the opposite polarity of the input voltage as the capacitor discharges in inverting mode. The input voltage appears across the MOSFET switch when the switch is turned off. When the switch is turned off,

the inductor that was charged during the switch on period is discharged. The capacitor is charged during this time, and the procedure is repeated.

6.3.3 Cuk Converter

Cuk converters are DC-DC converters with output voltage magnitudes that are either larger or less than the input voltage magnitude. The Cuk converter works in the same way as a buck-boost converter, increasing or decreasing the input voltage. Figure 3.5 depicts a circuit schematic in which the main energy storage device is a capacitor [57], rather than an inductor, as in buck, boost, and buck-boost converters. Slobodan Cuk, the circuit's creator, was given the name. The output voltage formulae are the same as the equation for a buck-boost converter given by,

$$V_{\text{out}} = \frac{D}{1 - D} V_{\text{in}}$$

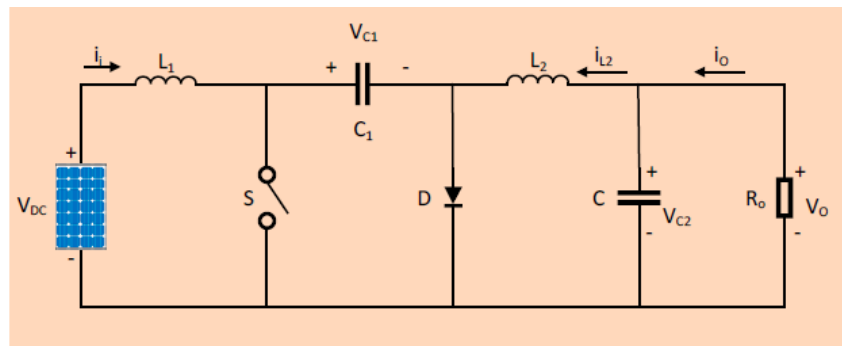


Figure 6.4: Cuk converter for PV application

The output voltage is controlled via a feedback loop since the output voltage equation is linear. The diode and the switch are either replaced by a short circuit when they are ON or by an open circuit when they are OFF in a non-isolated Cuk converter. When the input source is turned off, the capacitor C_1 is charged by the input source via the inductor L_1 . When the capacitor C_1 was turned on, it transferred energy to the output capacitor via the inductor L_2 . The Cuk converter's output voltage polarity is expected to be inverted in relation to the input voltage. The converter's output is inverted with the right connections, resulting in a ripple-free output.

6.3.4 Single-Ended Primary Inductance Converter (SEPIC)

The single-ended primary inductance converter, also known as a SEPIC converter, is depicted in Fig. 6.5. Basically, the ON period during switching is longer than the OFF time in order to achieve a greater output voltage (because of more time of charging for the inductor). If this is not the case, the converter will stop producing the required output. This is due to the capacitor's inability to fully charge. Based on the duty cycle, the output voltage equation [58] for SEPIC converter is,

$$V_{\text{out}} = \frac{D}{1 - D} V_{\text{in}}$$

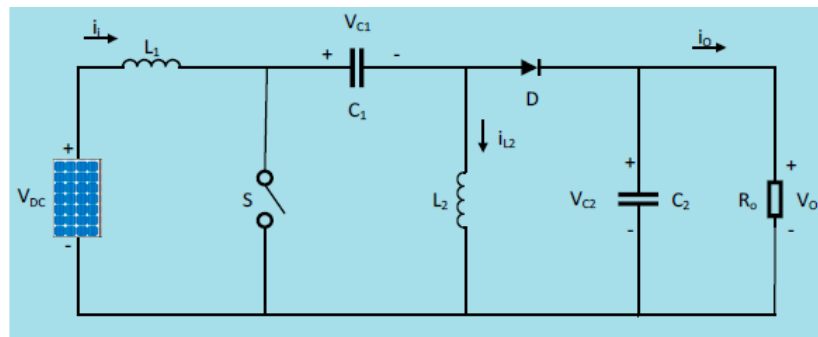


Figure 6.5: SEPIC converter for PV application

Several constraints must be taken into consideration when designing the converter. The ripple in the output voltage is claimed to be reduced when a high-frequency transformer is used with a traditional SEPIC converter. This arrangement benefits from crucial aspects such as constant output current, reduced switching stress, and reduced output ripple. Certain harmonics were created during AC-DC conversion, causing ripples in AC currents and subsequently lowering the power factor. The SEPIC converter can be used for power factor correction in AC lines when it is in the boundary conduction mode (BCM).

6.3.5 Zeta Converter

The zeta converter circuit diagram is depicted in Fig. 6.6. The zeta converter can convert input voltage to a noninverted output voltage with a value that is either lower or greater than the input voltage. Components in the zeta converter include a power electronic switch (S), inductors, a diode, capacitors, and a load (R). This converter's output voltage equation [59] is comparable to the buck-boost converter given by,

$$V_{\text{out}} = \frac{D}{1-D} V_{\text{in}}$$

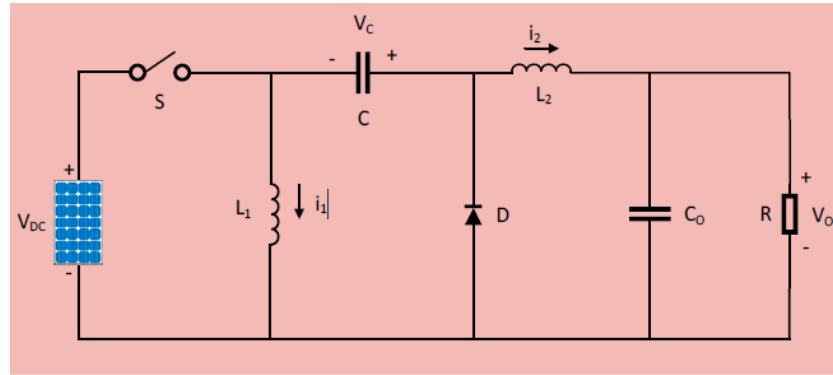


Figure 6.6: Zeta converter for PV application

It has two modes of operation. When the diode (D) is turned off and the switch (S) is turned on, mode 1 is accomplished. The source voltage V_s is used to draw current through the inductors L_1 and L_2 . Inductor currents i_{L1} and i_{L2} grow in a linear fashion. Charging mode is the name for this mode of operation. When the diode (D) is turned on and the switch (S) is turned off, mode 2 operation is achieved. The inductors' stored energy is released and delivered to the load. The current in the inductors falls in a linear fashion. Discharging mode is the name for this mode of operation.

6.3.6 Super-Lift Luo Converter

When compared to the Cuk and SEPIC converters [60], super-lift Luo converters, as shown in Fig. 6.7, are extremely powerful. This converter's distinguishing qualities are its increased efficiency and the output voltage generated in terms of arithmetic progression. When it comes to positive-output super-lift Luo converters, those that are operated in the first quadrant have a higher transfer voltage gain. Furthermore, these types of converters are still being studied for home and industrial applications. This converter's output voltage equation is as follows,

$$V_{\text{out}} = \frac{2 - D}{1 - D} V_{\text{in}}$$

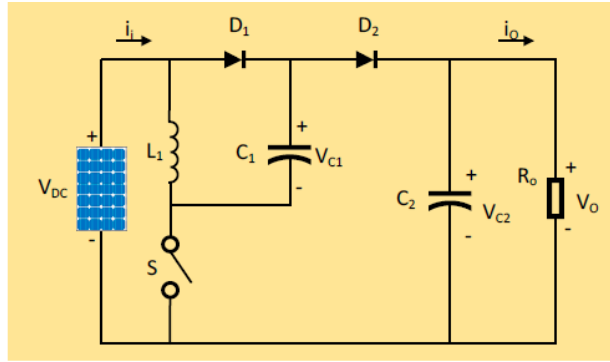


Figure 6.7: Super-Lift Luo converter for PV application

This super-lift technique was combined with series energy storage elements such as series capacitors and series inductors, which are responsible for higher voltages in the output resembling a higher geometric progression, and some modifications were made to the positive-output super-lift Luo converter, which now has a higher voltage transfer gain.

6.3.7 Ultra-Lift Luo Converter

The conversion of voltage transfer gain at the output of ultra-lift Luo converters, as shown in Fig. 6.8, is substantially higher. This converter's voltage transfer gain is the product of the voltage gains of buck-boost converter and the super-lift Luo converter. The output voltage equation of this converter is given by,

$$V_{\text{out}} = \frac{D(2 - D)}{(1 - D)^2} V_{\text{in}}$$

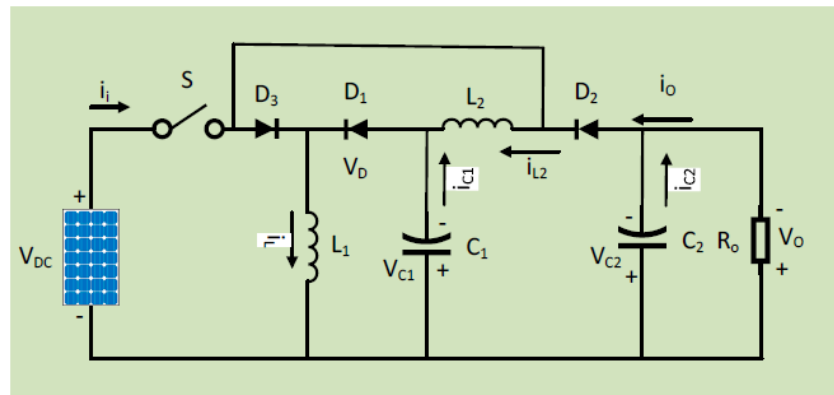


Figure 6.8: Ultra-Lift Luo converter for PV application

The closed-loop controller is difficult to design since the output voltage is believed to be the greatest value, with tiny fluctuations in the duty ratio produced. This converter's efficiency is expected to be the greatest among all non-isolated DC-DC converters.

6.4 Comparison of Gains of Non-Isolated Converters

Table 6.1: Converter's Gain comparison for different duty cycle (D)

Converters	Gain $\left(\frac{V_{out}}{V_{in}}\right)$	Duty Cycle (D)					
		0.2	0.33	0.5	0.67	0.8	0.9
Boost	$\frac{1}{1-D}$	1.25	1.5	2	3	5	10
Buck-Boost	$\frac{D}{1-D}$	0.25	0.5	1	2	4	9
Cuk	$\frac{D}{1-D}$	0.25	0.5	1	2	4	9
SEPIC	$\frac{D}{1-D}$	0.25	0.5	1	2	4	9
Zeta	$\frac{D}{1-D}$	0.25	0.5	1	2	4	9
Super-Lift Luo	$\frac{2-D}{1-D}$	2.25	2.5	3	4	6	11
Ultra-Lift Luo	$\frac{D(2-D)}{(1-D)^2}$	0.56	1.25	3	8	24	99

The above table compares the gain of different non-isolated DC-DC converters based on duty cycle. For less duty cycle, we can see that the Boost and Super-lift Luo converter has maximum gains whereas as duty cycle increases, the Ultra-lift Luo converters gain increases.

Since the formula of gain is same for Buck-Boost, Cuk, SEPIC and Zeta, it was obvious to obtain the same Gain value for the corresponding duty ratios of these converters.

6.5 Designing of Boost Converter

Given $P_o = 10000 \text{ W} @ V_o = 500 \text{ V}$

$$\text{From this, } R = \frac{V_o^2}{P_o} = 25 \Omega \text{ and } I_o = \frac{P_o}{V_o} = 20 \text{ A}$$

Assuming, $\Delta I_L = 5\% \text{ of } I_o = 1 \text{ A}$ and $\Delta V_o = 1\% \text{ of } V_o = 0.5 \text{ V}$

Let the Switching frequency $f_s = 10 \text{ KHz}$

$$V_{in} = 200 \text{ V and } V_o = 500 \text{ V} \quad \text{hence, } D = \frac{V_o - V_{in}}{V_o} = 0.6 = 60\%$$

Calculating L and C values:

$$L = \frac{DV_{in}}{\Delta I_L f_s} = 12 \text{ mH} \quad C = \frac{DI_o}{\Delta V_o f_s} = 2400 \mu\text{F}$$

Checking whether converter is in CCM or DCM:

$$L_{min} = \frac{D \cdot (1 - D)^2 R}{2f_s} = 0.12 \text{ mH} \quad C_{min} = \frac{D}{2f_s R} = 1.2 \mu\text{F}$$

Since the obtained values of L and C are greater than the critical values, the converter is working in **Continuous Conduction Mode**.

Similarly, Design Specification of all other converters are obtained from their design equations and are mentioned in the Table 6.2.

Table 6.2: Design Specification of DC-DC Converters

Elements Converters	L₁ (mH)	L₂ (mH)	C₁ (μF)	C₂ (μF)	R (Ω)
Boost	12	-	-	2400	25
Buck-Boost	14.3	-	-	2900	25
Cuk	14.3	14.3	571.43	25	25
SEPIC	14.3	14.3	571.43	2900	25
Zeta	14.3	14.3	571.43	25	25
Super-Lift Luo	6.7	-	2700	2700	25
Ultra-Lift Luo	9.3	17.4	696.67	1900	25

The design values of the various converters used in the simulations is tabulated in the Table 6.2. C_2 is the output capacitor to reduce the ripple content in the output voltage. R is the load resistor. L_1 and L_2 are the inductance value. Some converters use only one inductor whereas some converters require two inductors. Similarly, some converters need two capacitors for their operation.

Chapter - 7

SIMULATION IN MATLAB/SIMULINK

- **Introduction**
- **Simulink Model of Stand-Alone PV System**
- **Simulation Results and Discussions**

Chapter - 7

7.1 Introduction

In Stand-Alone PV (SAPV) System, the battery is crucial for power flow management if the load demands a constant voltage. However, in some applications like heating, cooking and water pumping system where the change in the load voltage will not affect the reliability of the system, the battery is not needed. In those applications, the battery is not applied to reduce cost, frequent maintenance and environmental issues caused by battery usages. The main objective of the system is to obtain power from the PV array as much as possible without having to regulate the output voltage and current. As per maximum power transfer theorem, maximum power is transferred to the load when equivalent load resistance referred to the input terminals of the converter (R_{in}) is match to the internal resistance of PV array at MPP (R_{MPP}). Fig. 7.1 shows such a system.

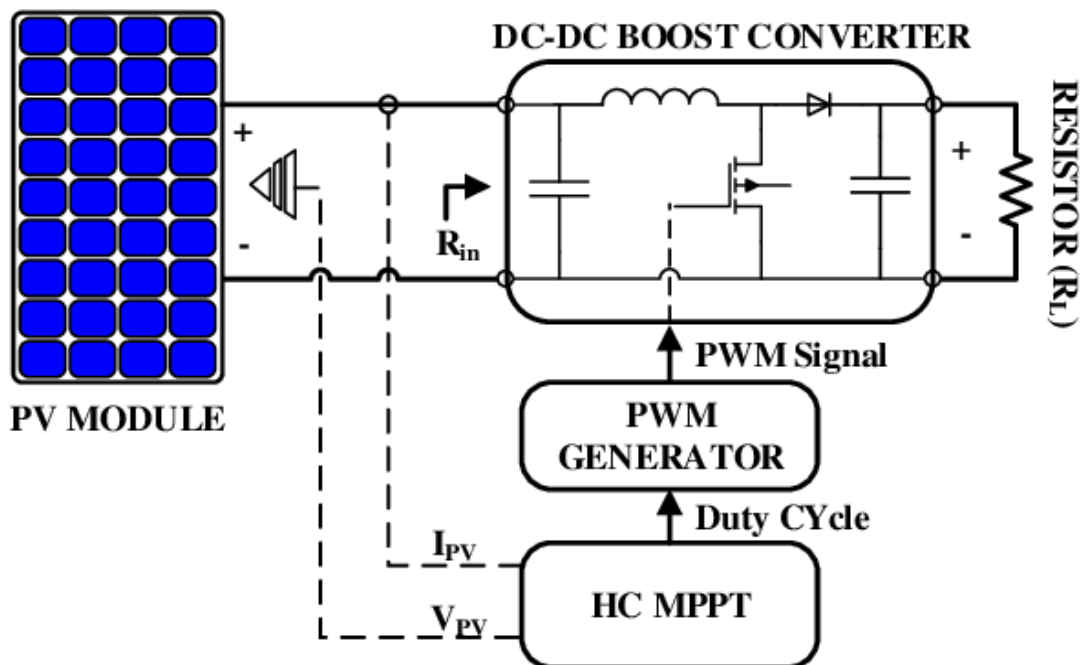


Figure 7.1: Block diagram of MPPT Stand-Slone PV system with load resistor

A maximum power point (MPPT) is used for extracting the maximum power from the solar panel and transferring maximum power from the PV module to the load. A DC-DC converter which interface between load and module, serve the purpose of transferring maximum power from PV module to the load. By changing the duty cycle the load

impedance as seen by the source is varied and matched at the point of the peak power with the source so as to transfer the maximum power. DC-DC converters are used in applications where an average output voltage is required, which can be higher or lower than the input voltage.

7.2 Simulink Model of Stand-Alone PV System

The simulation was run for 1 second for different partial shading conditions.

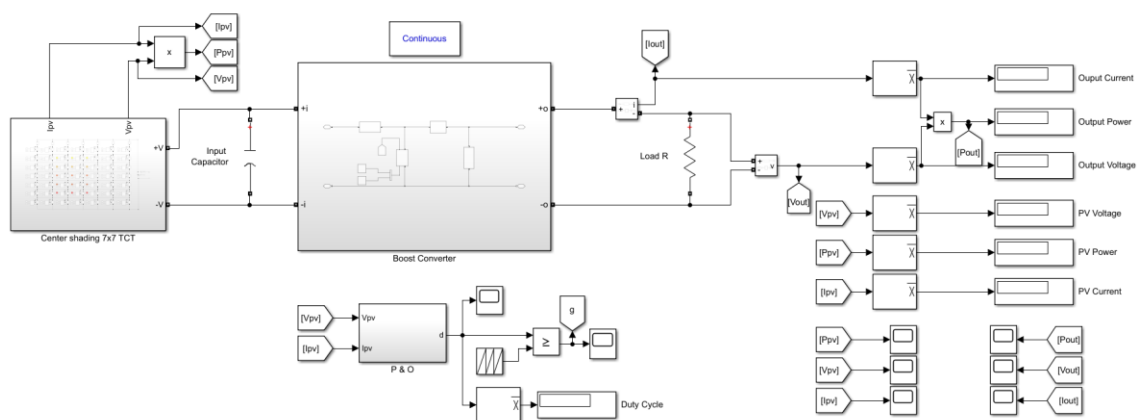


Figure 7.2: Simulink Model of Boost Converter with center shading on TCT PV Array

The Fig. 7.2 shows Simulink Model of Stand-Alone PV System which contains:

- A 7x7 TCT configured PV Array (using Kyocera KC200GT PV Modules)
- An intermediate DC-DC converter (Boost converter, in this case)
- MPPT Technique (Perturbation and Observation MPPT Technique)

Similarly, different converters such as Buck-Boost, Cuk, SEPIC, Zeta, Super-Lift Luo and Ultra-Lift Luo converters were used as an intermediate converter and were simulated using the design specification as specified in Table 6.2 in place of boost converter to compare the results of the MPPT for different Partial Shading Conditions (PSCs) mentioned in the Chapter - 4.

Various waveforms for each converter were obtained from the simulations results under different partial shading scenarios such as converter's output voltage, current and power. Converter's input parameter is nothing but the PV Voltage and PV current were also obtained and are available in the upcoming section.

7.3 Simulation Results and Discussions

7.3.1 Boost Converter Waveforms

7.3.1.1 Under center shading scenario

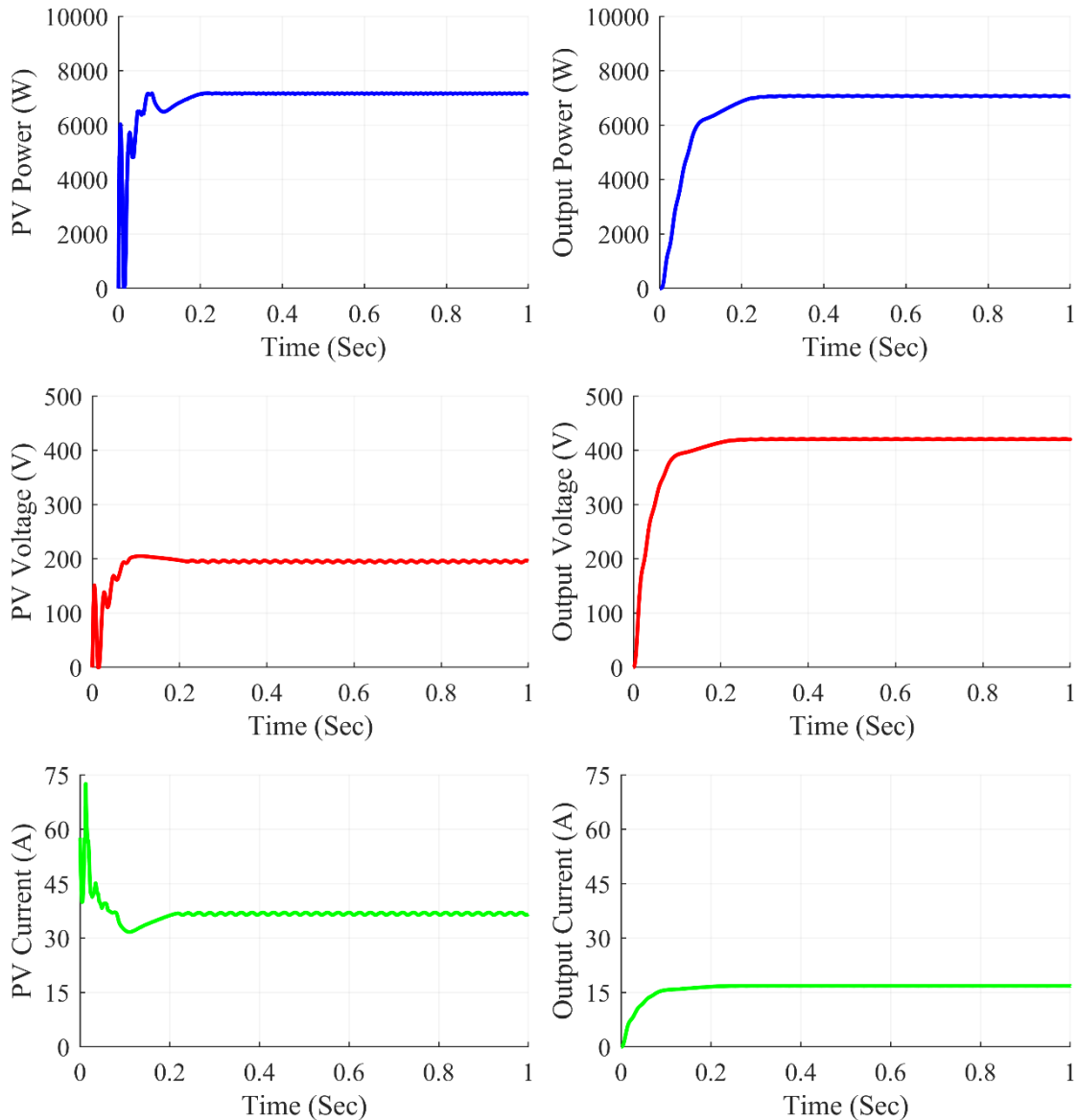


Figure 7.3: Boost converter waveforms under center shading condition

The Fig. 7.3 shows Boost Converter waveforms under center shading condition. At steady state, we can see that the converter gives average output power of 7063 W, the average output voltage at 420.2 V and the average output current of 16.81 A. The average value of PV power was at 7171 W and the PV current and PV voltage were at 195.8 V and 36.63 A respectively.

7.3.1.2 Under corner shading scenario

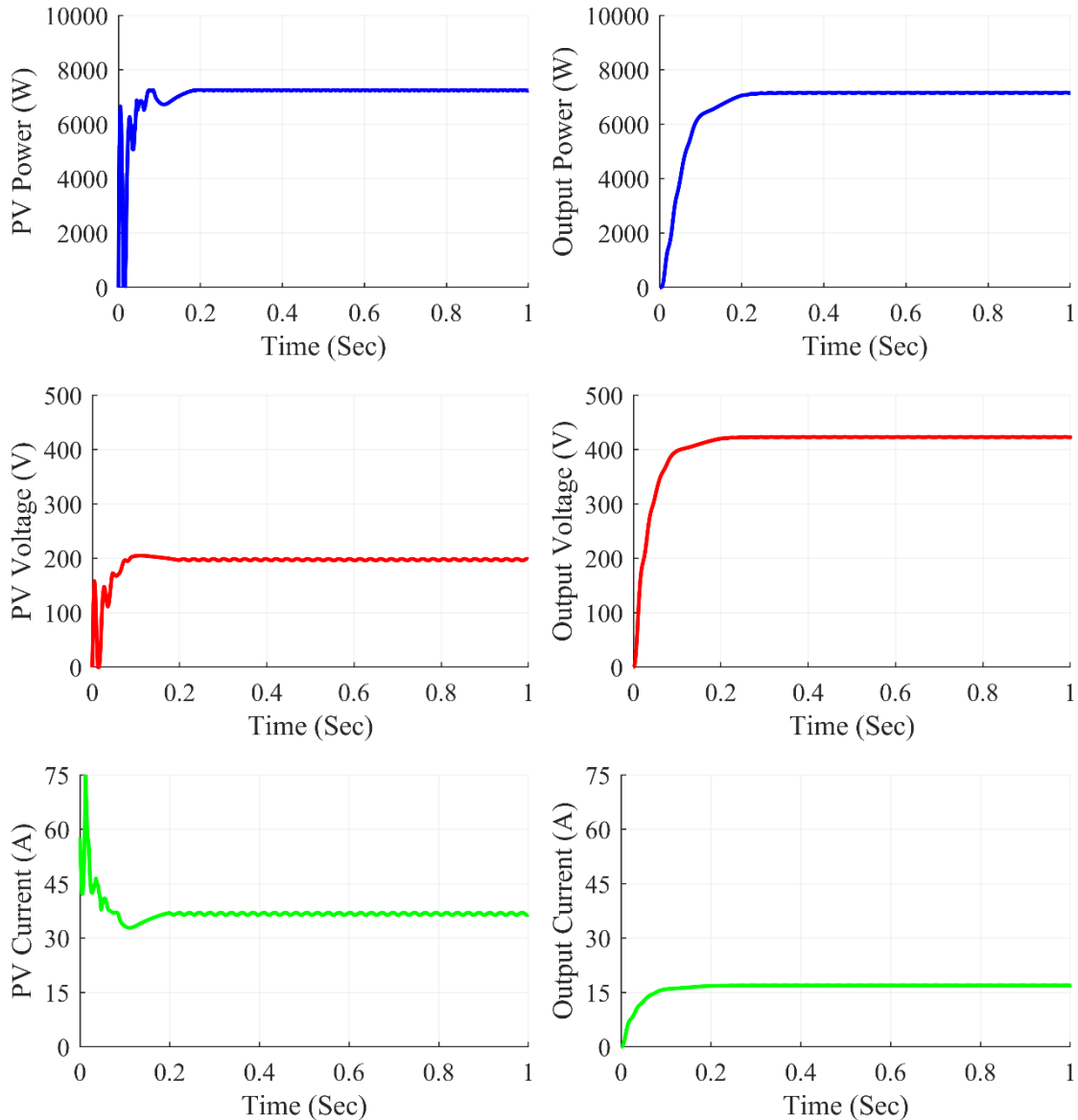


Figure 7.4: Boost converter waveforms under corner shading condition

The Fig. 7.4 shows Boost Converter waveforms under corner shading condition. At steady state, we can see that the converter gives average output power of 7144 W, the average output voltage at 422.6 V and the average output current of 16.9 A. The average value of PV power was at 7240 W and the PV current and PV voltage were at 198.7 V and 36.43 A respectively.

7.3.1.3 Under diagonal shading scenario

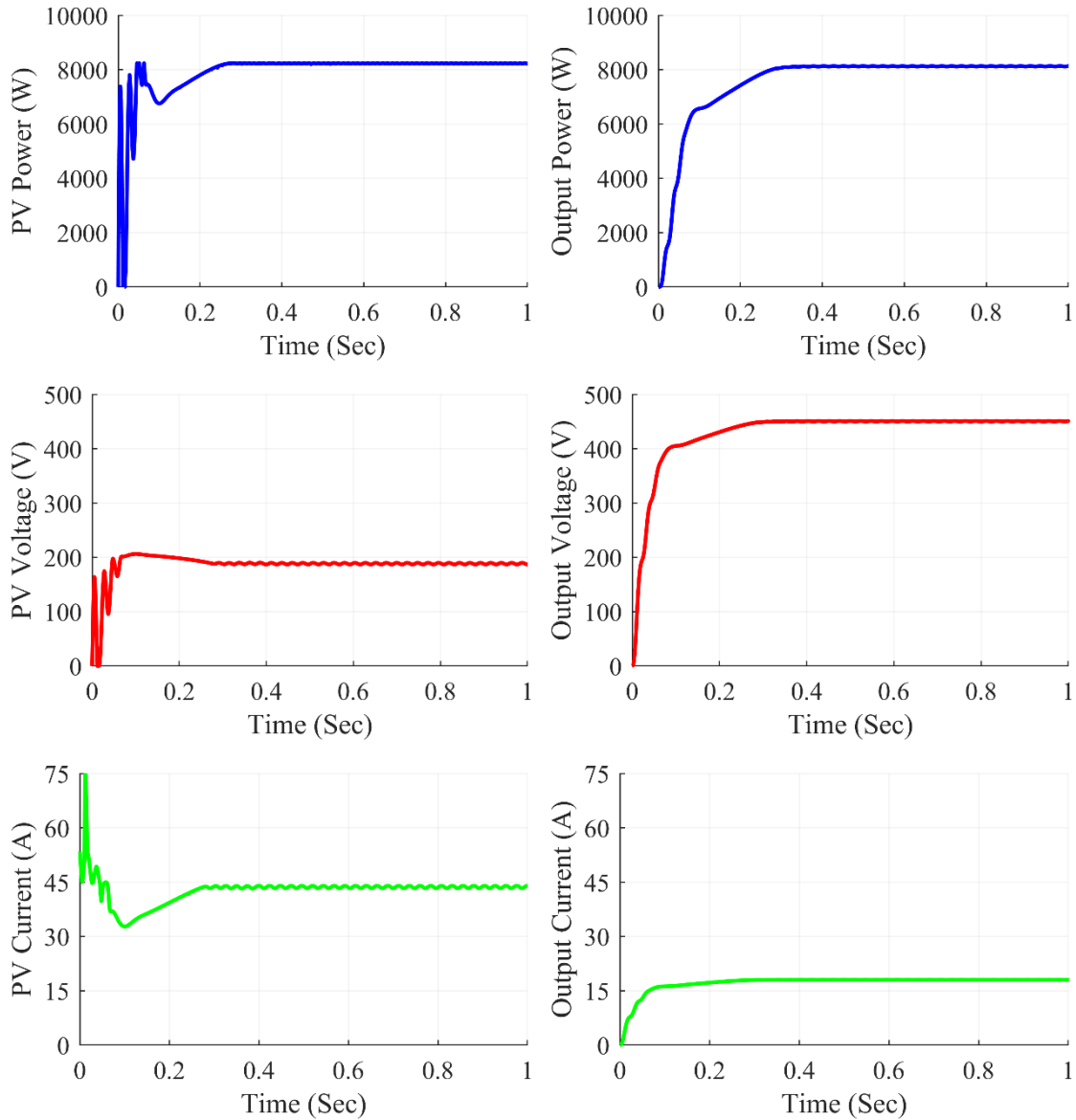


Figure 7.5: Boost converter waveforms under diagonal shading condition

The Fig. 7.5 shows Boost Converter waveforms under diagonal shading condition.

At steady state, we can see that the converter gives average output power of 8130 W, the average output voltage at 450.8 V and the average output current of 18.03 A. The average value of PV power was at 8224 W and the PV current and PV voltage were at 186.8 V and 44.02 A respectively.

7.3.1.4 Under frame shading scenario

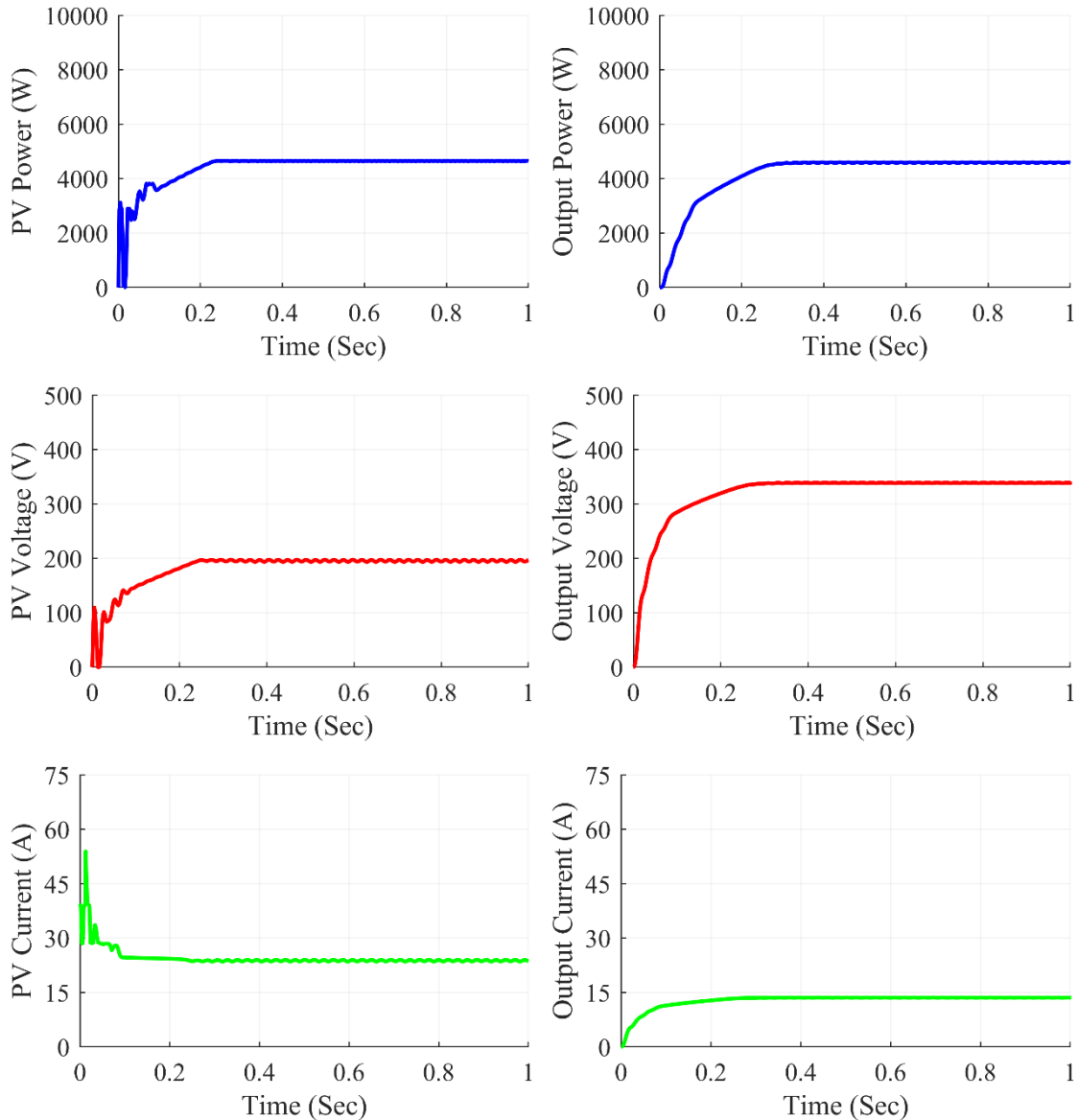


Figure 7.6: Boost converter waveforms under frame shading condition

The Fig. 7.6 shows Boost Converter waveforms under frame shading condition. At steady state, we can see that the converter gives average output power of 4582 W, the average output voltage at 338.4 V and the average output current of 13.54 A. The average value of PV power was at 4582 W and the PV current and PV voltage were at 197.0 V and 23.57 A respectively.

7.3.1.5 Under random shading scenario

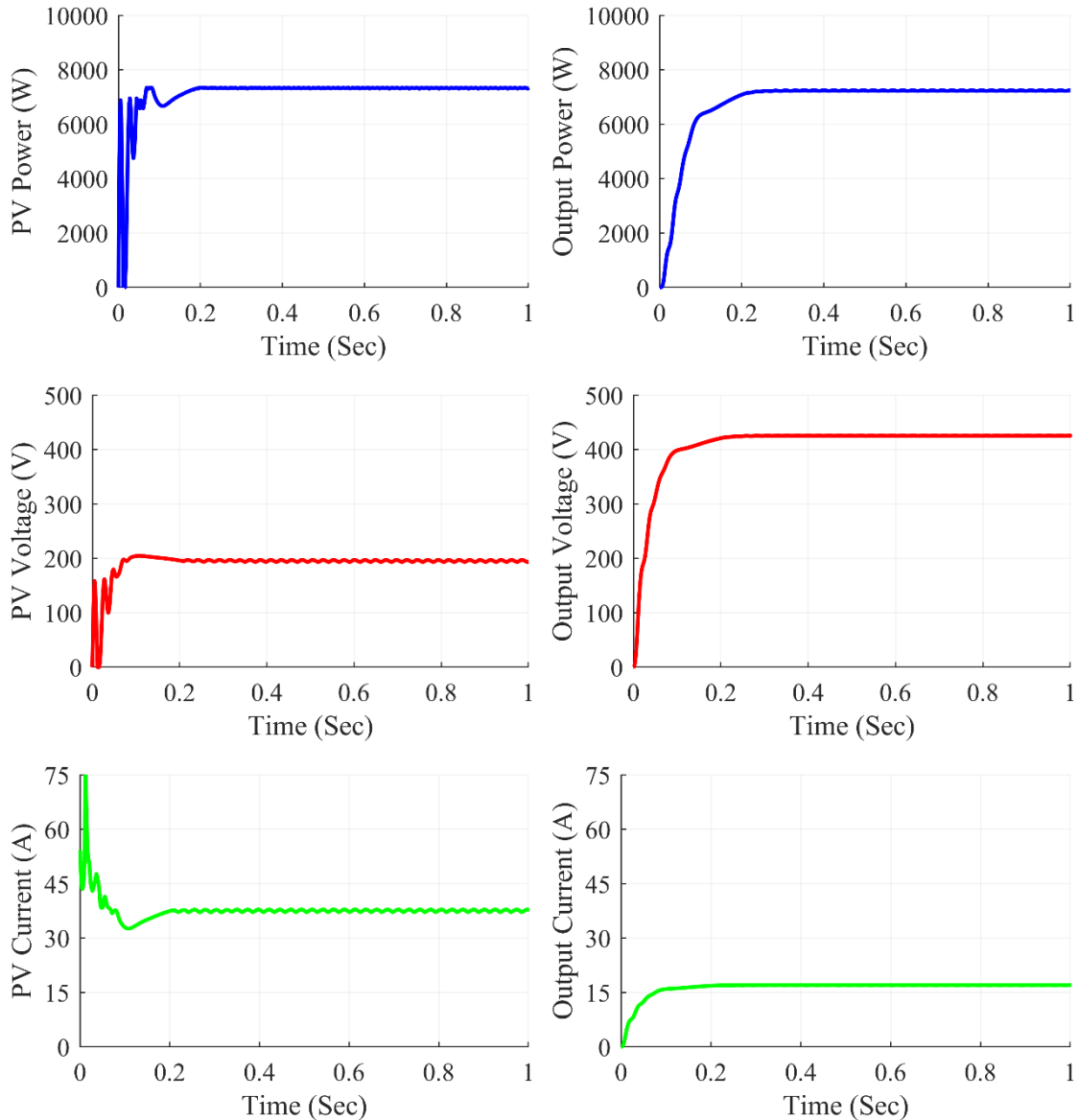


Figure 7.7: Boost converter waveforms under random shading condition

The Fig. 7.7 shows Boost Converter waveforms under random shading condition. At steady state, we can see that the converter gives average output power of 7245 W, the average output voltage at 425.6V and the average output current of 17.02 A. The average value of PV power was at 7322 W and the PV current and PV voltage were at 193.7 V and 37.80 A respectively.

7.3.1.6 Under right side end shading scenario

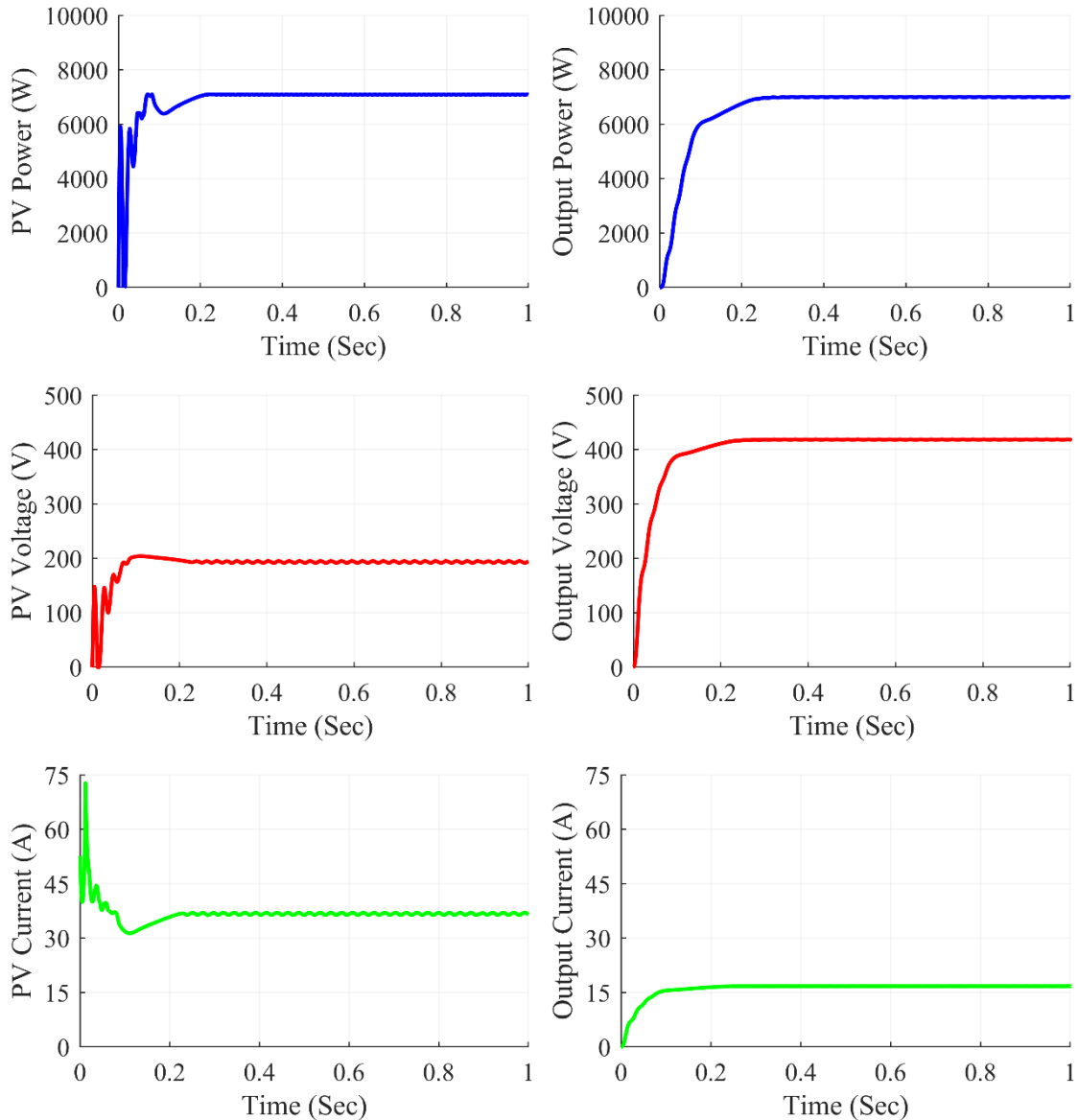


Figure 7.8: Boost converter waveforms under right side end shading condition

The Fig. 7.8 shows Boost Converter waveforms under right side end shading condition. At steady state, we can see that the converter gives average output power of 6998 W, the average output voltage at 418.3 V and the average output current of 16.73 A. The average value of PV power was at 7090 W and the PV current and PV voltage were at 194.4V and 36.47 A respectively.

7.3.1.7 Under uniform shading scenario

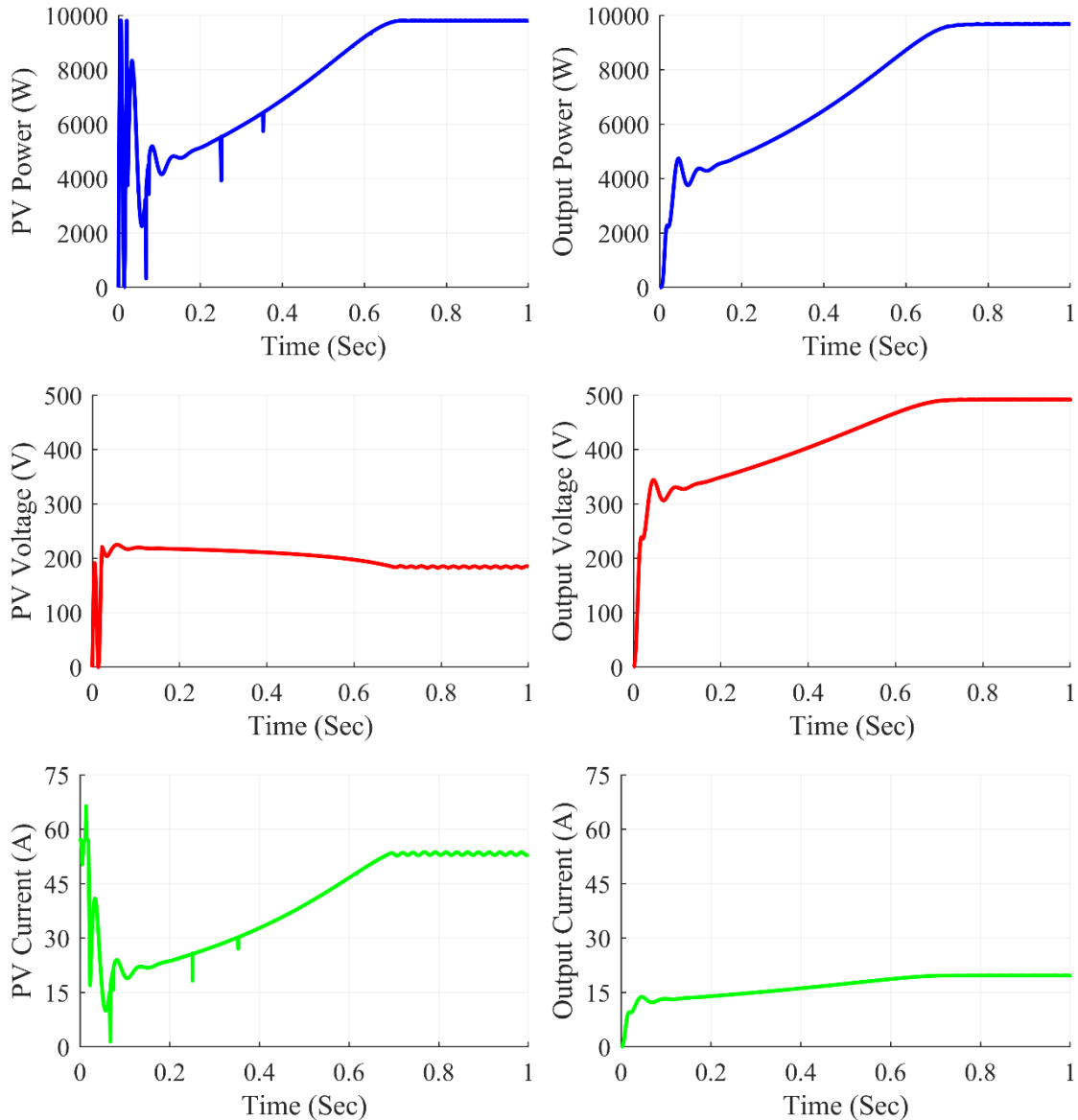


Figure 7.9: Boost converter waveforms under uniform shading condition

The Fig. 7.9 shows Boost Converter waveforms under uniform shading condition. At steady state, we can see that the converter gives average output power of 9683 W, the average output voltage at 492.0 V and the average output current of 19.68 A. The average value of PV power was at 9792 W and the PV current and PV voltage were at 186.4 V and 52.53 A respectively.

Table 7.1: Boost Converter Observations

Shading Conditions	PV Voltage (V_{PV})	PV Current (I_{PV})	PV Power (P_{PV})	Output Voltage (V_{out})	Output Current (I_{out})	Output Power (P_{out})	Duty Cycle (D)
Centre	195.8	36.63	7171	420.2	16.81	7063	0.537
Corner	198.7	36.43	7240	422.6	16.9	7144	0.533
Diagonal	186.8	44.02	8224	450.8	18.03	8130	0.583
Frame	197.0	23.57	4643	338.4	13.54	4582	0.421
Random	193.7	37.80	7322	425.6	17.02	7245	0.541
Right Side	194.4	36.47	7090	418.3	16.73	6998	0.535
Uniform	186.4	52.53	9792	492.0	19.68	9683	0.622

The results of the simulation are summarized in Table 7.1 for Boost converter. On the 7x7 TCT PV array design, various partial shading situations were produced, which fed power into the Boost converter in such a way that maximum power extraction from the PV array was achieved using the P&O method. The results were reasonably accurate and matched the expected value. The boost converter worked with a duty ratio ranging from 0.421 to 0.622 for frame shading to uniform shading respectively.

7.3.2 Buck-Boost Converter Waveforms

7.3.2.1 Under center shading scenario

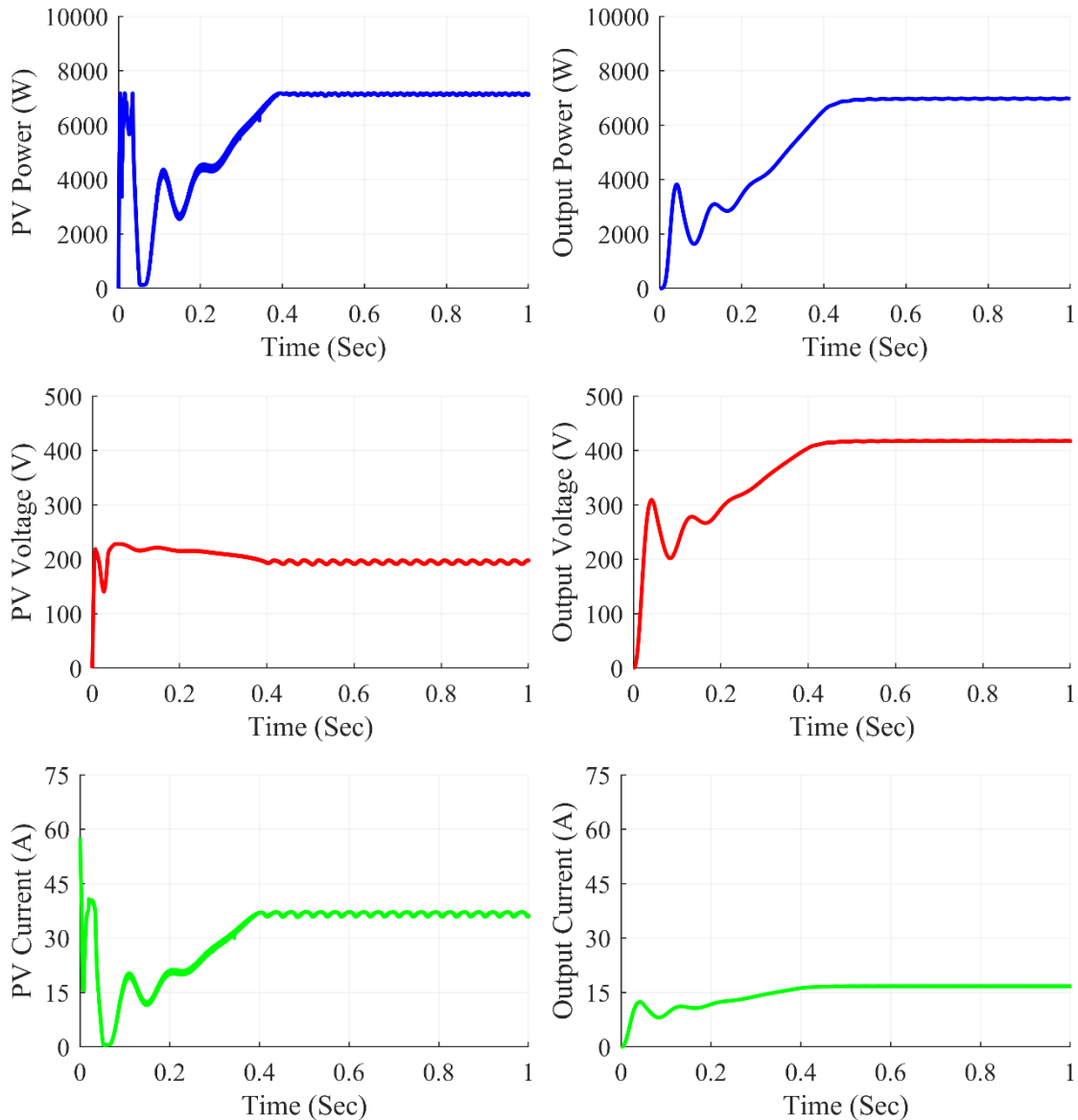


Figure 7.10: Buck-Boost converter waveforms under center shading condition

The Fig. 7.10 shows Buck-Boost Converter waveforms under center shading condition. At steady state, we can see that the converter gives average output power of 6970 W, the average output voltage at 417.4 V and the average output current of 16.7 A. The average value of PV power was at 7130 W and the PV current and PV voltage were at 197.7 V and 36.07 A respectively.

7.3.2.2 Under corner shading scenario

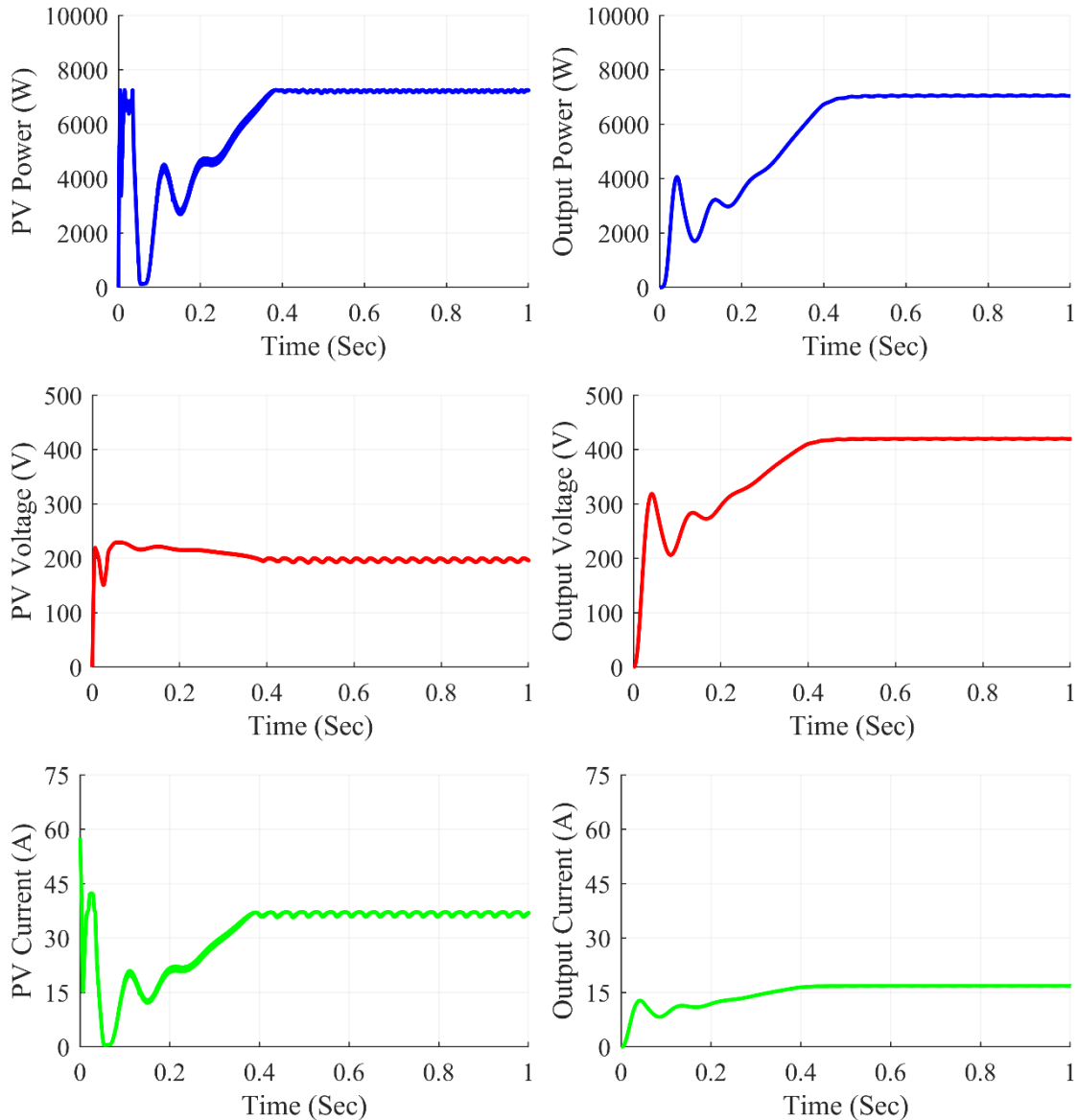


Figure 7.11: Buck-Boost converter waveforms under corner shading condition

The Fig. 7.11 shows Buck-Boost Converter waveforms under corner shading condition. At steady state, we can see that the converter gives average output power of 7036 W, the average output voltage at 419.4 V and the average output current of 16.78 A. The average value of PV power was at 7248 W and the PV current and PV voltage were at 36.95 A and 196.1 V respectively.

7.3.2.3 Under diagonal shading scenario

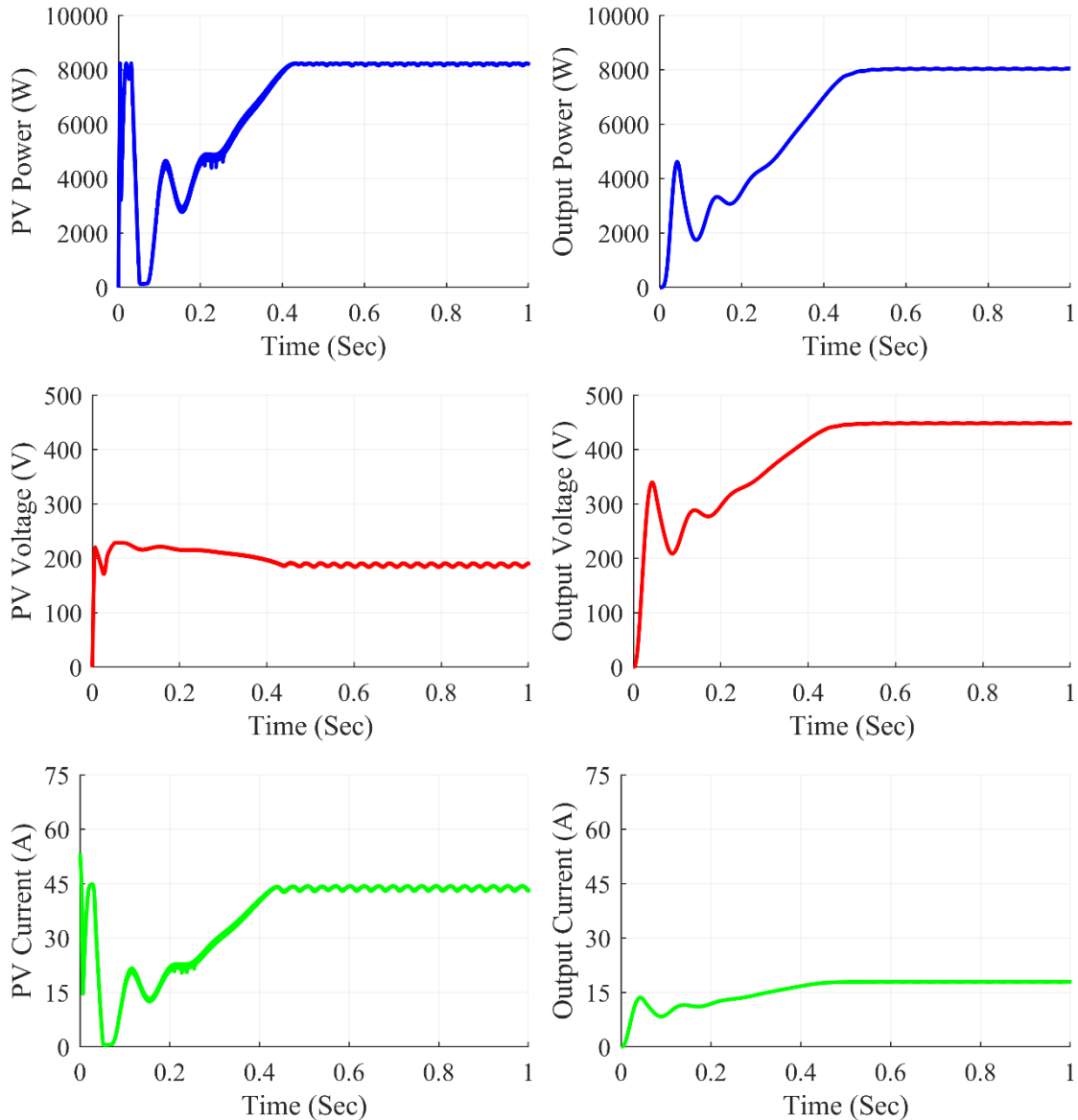


Figure 7.12: Buck-Boost converter waveforms under diagonal shading condition

The Fig. 7.12 shows Buck-Boost Converter waveforms under diagonal shading condition. At steady state, we can see that the converter gives average output power of 8039 W, the average output voltage at 448.3 V and the average output current of 17.93 A. The average value of PV power was at 8218 W and the PV current and PV voltage were at 190.5 V and 43.15 A respectively.

7.3.2.4 Under frame shading scenario

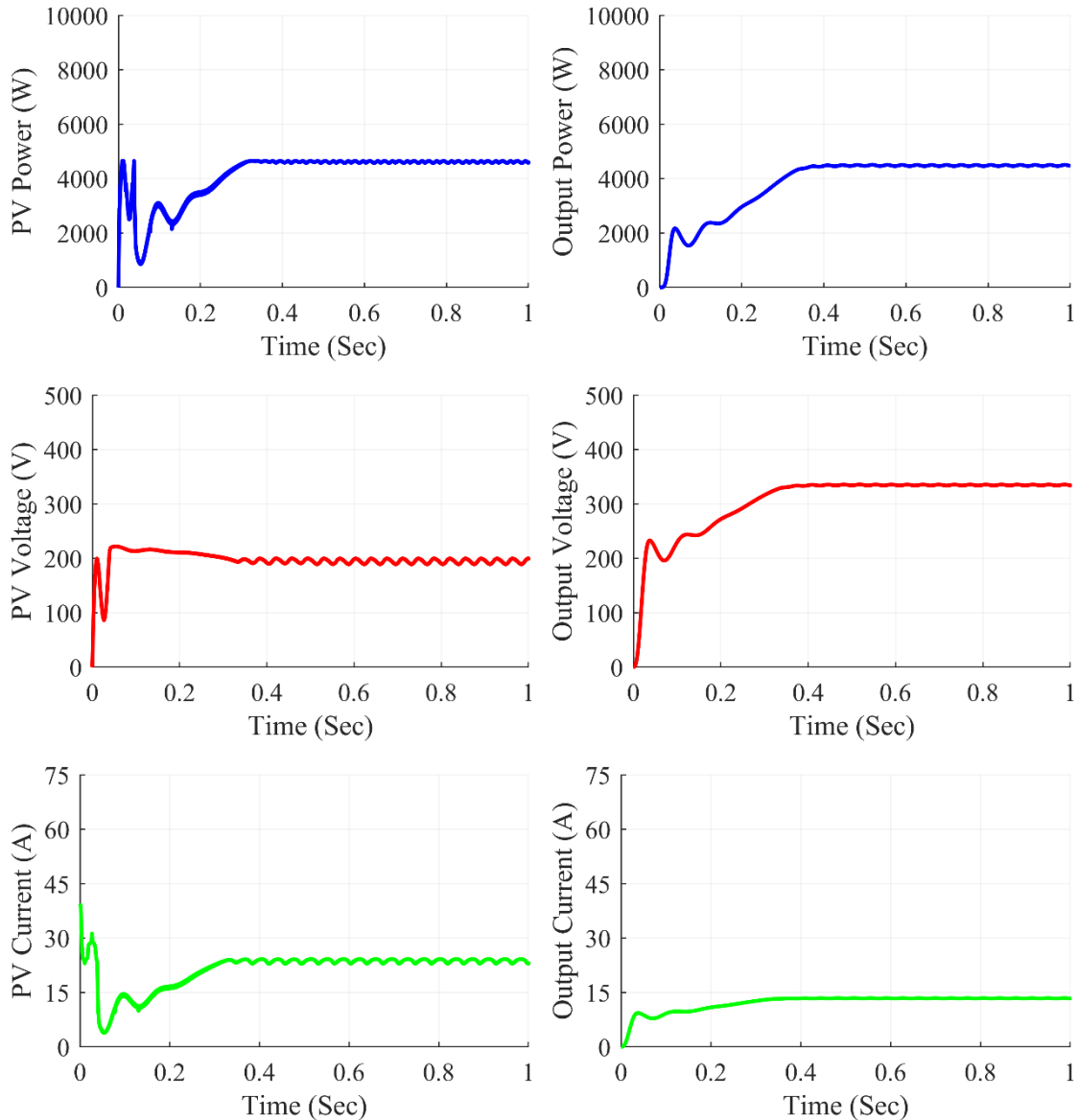


Figure 7.13: Buck-Boost converter waveforms under frame shading condition

The Fig. 7.13 shows Buck-Boost Converter waveforms under frame shading condition. At steady state, we can see that the converter gives average output power of 4466 W, the average output voltage at 334.1 V and the average output current of 13.37 A. The average value of PV power was at 4592 W and the PV current and PV voltage were at 199.3 V and 23.04 A respectively.

7.3.2.5 Under random shading scenario

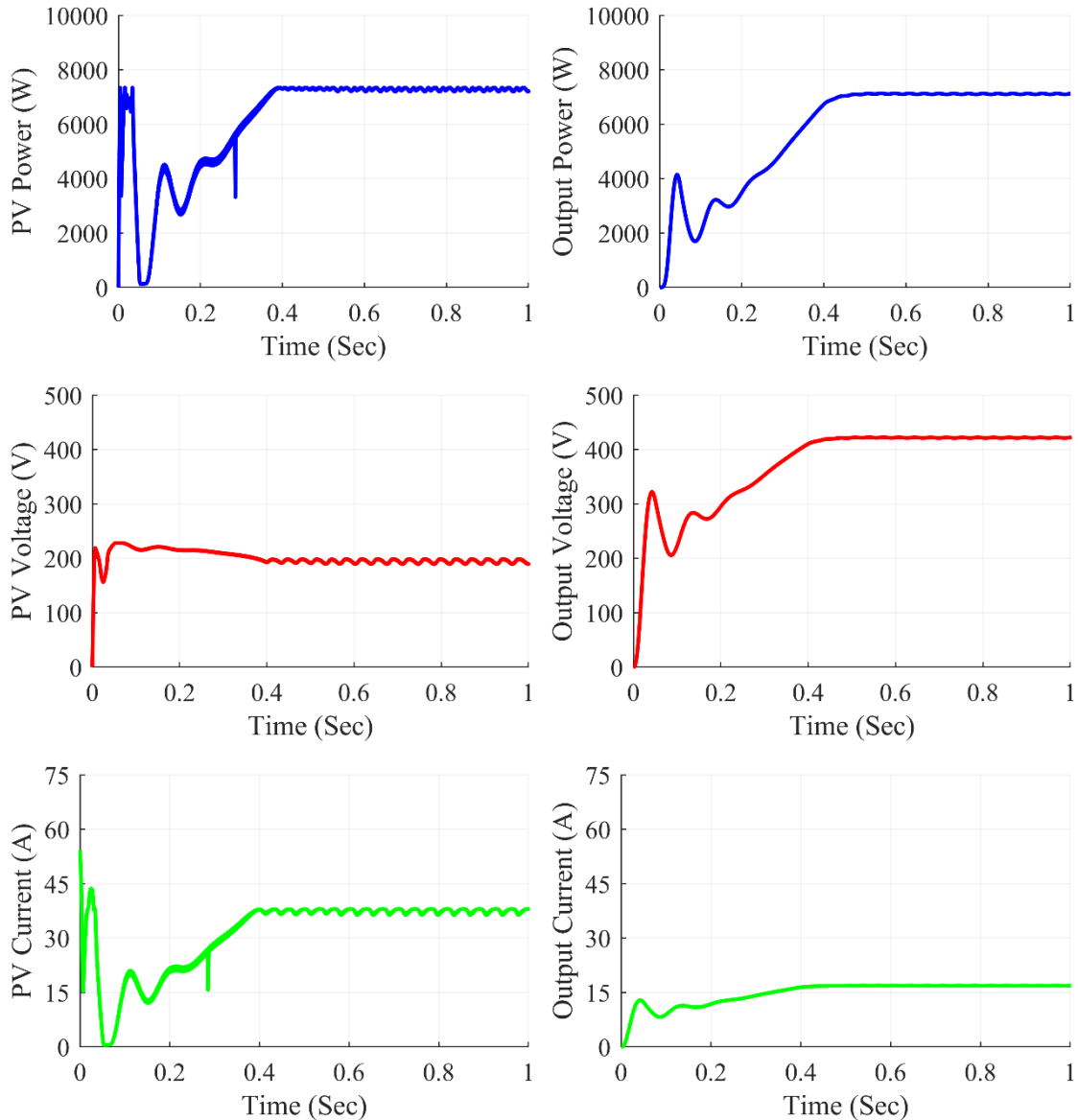


Figure 7.14: Buck-Boost converter waveforms under random shading condition

The Fig. 7.14 shows Buck-Boost Converter waveforms under random shading condition. At steady state, we can see that the converter gives average output power of 7126 W, the average output voltage at 422.1V and the average output current of 16.88 A. The average value of PV power was at 7216 W and the PV current and PV voltage were at 189.8 V and 38.02 A respectively.

7.3.2.6 Under right side end shading scenario

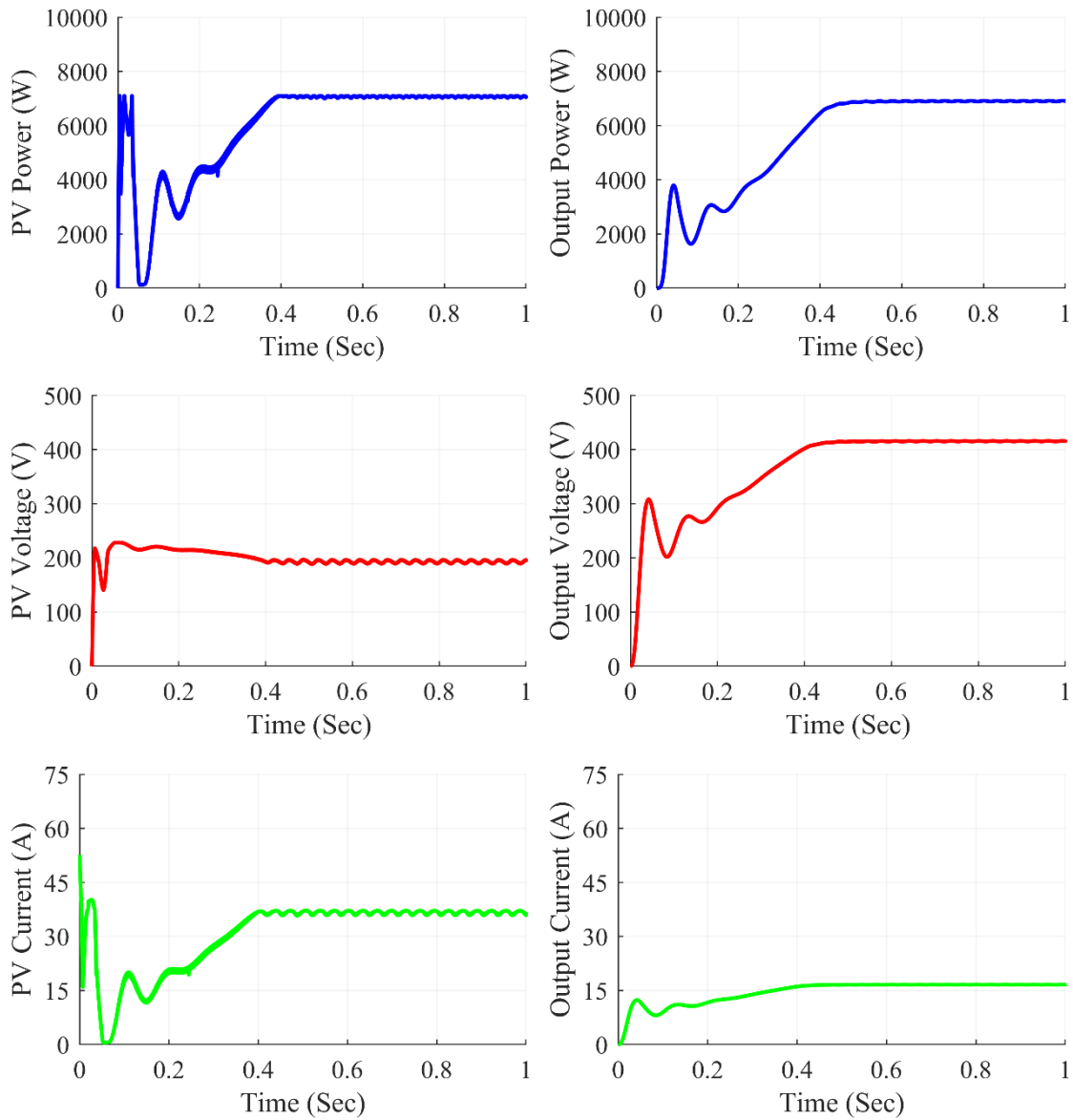


Figure 7.15: Buck-Boost converter waveforms under right side end shading condition

The Fig. 7.15 shows Buck-Boost Converter waveforms under right side end shading condition. At steady state, we can see that the converter gives average output power of 6904 W, the average output voltage at 415.5 V and the average output current of 16.62 A. The average value of PV power was at 7059 W and the PV current and PV voltage were at 36.07 A and 195.7V respectively.

7.3.2.7 Under uniform shading scenario

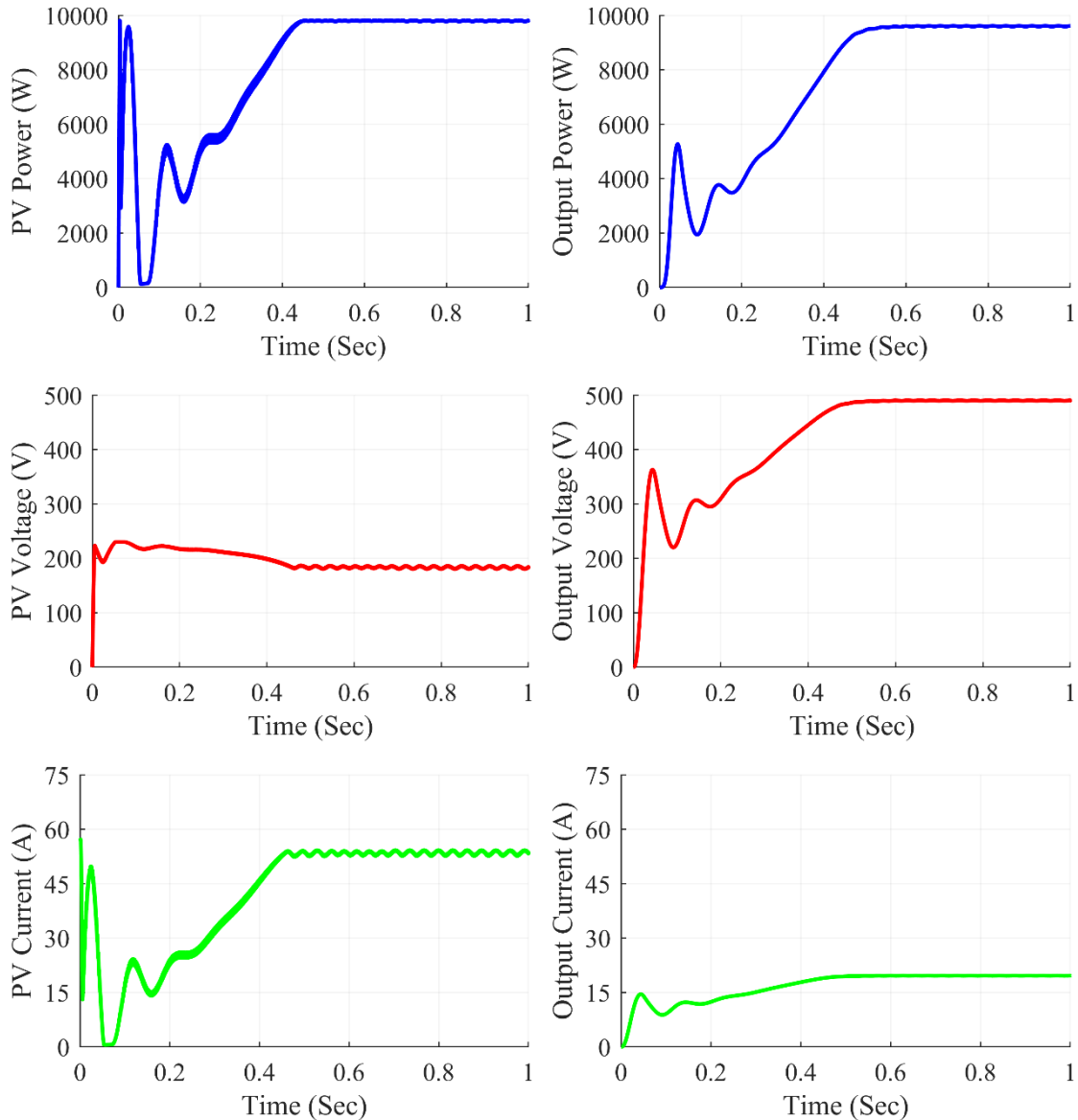


Figure 7.16: Buck-Boost converter waveforms under uniform shading condition

The Fig. 7.16 shows Buck-Boost Converter waveforms under uniform shading condition. At steady state, we can see that the converter gives average output power of 9614 W, the average output voltage at 490.3 V and the average output current of 19.61 A. The average value of PV power was at 9805 W and the PV current and PV voltage were at 183.5 V and 53.43 A respectively.

Table 7.2: Buck-Boost Converter Observations

Shading Conditions	PV Voltage (V_{PV})	PV Current (I_{PV})	PV Power (P_{PV})	Output Voltage (V_{out})	Output Current (I_{out})	Output Power (P_{out})	Duty Cycle (D)
Centre	197.7	36.07	7130	417.4	16.7	6970	0.681
Corner	196.1	36.95	7248	419.4	16.78	7036	0.685
Diagonal	190.5	43.15	8218	448.3	17.93	8039	0.703
Frame	199.3	23.04	4592	334.1	13.37	4466	0.631
Random	189.8	38.02	7216	422.1	16.88	7126	0.685
Right Side	195.7	36.07	7059	415.5	16.62	6904	0.681
Uniform	183.5	53.43	9805	490.3	19.61	9614	0.725

The results of the simulation are summarized in Table 7.2. for Buck-Boost converter. On the 7x7 TCT PV array design, various partial shading situations were produced, which fed power into the Buck-Boost converter in such a way that maximum power extraction from the PV array was achieved using the P&O method. The results were reasonably accurate and matched the expected value. The Buck-Boost converter worked with a duty ratio ranging from 0.631 to 0.725 for frame shading to uniform shading respectively.

7.3.3 Cuk Converter Waveforms

7.3.3.1 Under center shading scenario

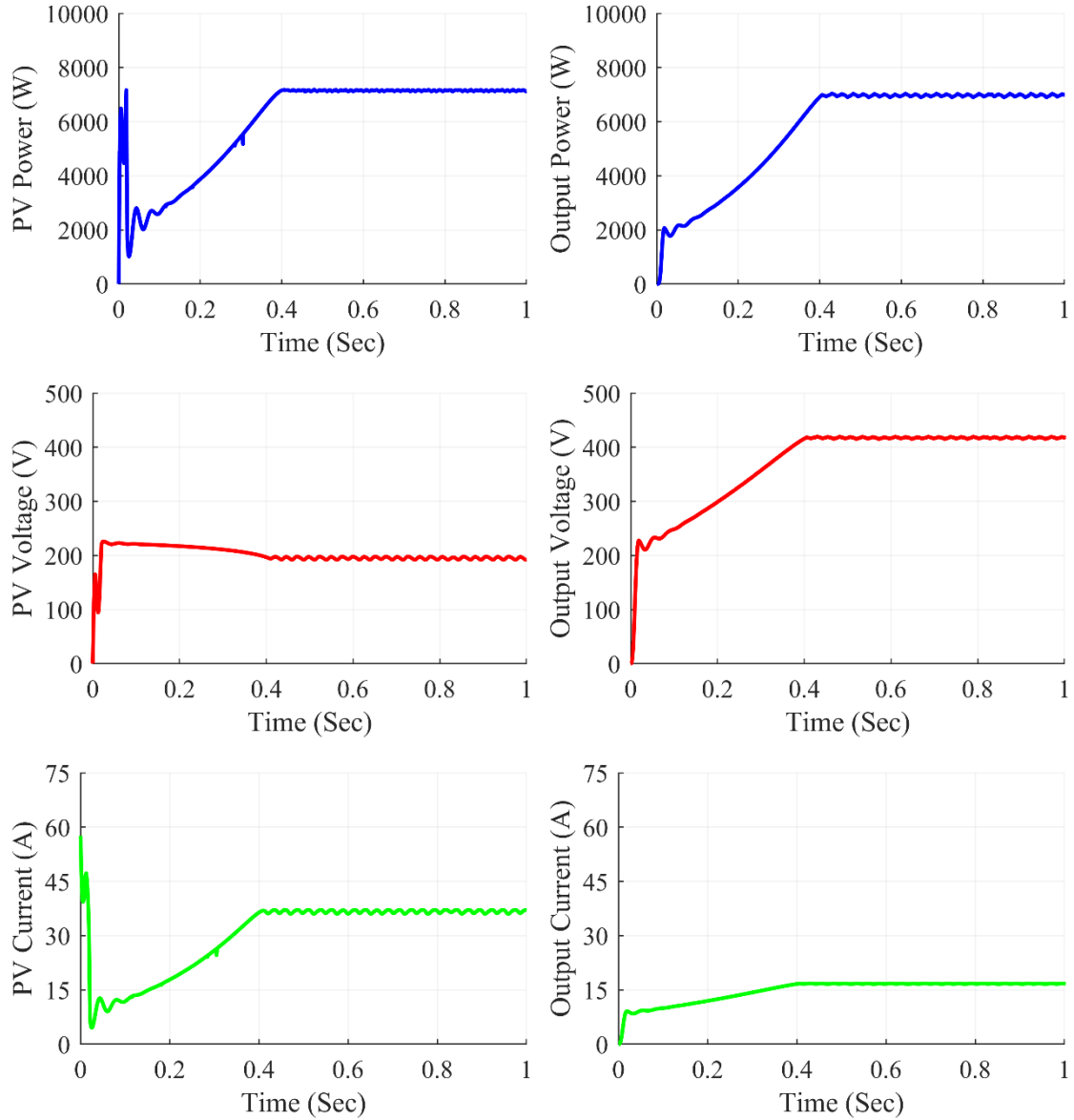


Figure 7.17: Cuk converter waveforms under center shading condition

The Fig. 7.17 shows Cuk Converter waveforms under center shading condition. At steady state, we can see that the converter gives average output power of 6988 W, the average output voltage at 418 V and the average output current of 16.72 A. The average value of PV power was at 7123 W and the PV current and PV voltage were at 192.1 V and 37.09 A respectively.

7.3.3.2 Under corner shading scenario

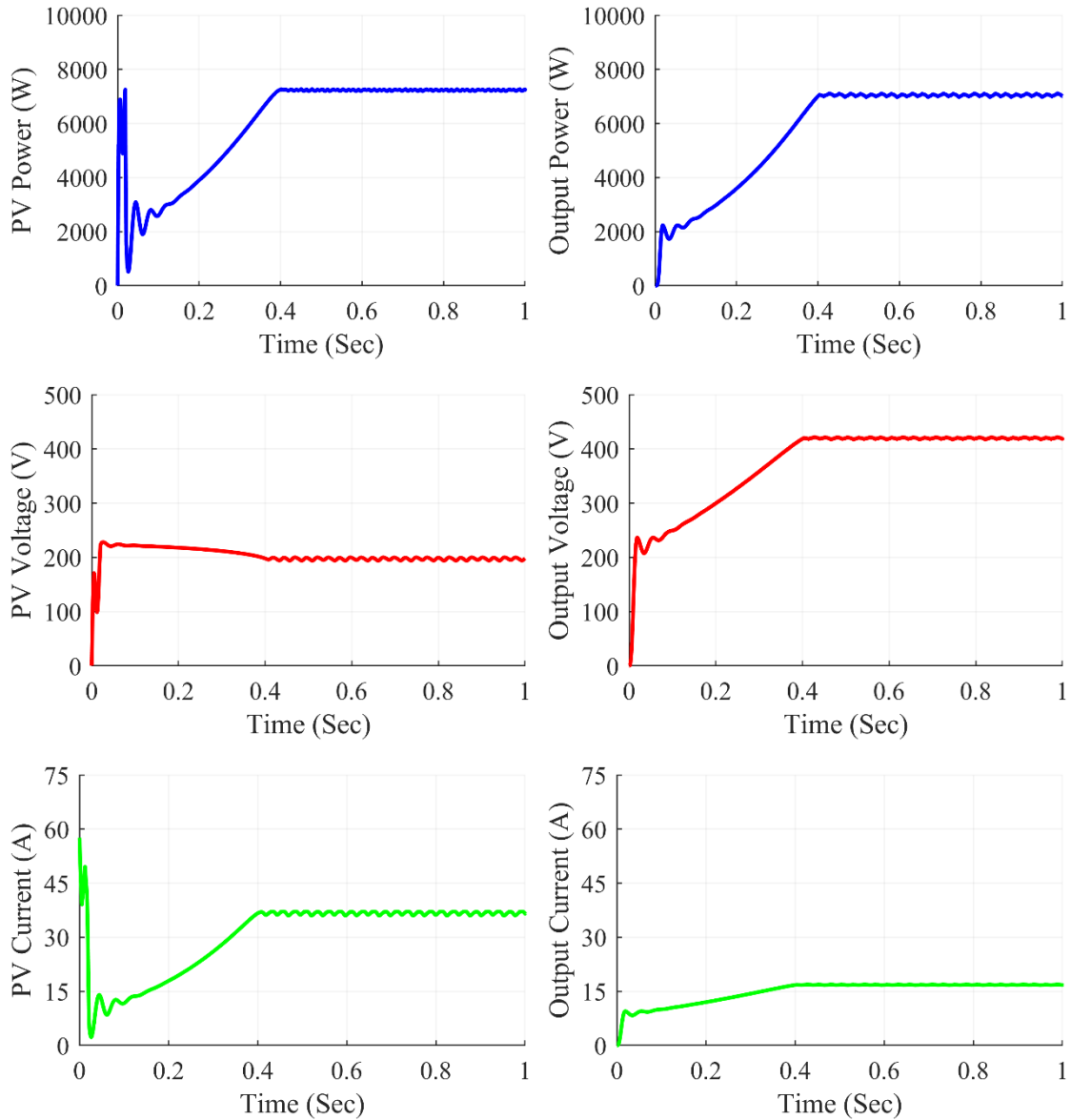


Figure 7.18: Cuk converter waveforms under corner shading condition

The Fig. 7.18 shows Cuk Converter waveforms under corner shading condition. At steady state, we can see that the converter gives average output power of 7005 W, the average output voltage at 418.5 V and the average output current of 16.74 A. The average value of PV power was at 7250 W and the PV current and PV voltage were at 198.2 V and 36.59 A respectively.

7.3.3.3 Under diagonal shading scenario

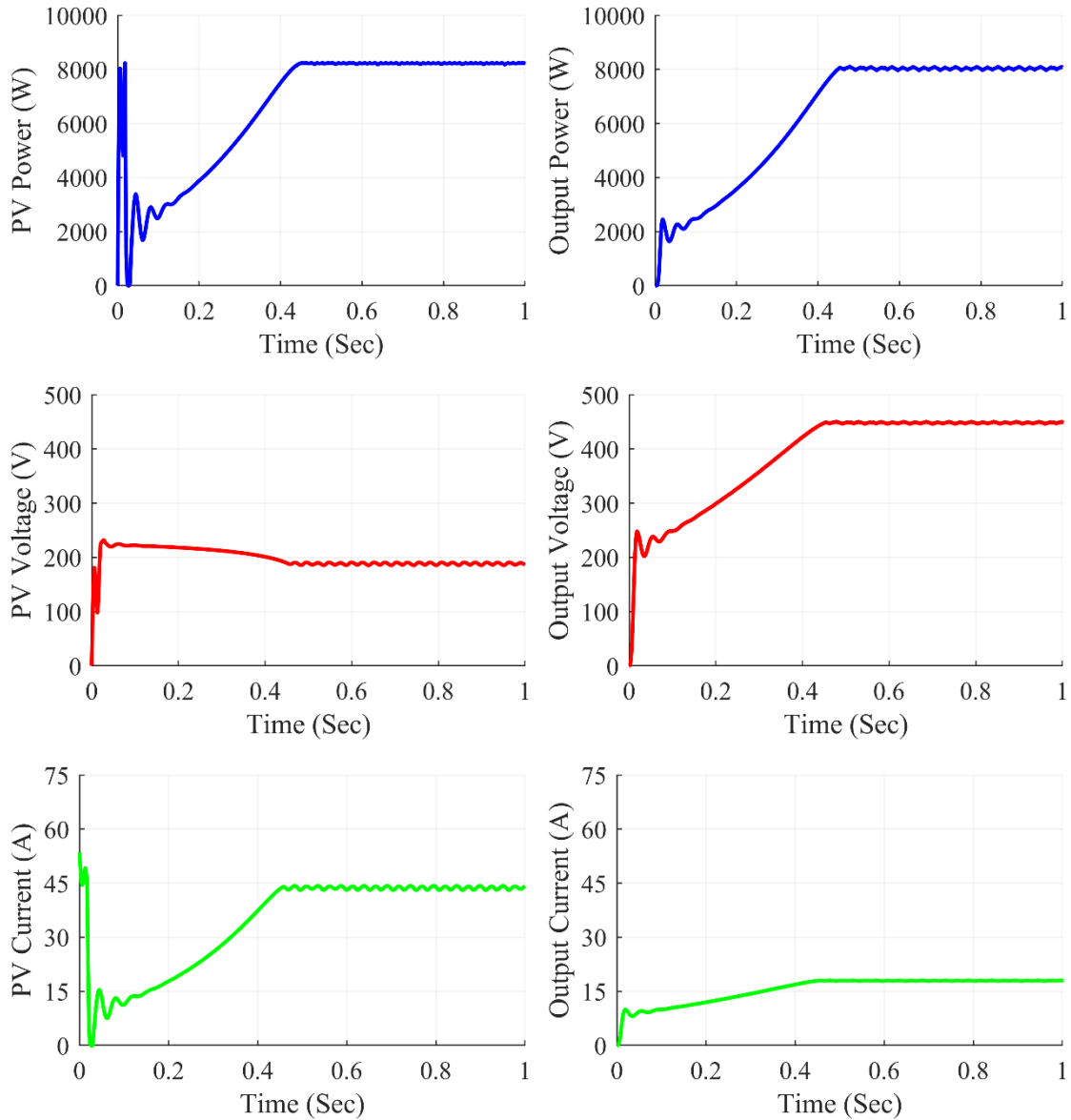


Figure 7.19: Cuk converter waveforms under diagonal shading condition

The Fig. 7.19 shows Cuk Converter waveforms under diagonal shading condition.

At steady state, we can see that the converter gives average output power of 8069 W, the average output voltage at 449.1 V and the average output current of 17.97 A. The average value of PV power was at 8211 W and the PV current and PV voltage were at 186.1 V and 44.12 A respectively.

7.3.2.4 Under frame shading scenario

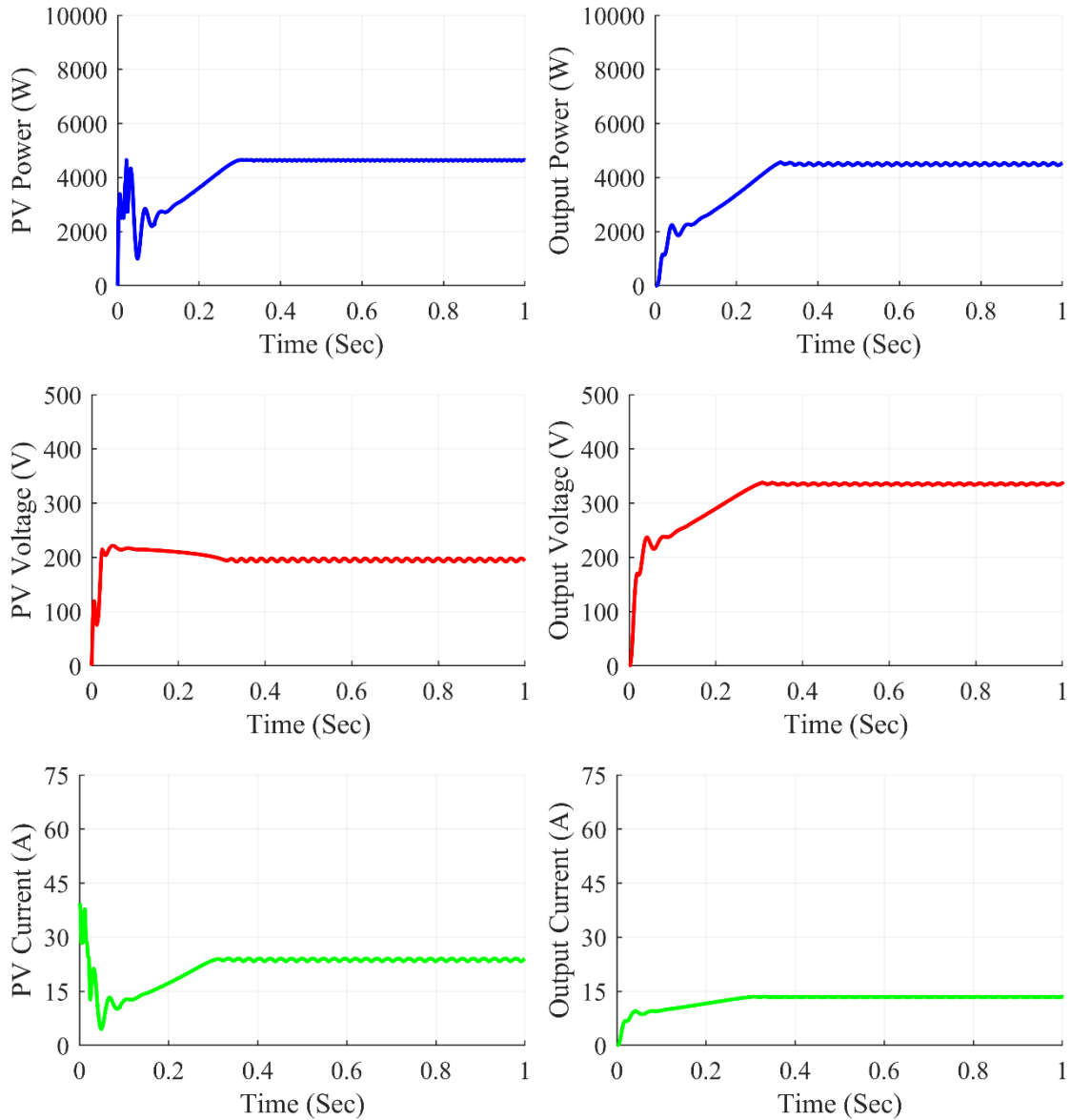


Figure 7.20: Cuk converter waveforms under frame shading condition

The Fig. 7.20 shows Cuk Converter waveforms under frame shading condition. At steady state, we can see that the converter gives average output power of 4543 W, the average output voltage at 337.0 V and the average output current of 13.48 A. The average value of PV power was at 4643 W and the PV current and PV voltage were at 193.7 V and 23.97 A respectively.

7.3.2.5 Under random shading scenario

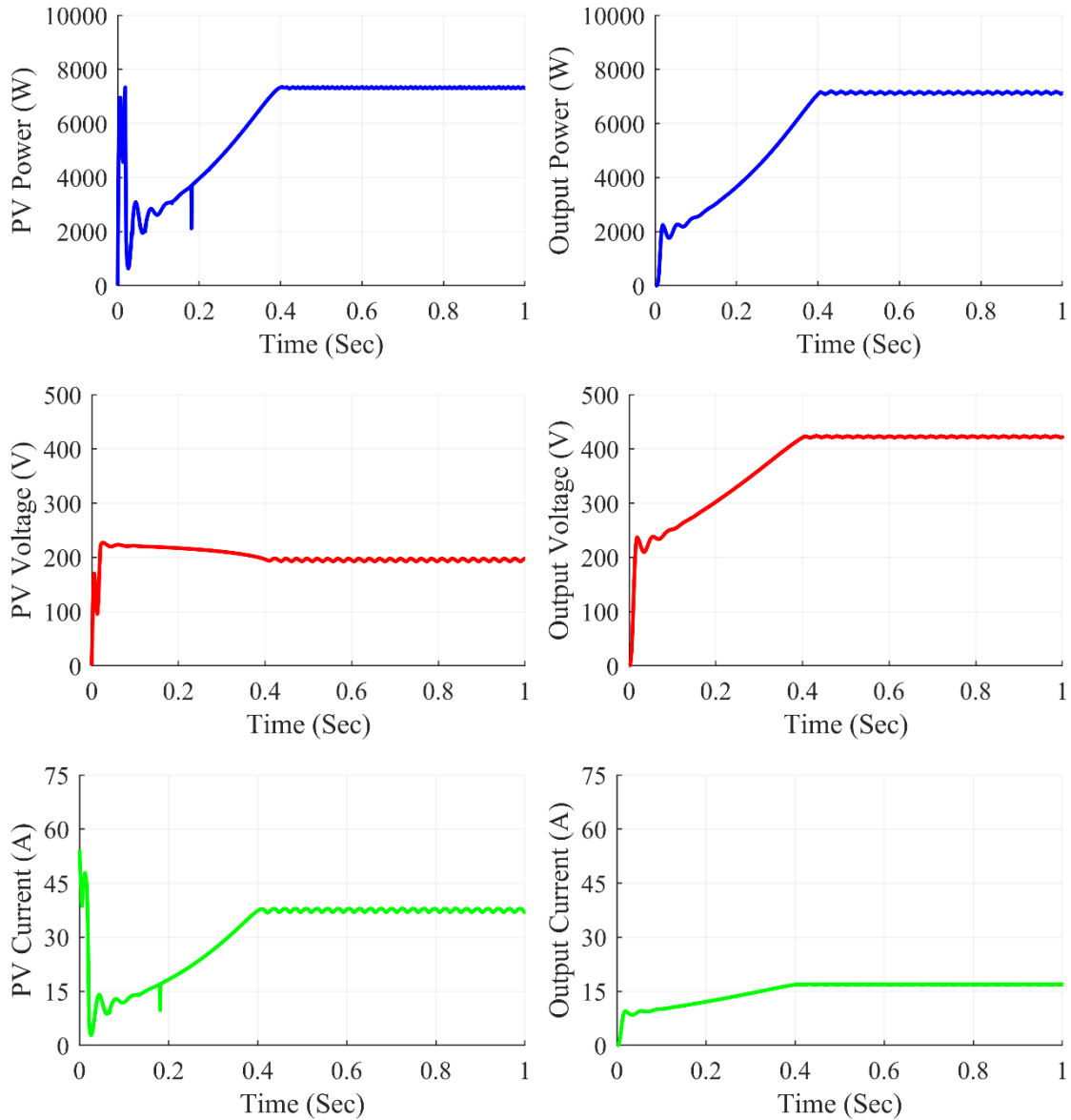


Figure 7.21: Cuk converter waveforms under random shading condition

The Fig. 7.21 shows Cuk Converter waveforms under random shading condition. At steady state, we can see that the converter gives average output power of 7118 W, the average output voltage at 421.9V and the average output current of 16.87 A. The average value of PV power was at 7298 W and the PV current and PV voltage were at 197.7 V and 36.92 A respectively.

7.3.2.6 Under right side end shading scenario

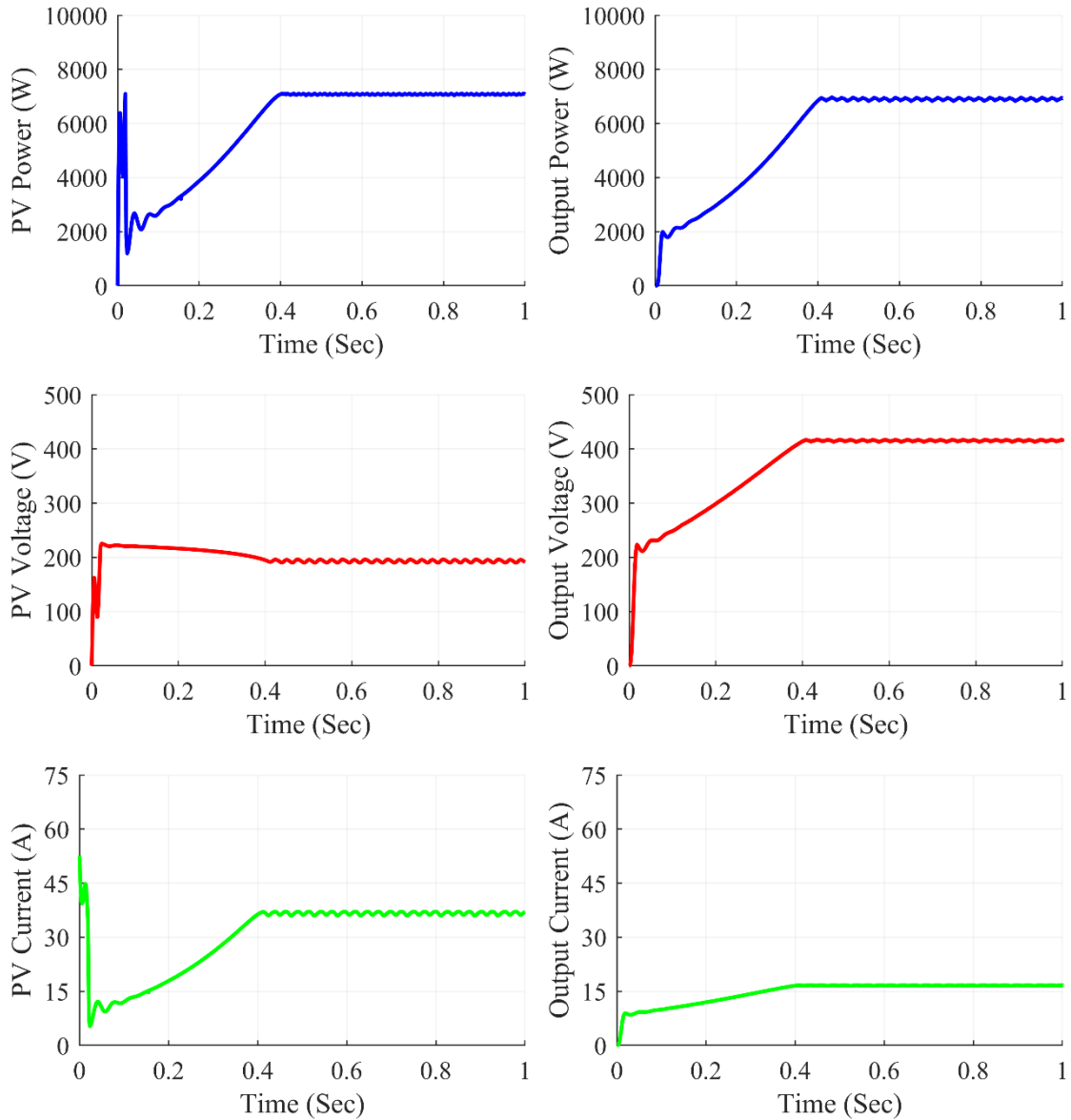


Figure 7.22: Cuk converter waveforms under right side end shading condition

The Fig. 7.22 shows Cuk Converter waveforms under right side end shading condition. At steady state, we can see that the converter gives average output power of 6928 W, the average output voltage at 416.2 V and the average output current of 16.65 A. The average value of PV power was at 7070 W and the PV current and PV voltage were at 191.0V and 37.02 A respectively.

7.3.2.7 Under uniform shading scenario

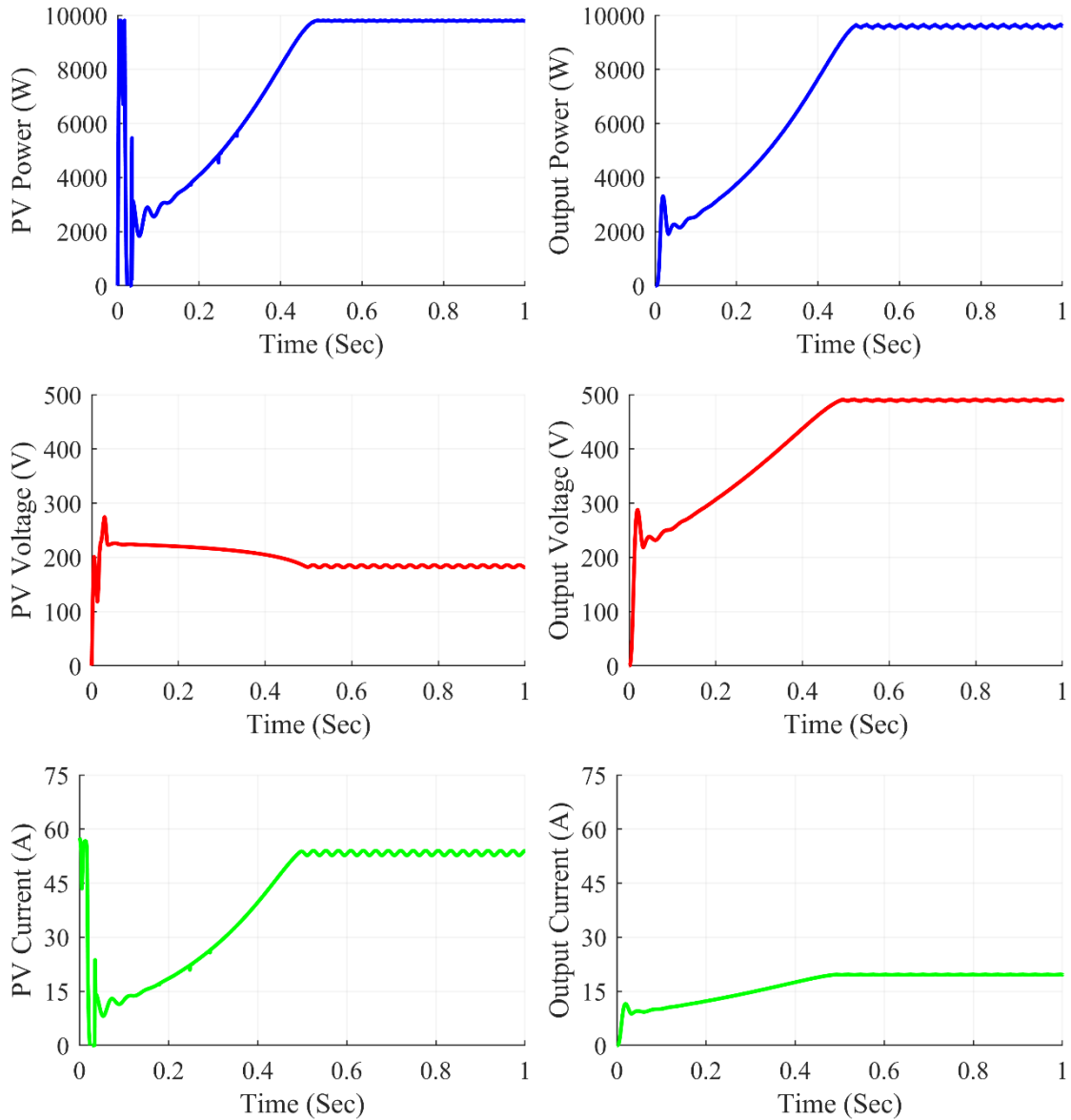


Figure 7.23: Cuk converter waveforms under uniform shading condition

The Fig. 7.23 shows Cuk Converter waveforms under uniform shading condition.

At steady state, we can see that the converter gives average output power of 9602 W, the average output voltage at 489.9 V and the average output current of 19.6 A. The average value of PV power was at 9787 W and the PV current and PV voltage were at 181.2 V and 54.01 A respectively.

Table 7.3: Cuk Converter Observations

Shading Conditions	PV Voltage (V_{PV})	PV Current (I_{PV})	PV Power (P_{PV})	Output Voltage (V_{out})	Output Current (I_{out})	Output Power (P_{out})	Duty Cycle (D)
Centre	192.1	37.09	7123	418	16.72	6988	0.682
Corner	198.2	36.59	7250	418.5	16.74	7005	0.678
Diagonal	186.1	44.12	8211	449.1	17.97	8069	0.707
Frame	193.7	23.97	4643	337.0	13.48	4543	0.635
Random	197.7	36.92	7298	421.9	16.87	7118	0.683
Right Side	191.0	37.02	7070	416.2	16.65	6928	0.685
Uniform	181.2	54.01	9787	489.9	19.6	9602	0.729

Table 7.3 summarizes the simulation results for the Cuk converter. Various partial shade scenarios were created on the 7x7 TCT PV array design, feeding power into the Cuk converter in such a way that maximum power extraction from the PV array was accomplished using the P&O method. The results were fairly accurate, and the desired value was met. From frame shading to uniform shading, the Cuk converter used duty ratios ranging from 0.635 to 0.729 respectively.

7.3.4 SEPIC Converter Waveforms

7.3.4.1 Under center shading scenario

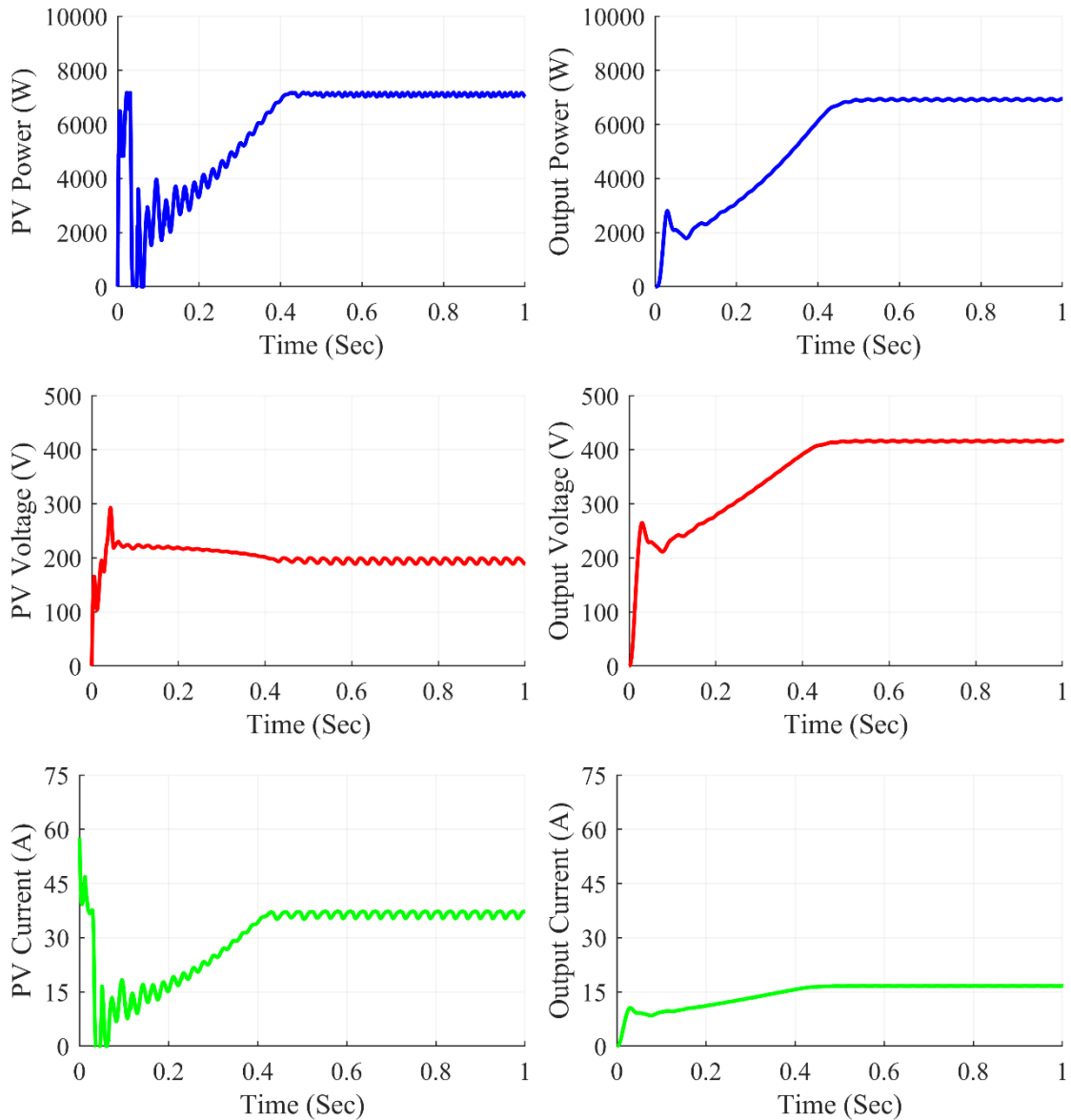


Figure 7.24: SEPIC converter waveforms under center shading condition

The Fig. 7.24 shows SEPIC Converter waveforms under center shading condition.

At steady state, we can see that the converter gives average output power of 6953 W, the average output voltage at 416.9 V and the average output current of 16.68 A. The average value of PV power was at 7020 W and the PV current and PV voltage were at 188.5V and 37.23 A respectively.

7.3.4.2 Under corner shading scenario

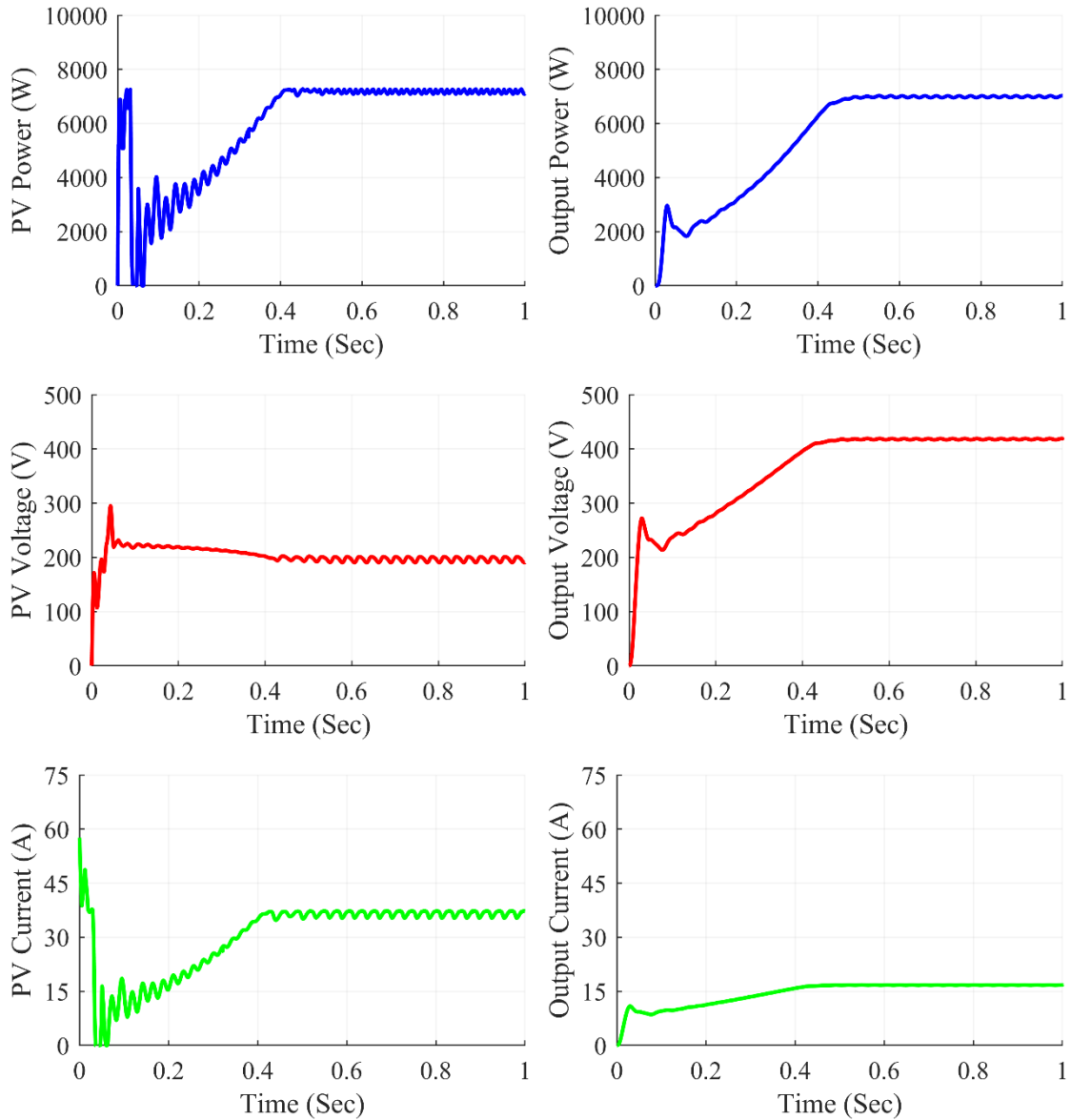


Figure 7.25: SEPIC converter waveforms under corner shading condition

The Fig. 7.25 shows SEPIC Converter waveforms under corner shading condition.

At steady state, we can see that the converter gives average output power of 7023 W, the average output voltage at 419 V and the average output current of 16.76 A. The average value of PV power was at 7105 W and the PV current and PV voltage were at 190.8 V and 37.24 A respectively.

7.3.4.3 Under diagonal shading scenario

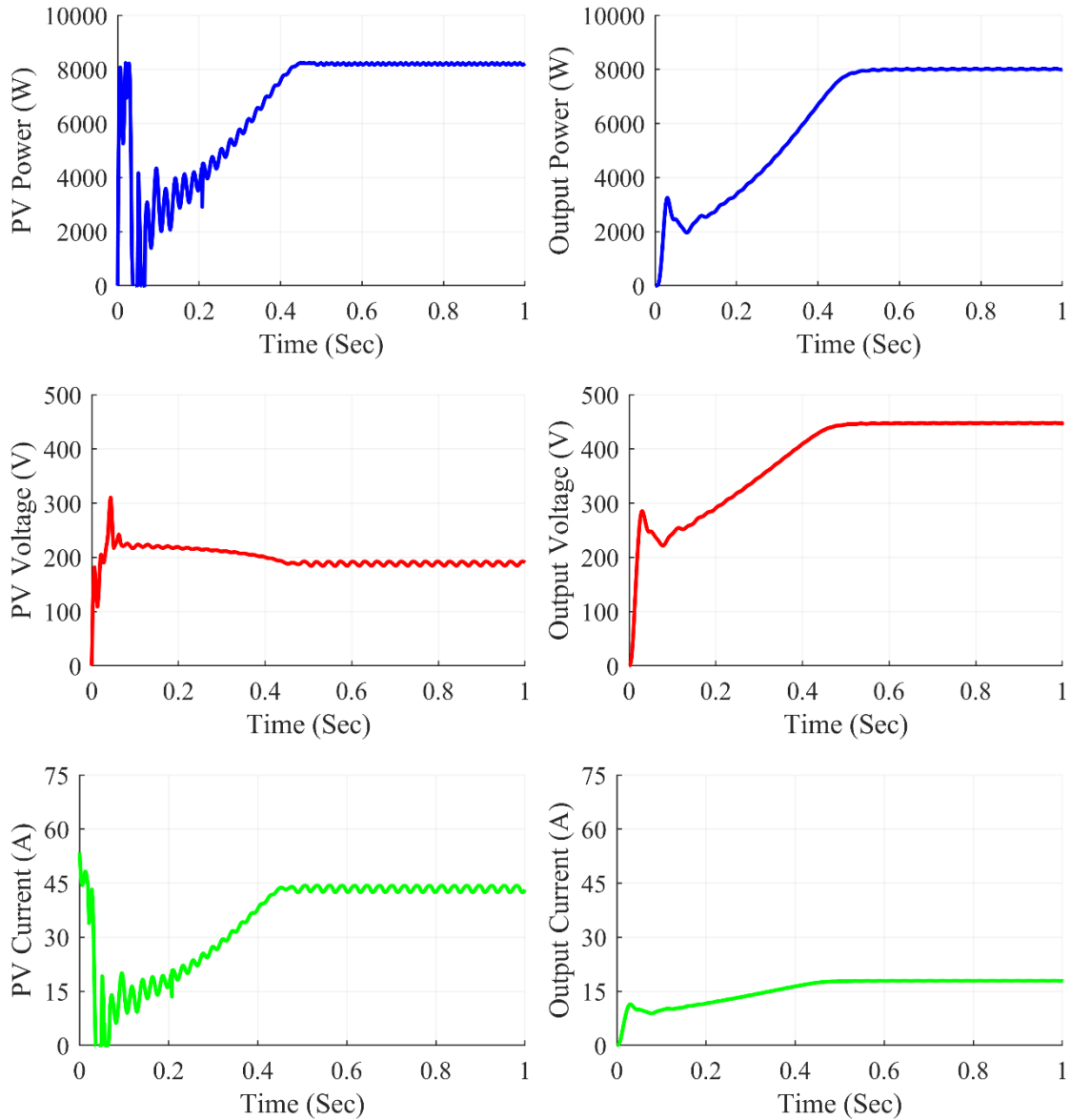


Figure 7.26: SEPIC converter waveforms under diagonal shading condition

The Fig. 7.26 shows SEPIC Converter waveforms under diagonal shading condition. At steady state, we can see that the converter gives average output power of 800 W, the average output voltage at 447.2 V and the average output current of 17.89A. The average value of PV power was at 8220 W and the PV current and PV voltage were at 190.4 V and 43.18 A respectively.

7.3.4.4 Under frame shading scenario

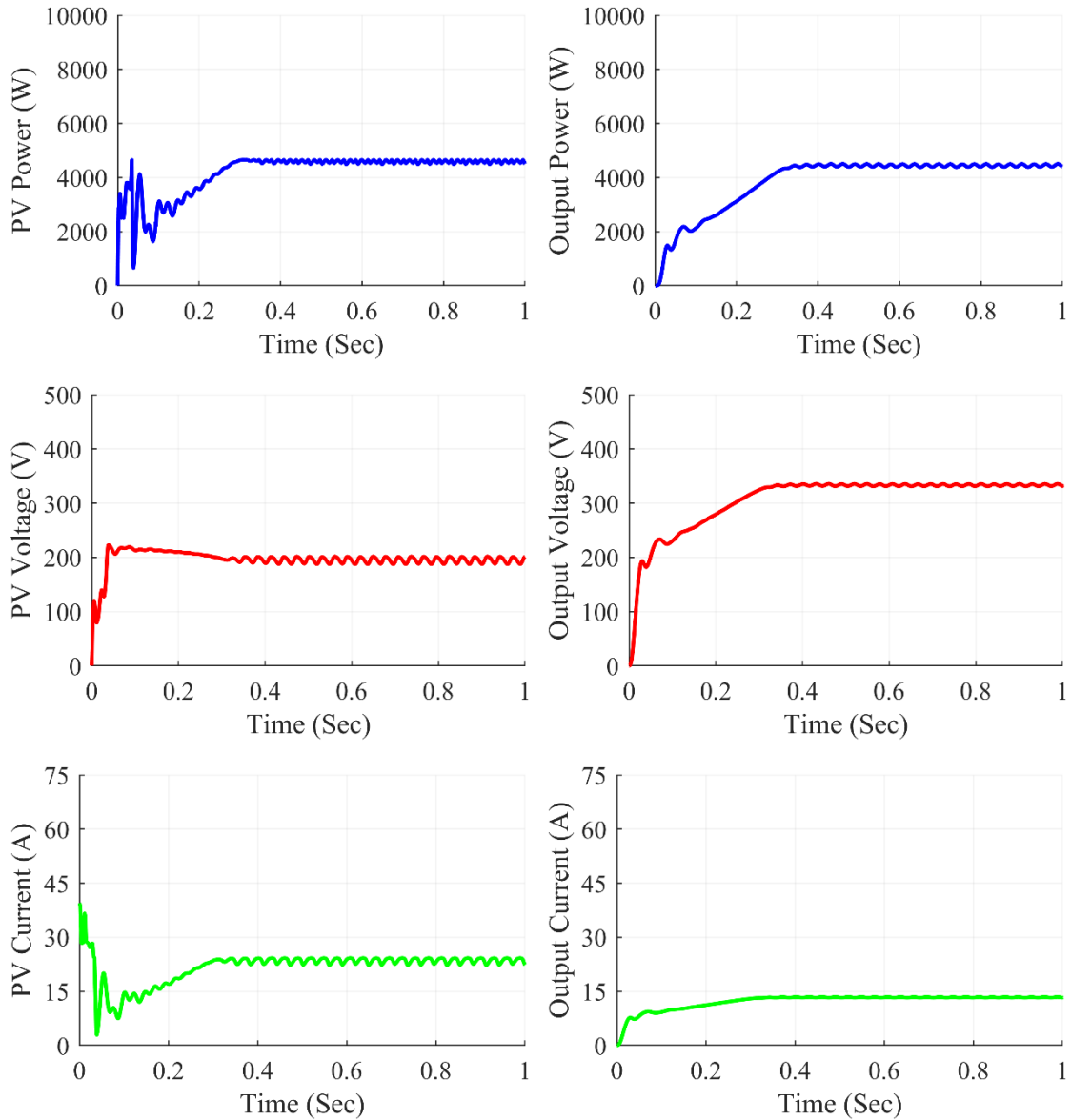


Figure 7.27: SEPIC converter waveforms under frame shading condition

The Fig. 7.27 shows SEPIC Converter waveforms under frame shading condition. At steady state, we can see that the converter gives average output power of 4400 W, the average output voltage at 331.6 V and the average output current of 13.27 A. The average value of PV power was at 331.6 W and the PV current and PV voltage were at 201.5 V and 22.33 A respectively.

7.3.4.5 Under random shading scenario

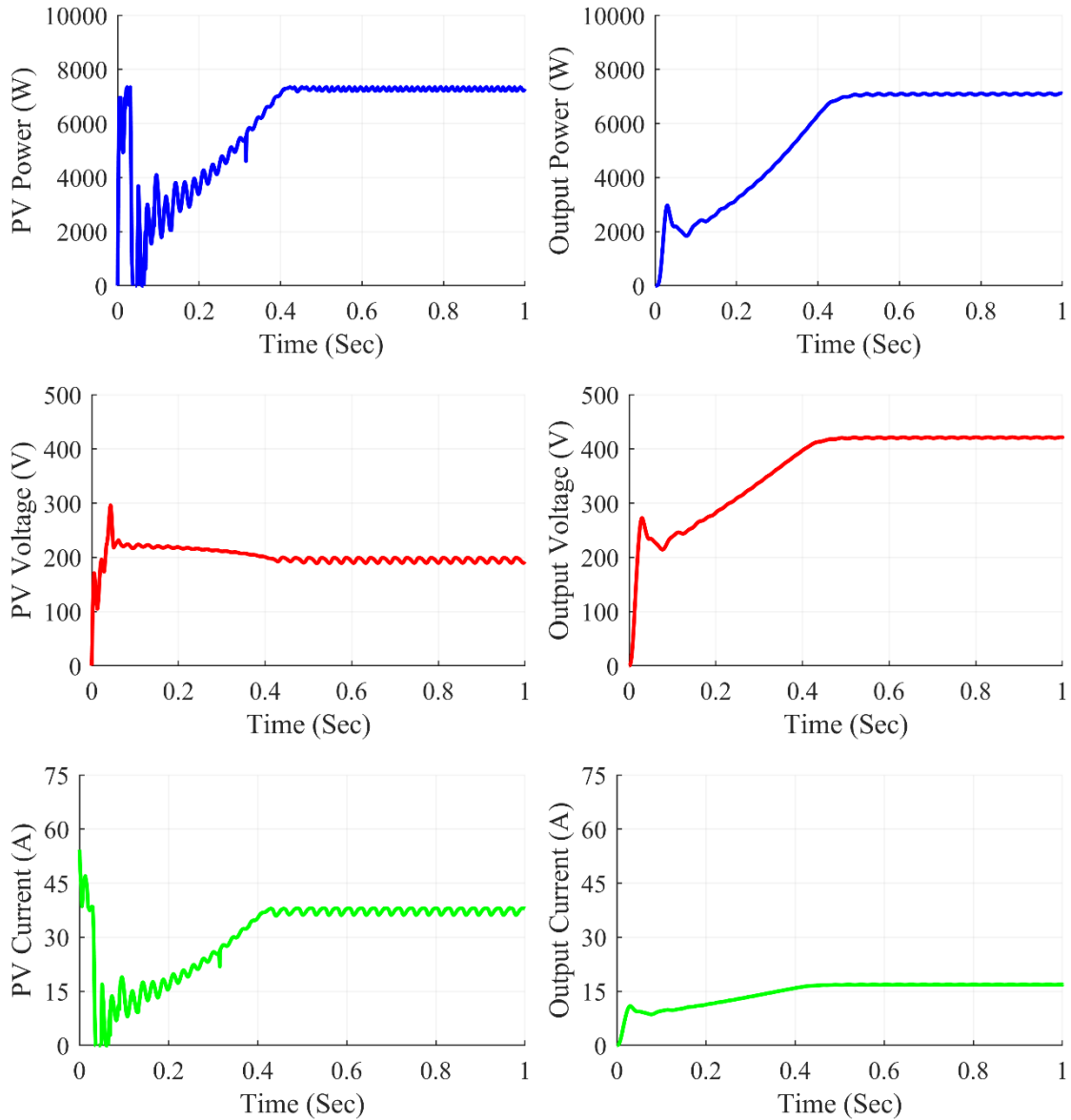


Figure 7.28: SEPIC converter waveforms under random shading condition

The Fig. 7.28 shows SEPIC Converter waveforms under random shading condition. At steady state, we can see that the converter gives average output power of 7087 W, the average output voltage at 420.9 V and the average output current of 16.84 A. The average value of PV power was at 7310 W and the PV current and PV voltage were at 193.1 V and 37.85 A respectively.

7.3.4.6 Under right side end shading scenario

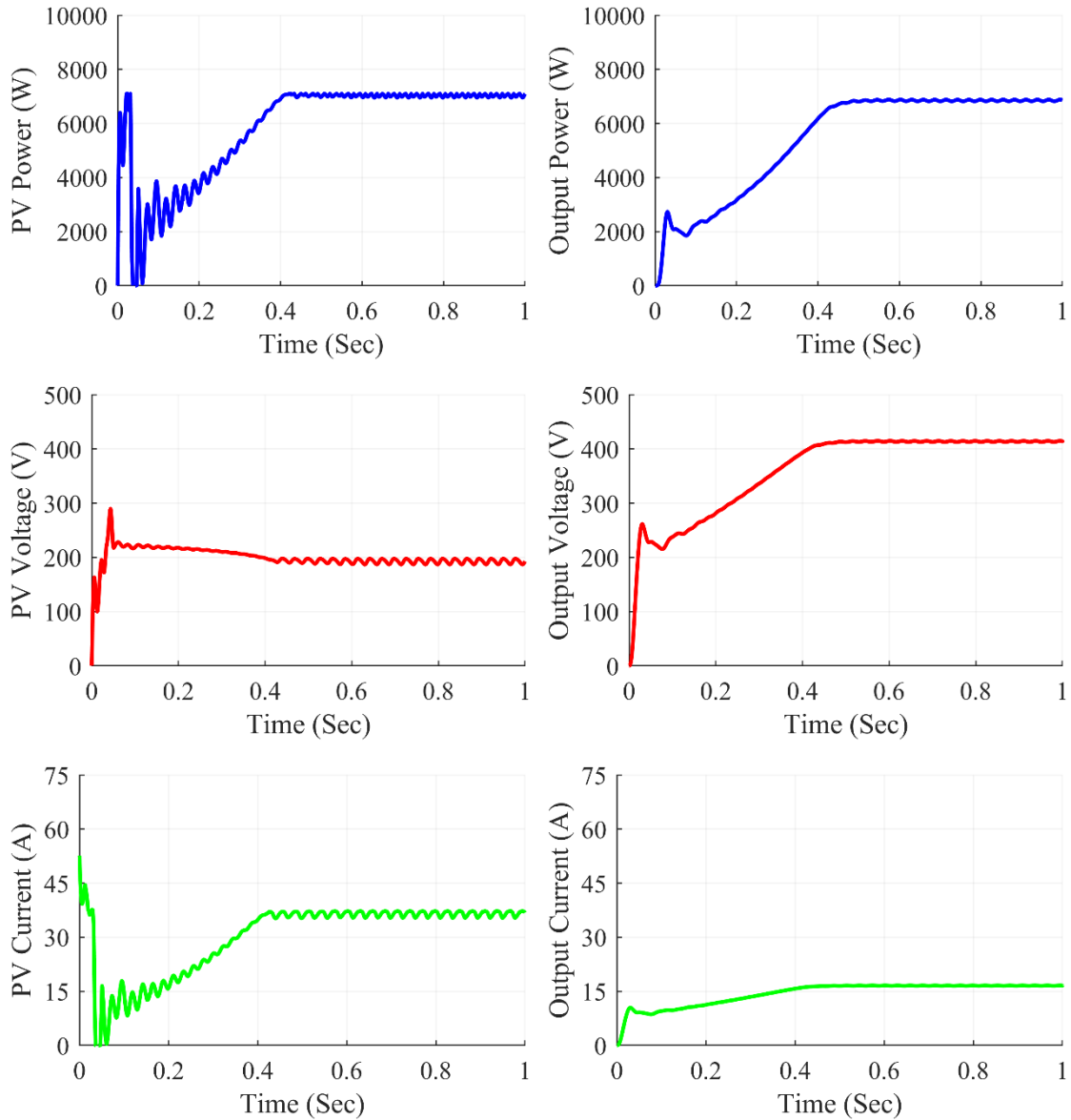


Figure 7.29: SEPIC converter waveforms under right side end shading condition

The Fig. 7.29 shows SEPIC Converter waveforms under right side end shading condition. At steady state, we can see that the converter gives average output power of 6874 W, the average output voltage at 414.5 V and the average output current of 16.58 A. The average value of PV power was at 7095 W and the PV current and PV voltage were at 192.9V and 36.79 A respectively.

7.3.4.7 Under uniform shading scenario

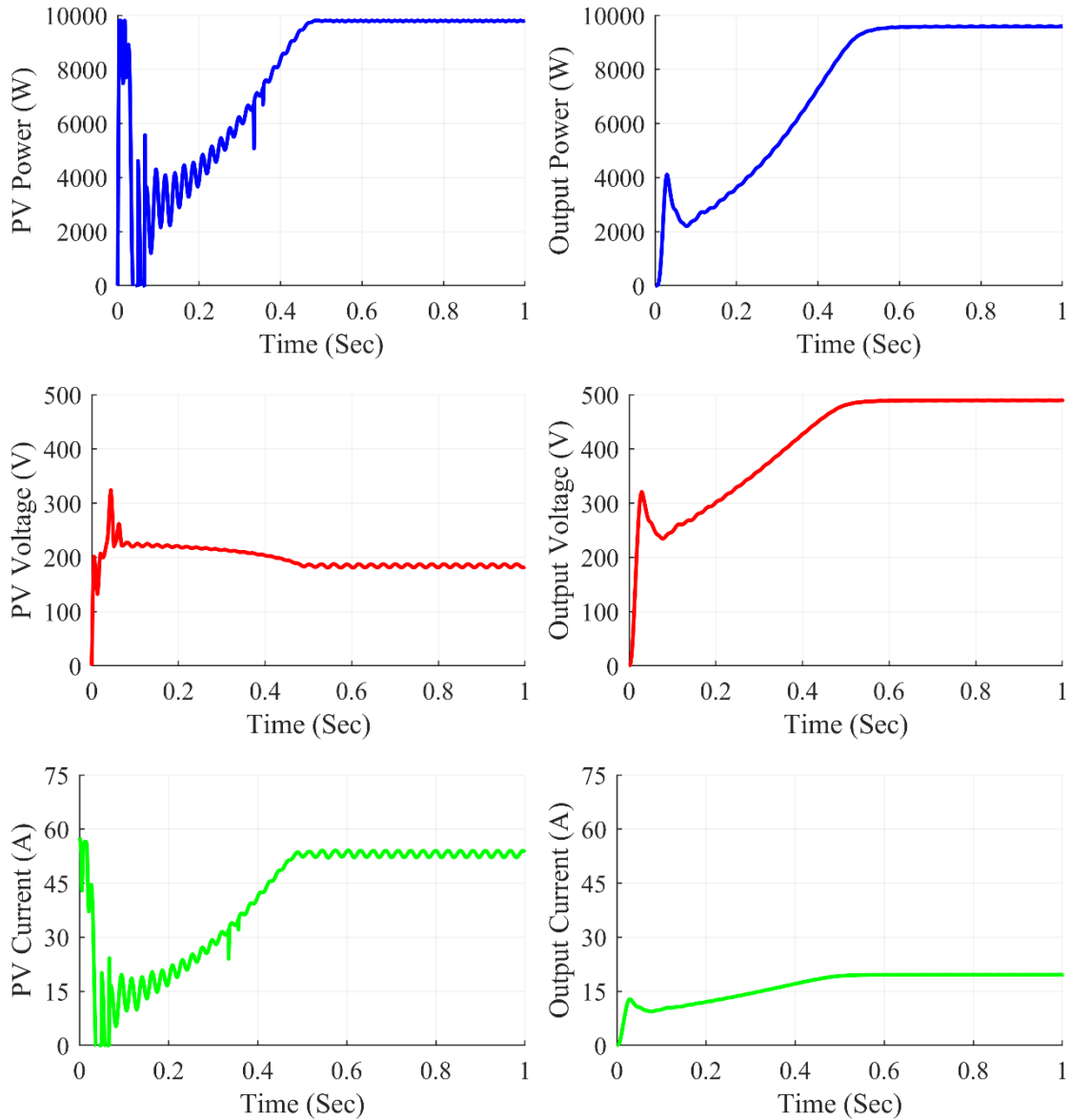


Figure 7.30: SEPIC converter waveforms under uniform shading condition

The Fig. 7.30 shows SEPIC Converter waveforms under uniform shading condition. At steady state, we can see that the converter gives average output power of 9668 W, the average output voltage at 496.1 V and the average output current of 19.67 A. The average value of PV power was at 9801 W and the PV current and PV voltage were at 52.85 A and 185.4 V respectively.

Table 7.4: SEPIC Converter Observations

Shading Conditions	PV Voltage (V_{PV})	PV Current (I_{PV})	PV Power (P_{PV})	Output Voltage (V_{out})	Output Current (I_{out})	Output Power (P_{out})	Duty Cycle (D)
Centre	188.5	37.23	7020	416.9	16.68	6953	0.682
Corner	190.8	37.24	7105	419	16.76	7023	0.680
Diagonal	190.4	43.18	8220	447.2	17.89	8000	0.705
Frame	201.5	22.33	4499	331.6	13.27	4400	0.628
Random	192.1	37.90	7283	421.5	16.86	7107	0.682
Right Side	192.7	36.82	7094	414.1	16.57	6860	0.680
Uniform	183.2	53.53	9804	489.7	19.59	9592	0.725

The results of the simulation are summarized in Table 7.4 for SEPIC converter. On the 7x7 TCT PV array design, various partial shading situations were produced, which fed power into the SEPIC converter in such a way that maximum power extraction from the PV array was achieved using the P&O method. The results were reasonably accurate and matched the expected value. The SEPIC converter worked with a duty ratio ranging from 0.628 to 0.725 for frame shading to uniform shading respectively.

7.3.5 Zeta Converter Waveforms

7.3.5.1 Under center shading scenario

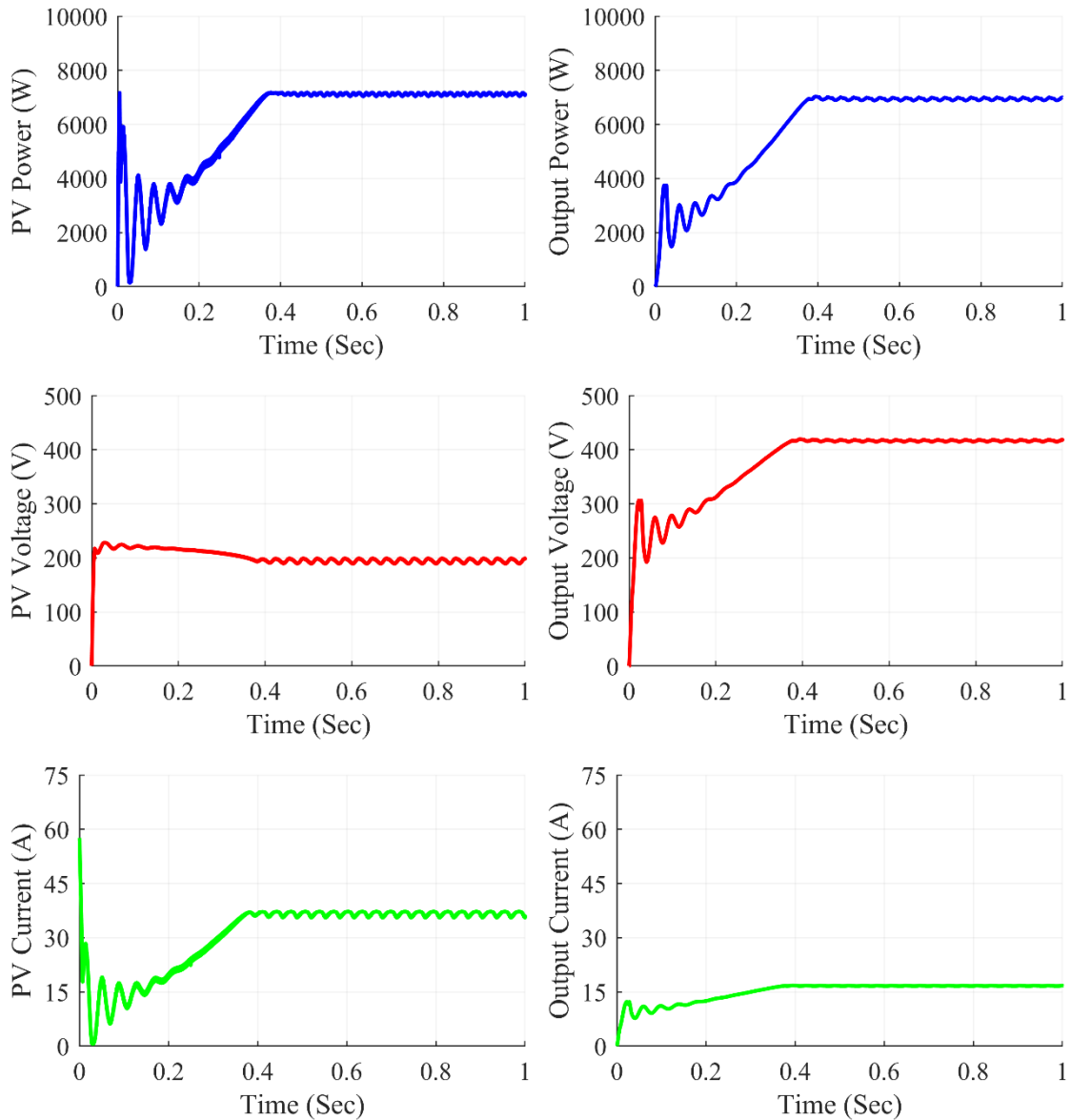


Figure 7.31: Zeta converter waveforms under center shading condition

The Fig. 7.31 shows Zeta Converter waveforms under center shading condition. At steady state, we can see that the converter gives average output power of 6996 W, the average output voltage at 418.2 V and the average output current of 16.73 A. The average value of PV power was at 7099 W and the PV current and PV voltage were at 198.4V and 35.77 A respectively.

7.3.5.2 Under corner shading scenario

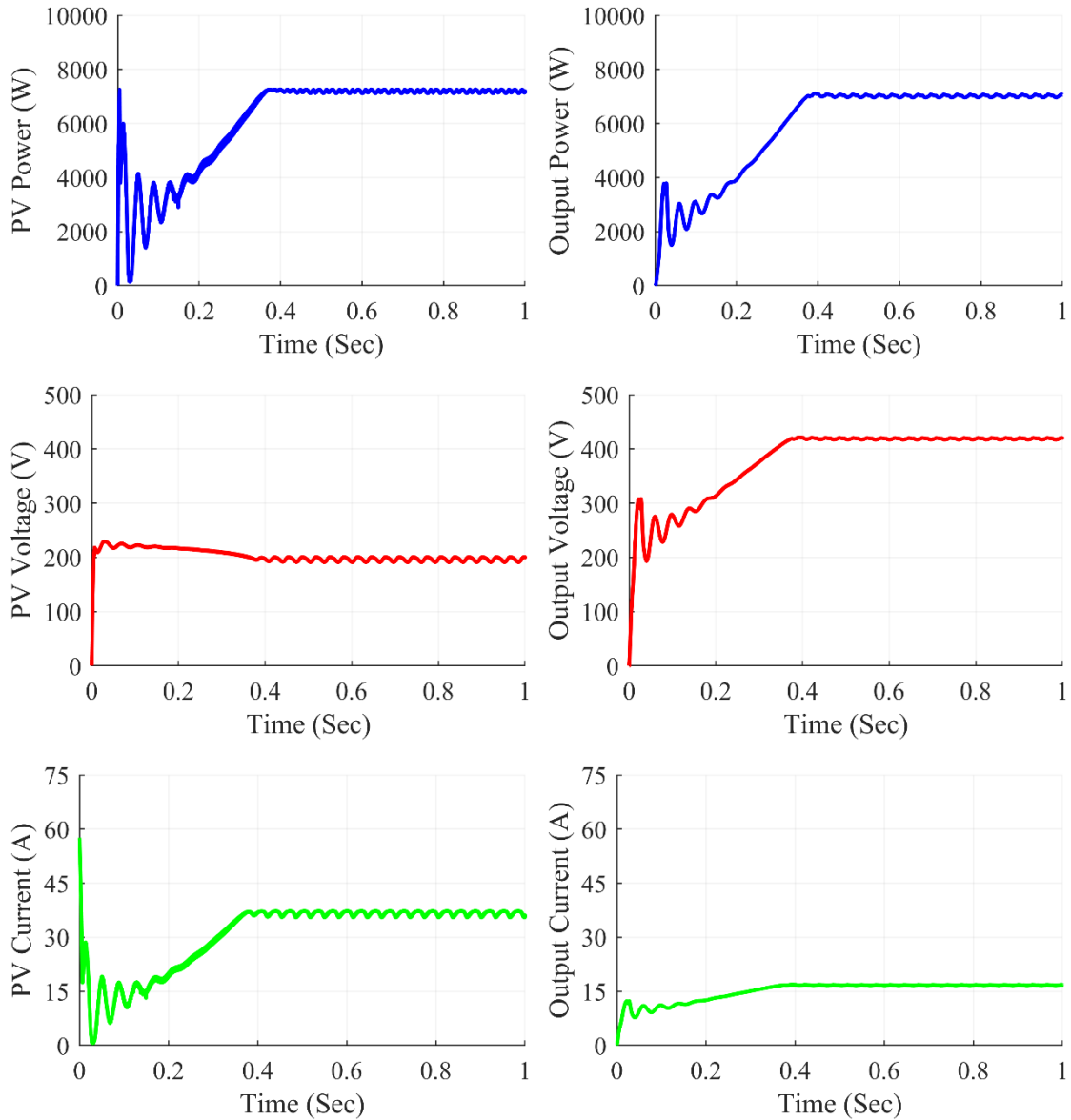


Figure 7.32: Zeta converter waveforms under corner shading condition

The Fig. 7.32 shows Zeta Converter waveforms under corner shading condition. At steady state, we can see that the converter gives average output power of 7059 W, the average output voltage at 420.1V and the average output current of 16.8A. The average value of PV power was at 7177 W and the PV current and PV voltage were at 200.3 V and 35.83 A respectively.

7.3.5.3 Under diagonal shading scenario

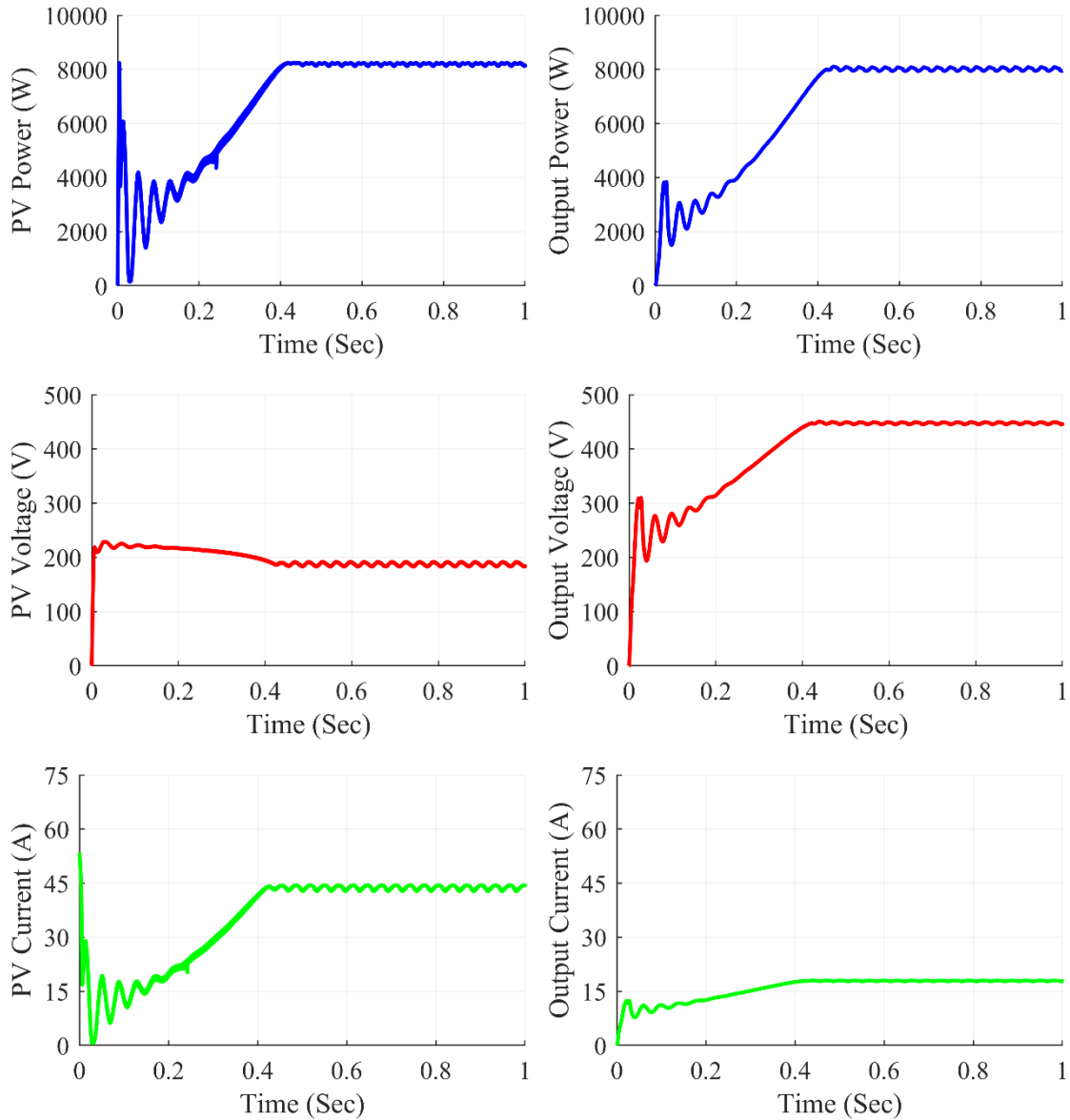


Figure 7.33: Zeta converter waveforms under diagonal shading condition

The Fig. 7.33 shows Zeta Converter waveforms under diagonal shading condition.

At steady state, we can see that the converter gives average output power of 7946 W, the average output voltage at 445.7 V and the average output current of 17.83 A. The average value of PV power was at 8147 W and the PV current and PV voltage were at 183.7 V and 44.34 A respectively.

7.3.5.4 Under frame shading scenario

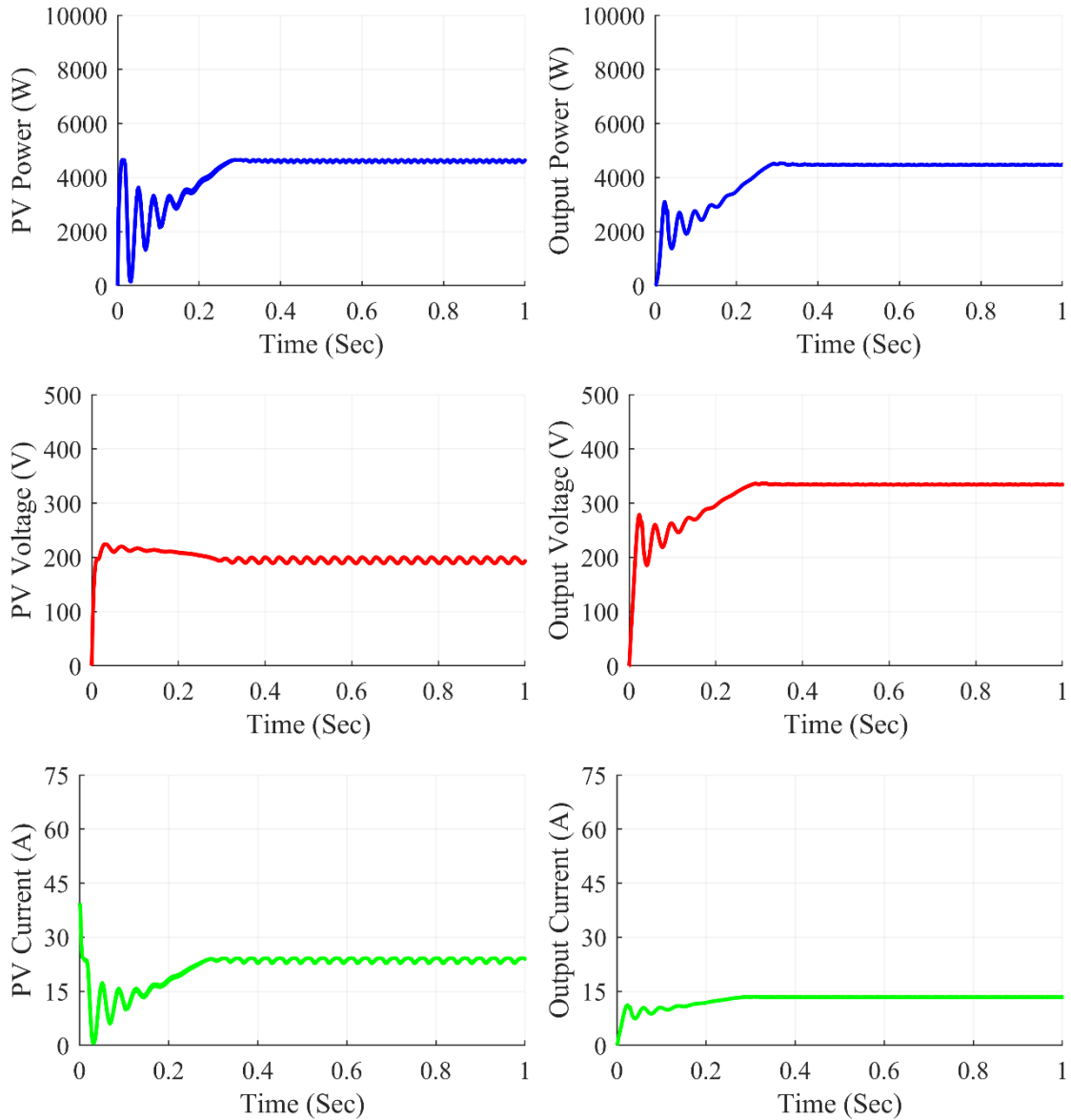


Figure 7.34: Zeta converter waveforms under frame shading condition

The Fig. 7.34 shows Zeta Converter waveforms under frame shading condition. At steady state, we can see that the converter gives average output power of 4472 W, the average output voltage at 334.4 V and the average output current of 13.38 A. The average value of PV power was at 4637 W and the PV current and PV voltage were at 193.2 V and 24.01 A respectively.

7.3.5.5 Under random shading scenario

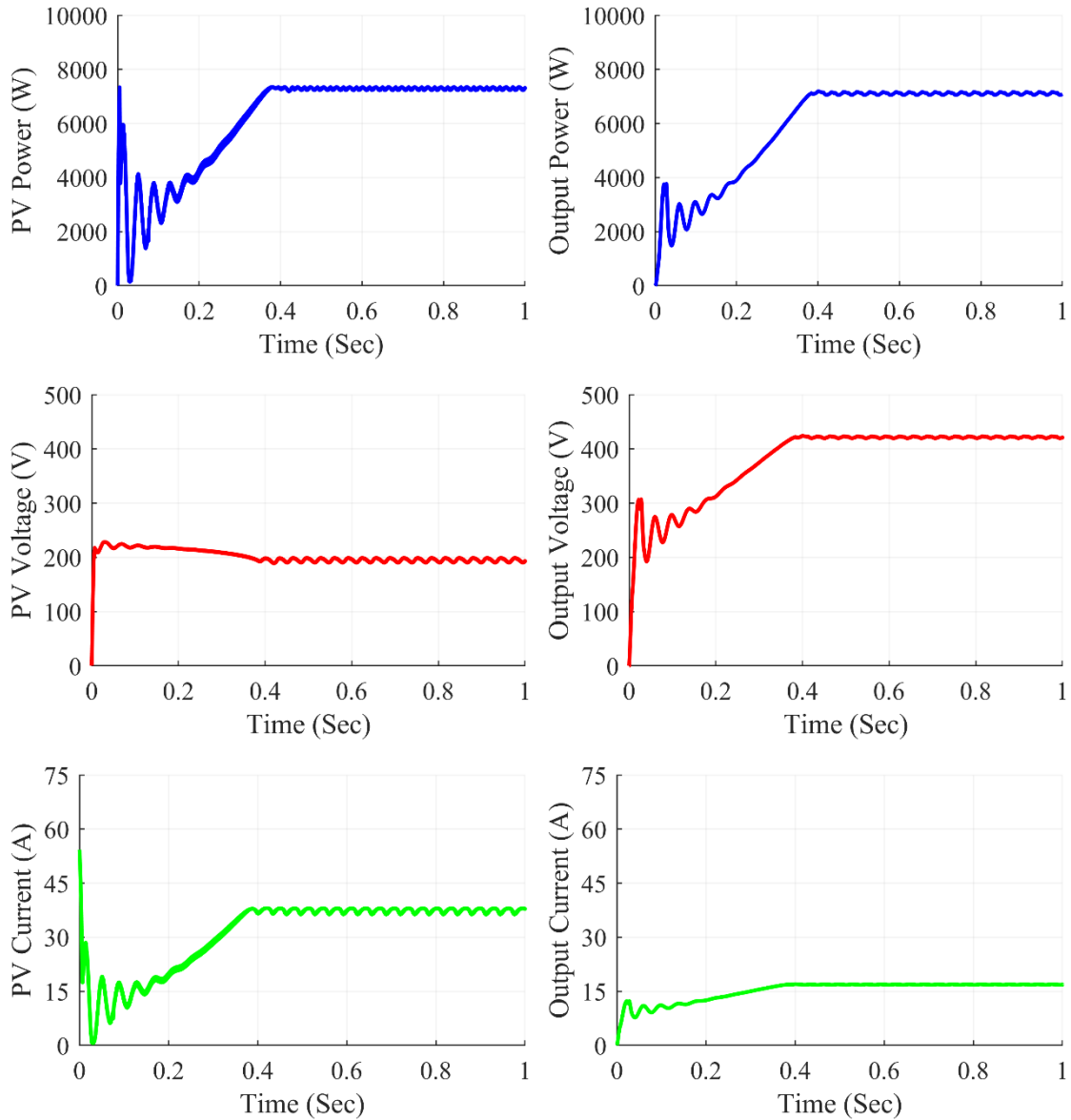


Figure 7.35: Zeta converter waveforms under random shading condition

The Fig. 7.35 shows Zeta Converter waveforms under random shading condition. At steady state, we can see that the converter gives average output power of 7087 W, the average output voltage at 420.9V and the average output current of 16.84A. The average value of PV power was at 7310 W and the PV current and PV voltage were at 193.1 V and 37.85 A respectively.

7.3.5.6 Under right side end shading scenario

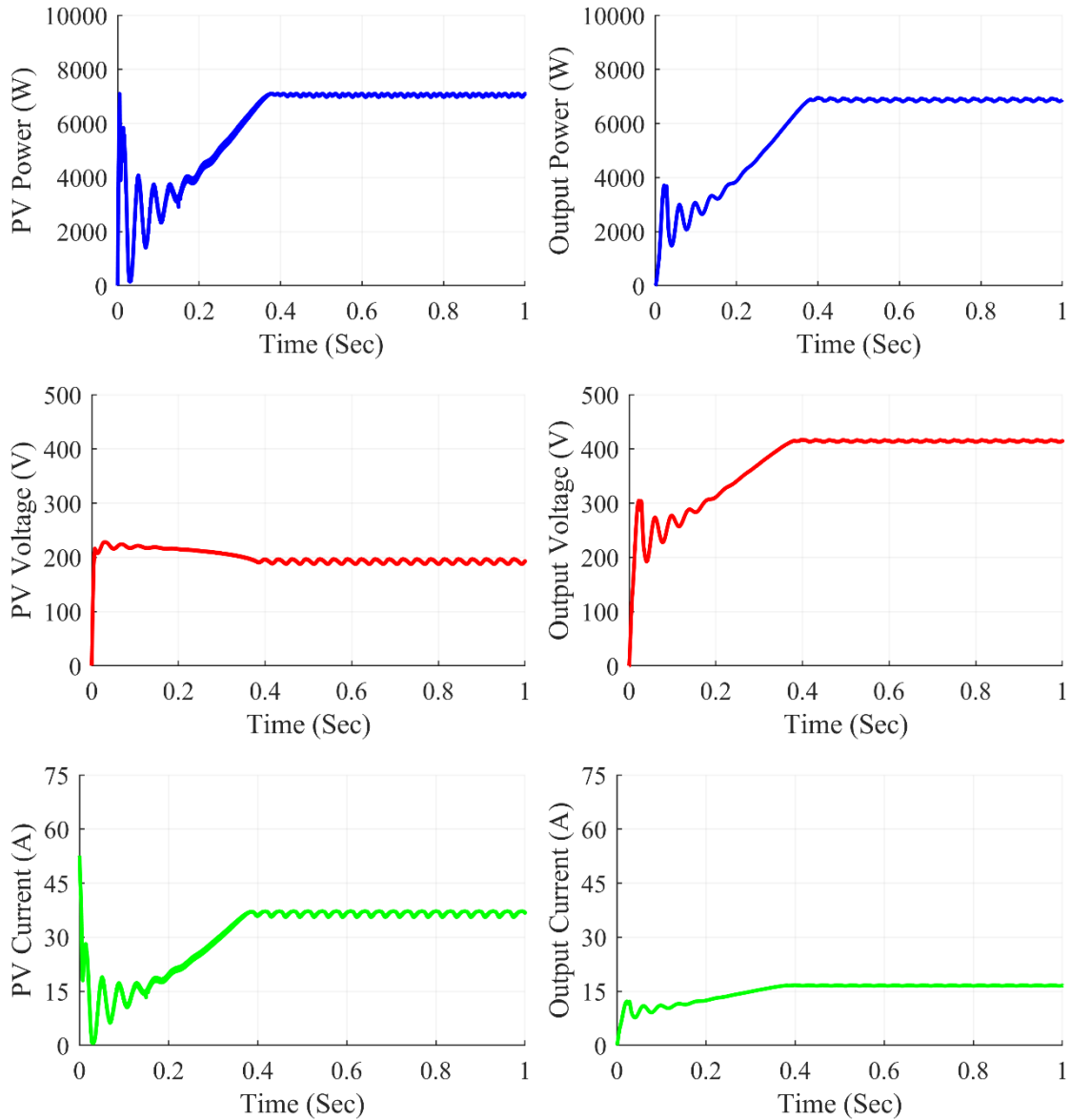


Figure 7.36: Zeta converter waveforms under right side end shading condition

The Fig. 7.36 shows Zeta Converter waveforms under right side end shading condition. At steady state, we can see that the converter gives average output power of 6874 W, the average output voltage at 414.5 V and the average output current of 16.58 A. The average value of PV power was at 7095 W and the PV current and PV voltage were at 36.79V and 192.9A respectively.

7.3.5.7 Under uniform shading scenario

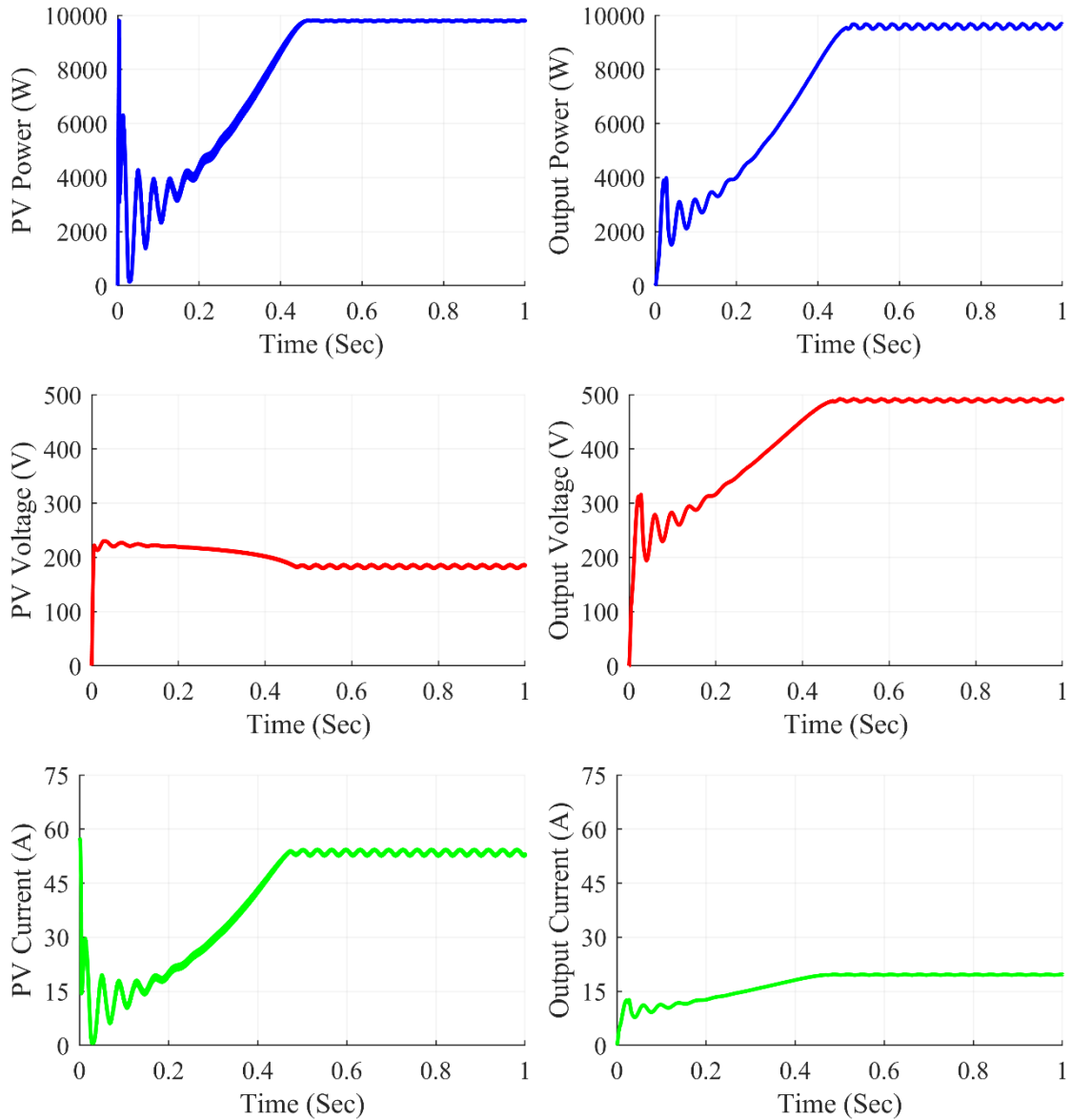


Figure 7.37: Zeta converter waveforms under uniform shading condition

The Fig. 7.37 shows Zeta Converter waveforms under uniform shading condition.

At steady state, we can see that the converter gives average output power of 9668 W, the average output voltage at 496.1 V and the average output current of 19.67 A. The average value of PV power was at 9801 W and the PV current and PV voltage were at 185.4 V and 52.85 A respectively.

Table 7.5: Zeta Converter Observations

Shading Conditions	PV Voltage (V_{PV})	PV Current (I_{PV})	PV Power (P_{PV})	Output Voltage (V_{out})	Output Current (I_{out})	Output Power (P_{out})	Duty Cycle (D)
Centre	198.4	35.77	7099	418.2	16.73	6996	0.680
Corner	200.3	35.83	7177	420.1	16.8	7059	0.680
Diagonal	183.7	44.34	8147	445.7	17.83	7946	0.705
Frame	1932.	24.01	4637	334.4	13.38	4472	0.630
Random	193.1	37.85	7310	420.9	16.84	7087	0.682
Right Side	192.9	36.79	7095	414.5	16.58	6874	0.680
Uniform	185.4	52.85	9801	496.1	19.67	9668	0.728

Table 7.5 summarizes the simulation results for the Zeta converter. Various partial shade scenarios were created on the 7x7 TCT PV array design, feeding power into the Zeta converter in such a way that maximum power extraction from the PV array was accomplished using the P&O method. The results were fairly accurate, and the desired value was met. From frame shading to uniform shading, the Zeta converter used the duty ratios ranging from 0.630 to 0.728 respectively.

7.3.6 Super-Lift Luo Converter Waveforms

7.3.6.1 Under center shading scenario

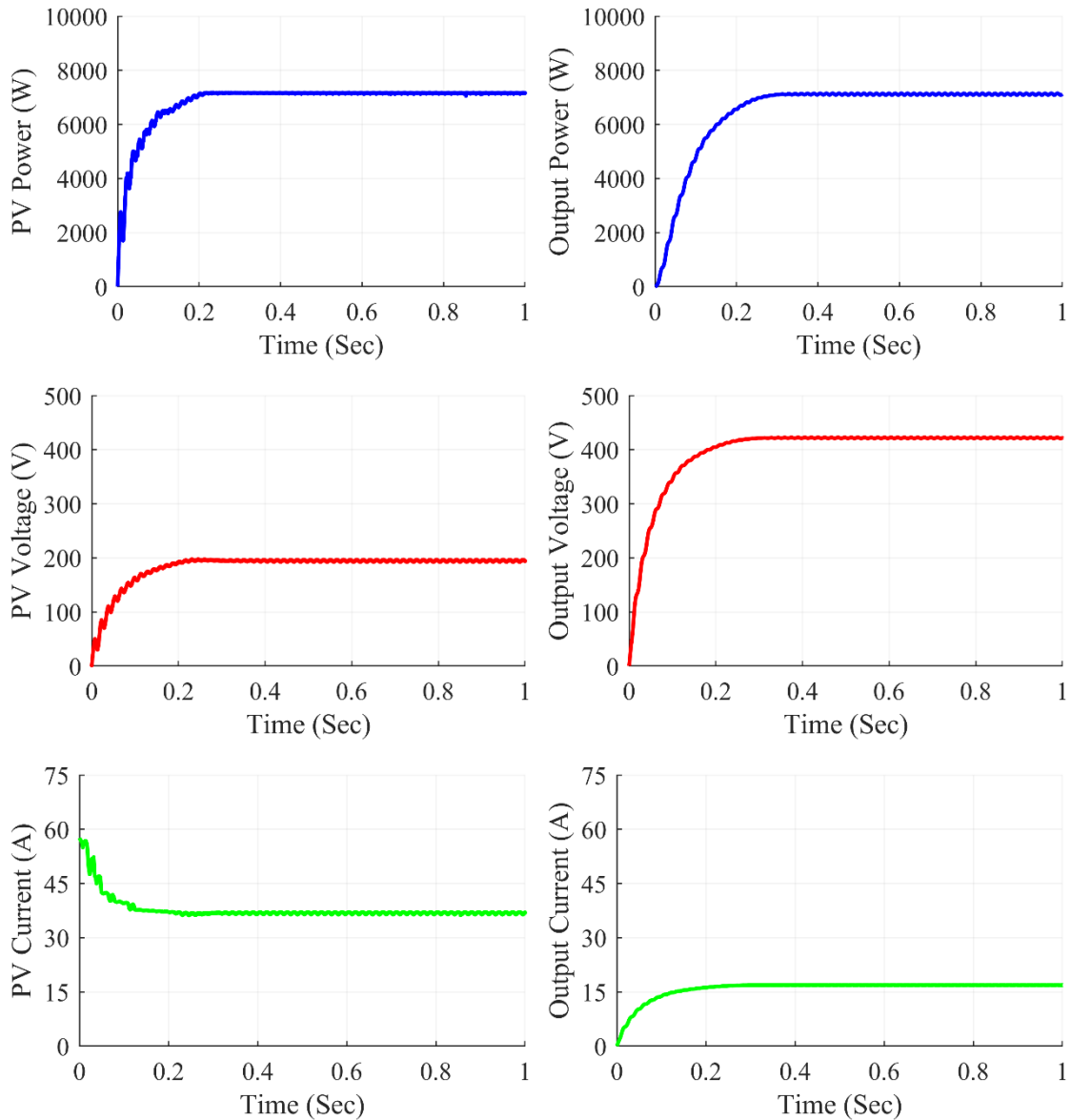


Figure 7.38: Super-Lift Luo converter waveforms under center shading condition

The Fig. 7.38 shows Super-Lift Luo Converter waveforms under center shading condition. At steady state, we can see that the converter gives average output power of 7126 W, the average output voltage at 422.1 V and the average output current of 16.88 A. The average value of PV power was at 7162 W and the PV current and PV voltage were at 194.0V and 36.93 A respectively.

7.3.6.2 Under corner shading scenario

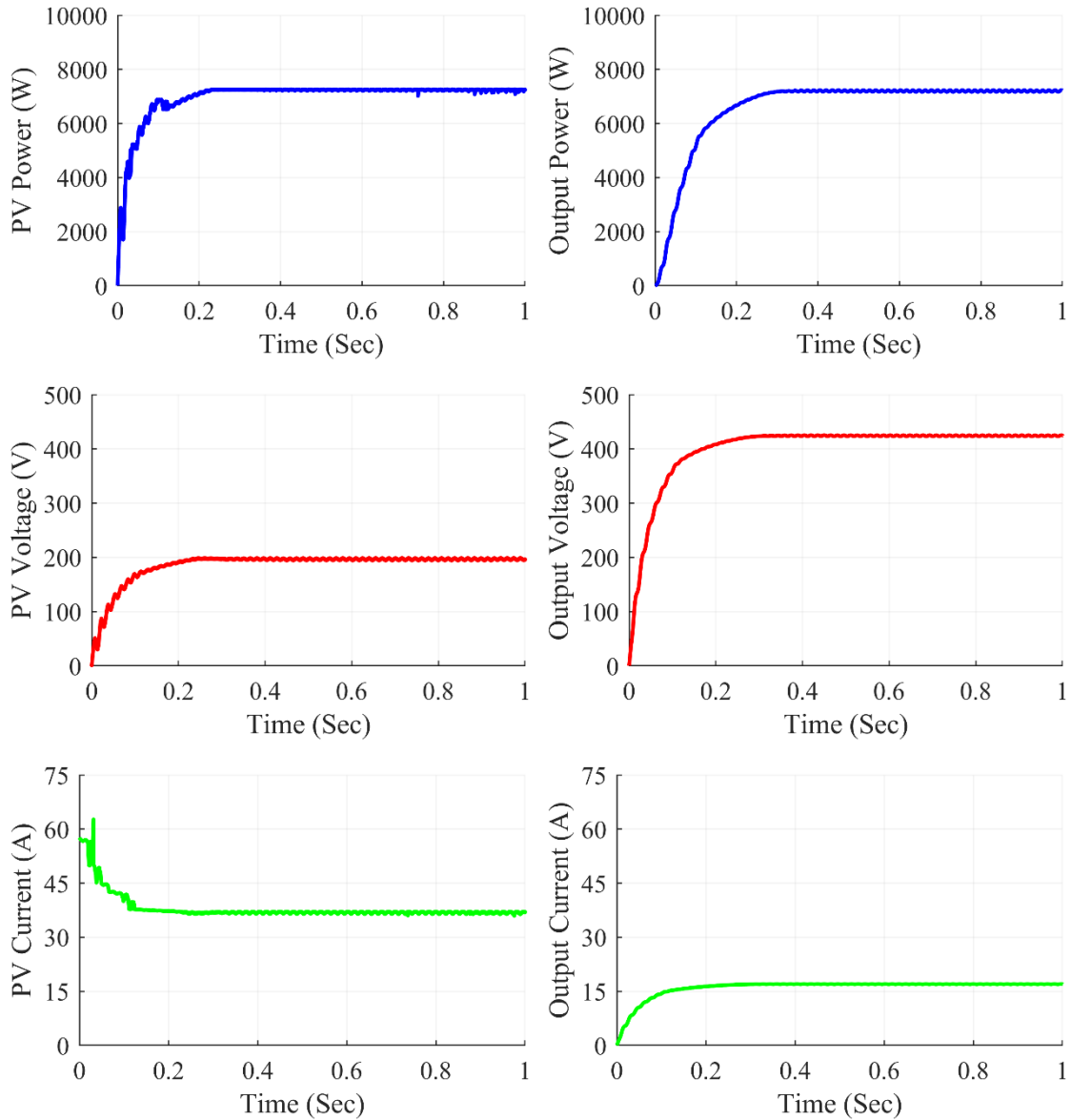


Figure 7.39: Super-Lift Luo converter waveforms under corner shading condition

The Fig. 7.39 shows Super-Lift Luo Converter waveforms under corner shading condition. At steady state, we can see that the converter gives average output power of 7216 W, the average output voltage at 424.7V and the average output current of 16.99 A. The average value of PV power was at 7245 W and the PV current and PV voltage were at 196.1 V and 36.95 A respectively.

7.3.6.3 Under diagonal shading scenario

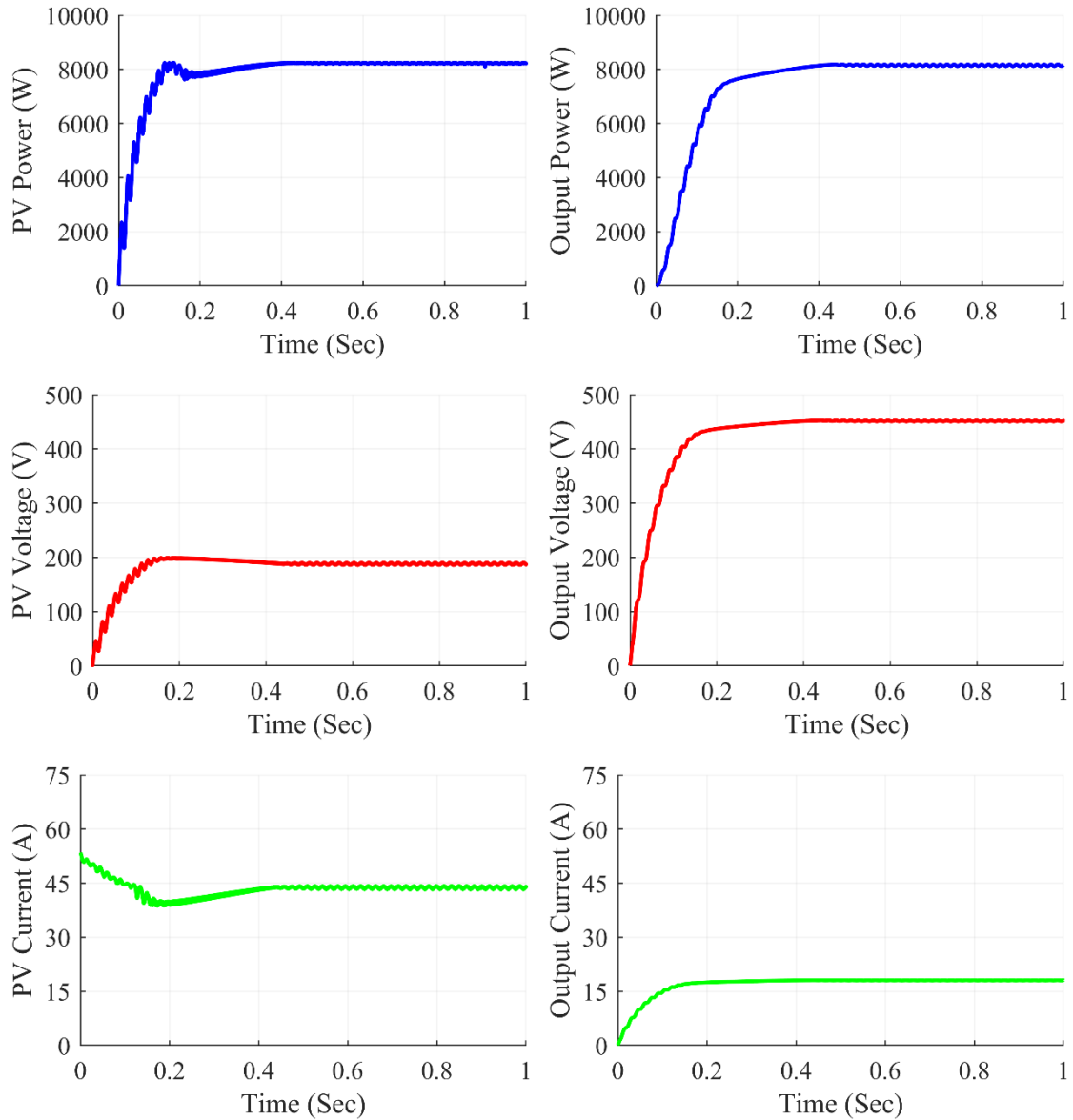


Figure 7.40: Super-Lift Luo converter waveforms under diagonal shading condition

The Fig. 7.40 shows Super-Lift Luo Converter waveforms under diagonal shading condition. At steady state, we can see that the converter gives average output power of 8165 W, the average output voltage at 451.8 V and the average output current of 18.07 A. The average value of PV power was at 8224 W and the PV current and PV voltage were at 186.9 V and 44.00 A respectively.

7.3.6.4 Under frame shading scenario

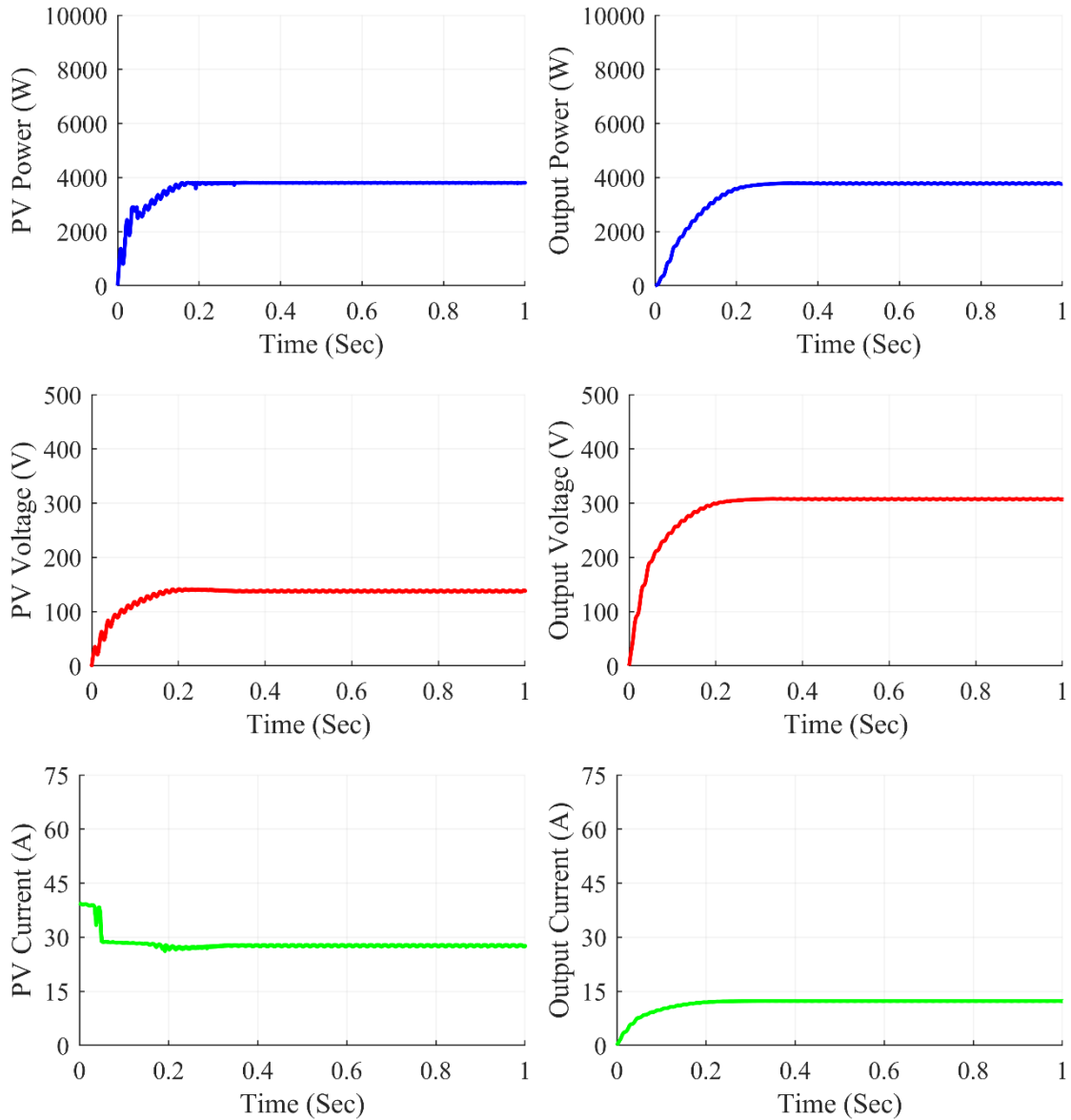


Figure 7.41: Super-Lift Luo converter waveforms under frame shading condition

The Fig. 7.41 shows Super-Lift Luo Converter waveforms under frame shading condition. At steady state, we can see that the converter gives average output power of 3370 W, the average output voltage at 307.0 V and the average output current of 12.28 A. The average value of PV power was at 3810 W and the PV current and PV voltage were at 138.1 V and 27.59 A respectively.

7.3.6.5 Under random shading scenario

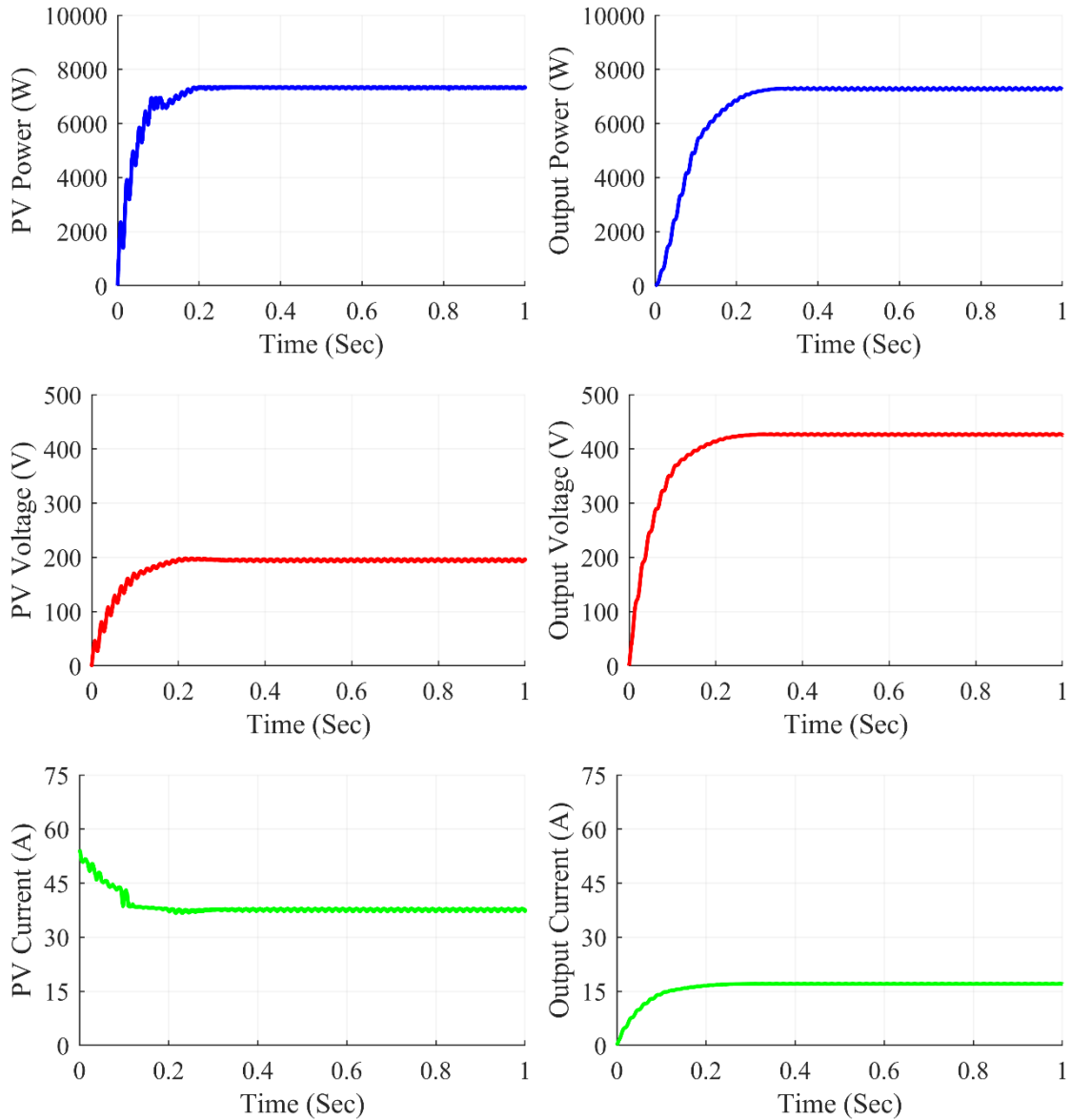


Figure 7.42: Super-Lift Luo converter waveforms under random shading condition

The Fig. 7.42 shows Super-Lift Luo Converter waveforms under random shading condition. At steady state, we can see that the converter gives average output power of 7245 W, the average output voltage at 425.8V and the average output current of 17.03 A. The average value of PV power was at 7336 W and the PV current and PV voltage were at 196.0 V and 37.44 A respectively.

7.3.6.6 Under right side end shading scenario

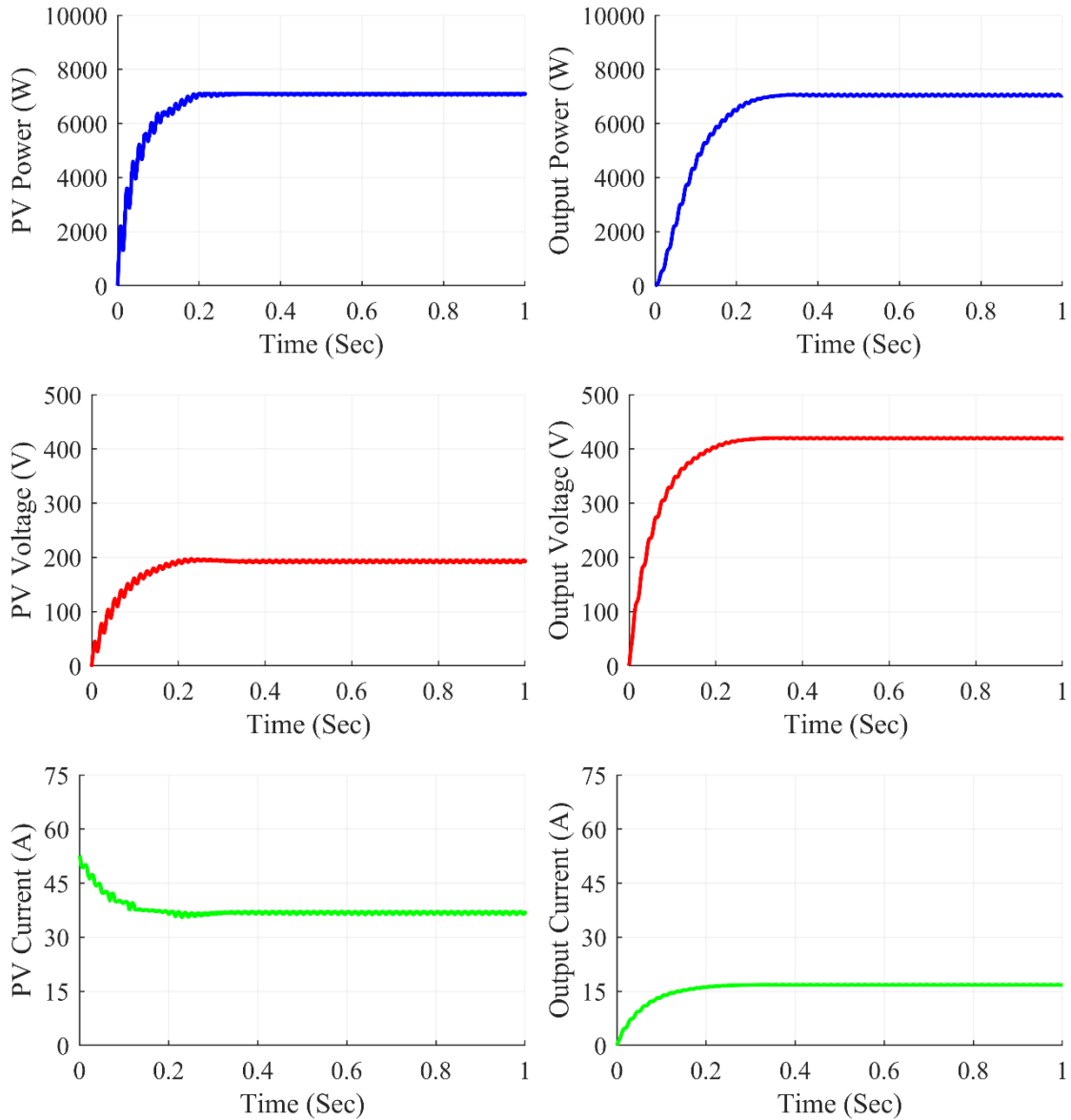


Figure 7.43: Super-Lift Luo converter waveforms under right side shading condition

The Fig. 7.43 shows Super-Lift Luo Converter waveforms under right side end shading condition. At steady state, we can see that the converter gives average output power of 7037 W, the average output voltage at 419.4 V and the average output current of 16.78 A. The average value of PV power was at 7095 W and the PV current and PV voltage were at 192.8V and 36.8 A respectively.

7.3.6.7 Under uniform shading scenario

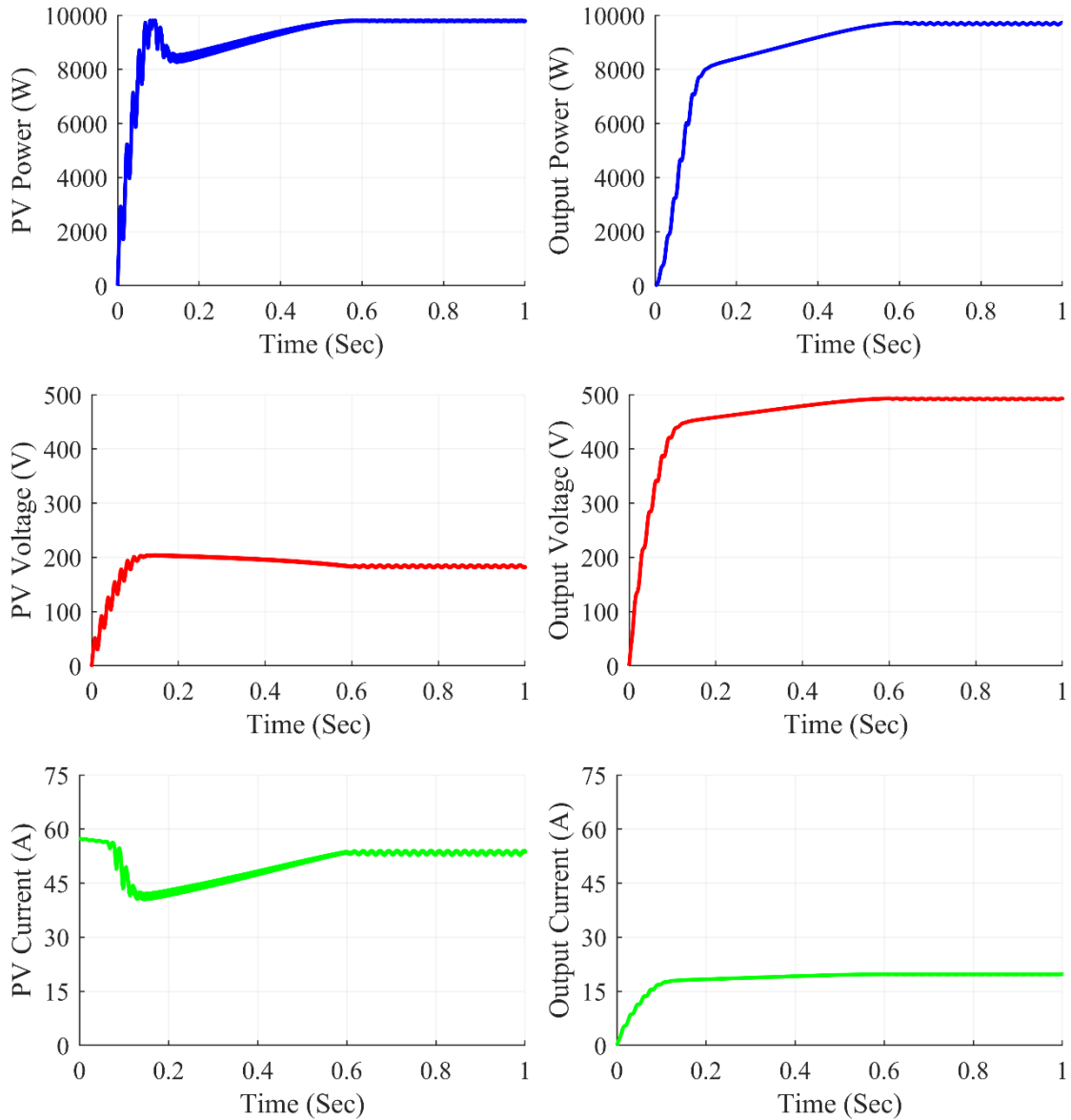


Figure 7.44: Super-Lift Luo converter waveforms under uniform shading condition

The Fig. 7.38 shows Super-Lift Luo Converter waveforms under uniform shading condition. At steady state, we can see that the converter gives average output power of 9717 W, the average output voltage at 492.5 V and the average output current of 19.71 A. The average value of PV power was at 9795 W and the PV current and PV voltage were at 181.9 V and 53.84 A respectively.

Table 7.6: Super-Lift Luo Converter Observations

Shading Conditions	PV Voltage (V_{PV})	PV Current (I_{PV})	PV Power (P_{PV})	Output Voltage (V_{out})	Output Current (I_{out})	Output Power (P_{out})	Duty Cycle (D)
Centre	194.0	36.93	7162	422.1	16.88	7126	0.150
Corner	196.1	36.95	7245	424.7	16.99	7216	0.140
Diagonal	186.9	44.00	8224	451.8	18.07	8165	0.293
Frame	138.1	27.59	3810	307.0	12.28	3770	0.194
Random	196.0	37.44	7336	425.8	17.03	7245	0.163
Right Side	192.8	36.8	7095	419.4	16.78	7037	0.157
Uniform	181.9	53.84	9795	492.5	19.71	9717	0.409

The results of the simulation are summarized in Table 7.6 for Super-Lift Luo converter. On the 7x7 TCT PV array design, various partial shading situations were produced, which fed power into the Super-Lift Luo converter in such a way that maximum power extraction from the PV array was achieved using the P&O method. The results were reasonably accurate and matched the expected value. The Super-Lift Luo converter worked with a duty ratio ranging from 0.140 to 0.409 for corner shading to uniform shading respectively.

7.3.7 Ultra-Lift Luo Converter Waveforms

7.3.7.1 Under center shading scenario

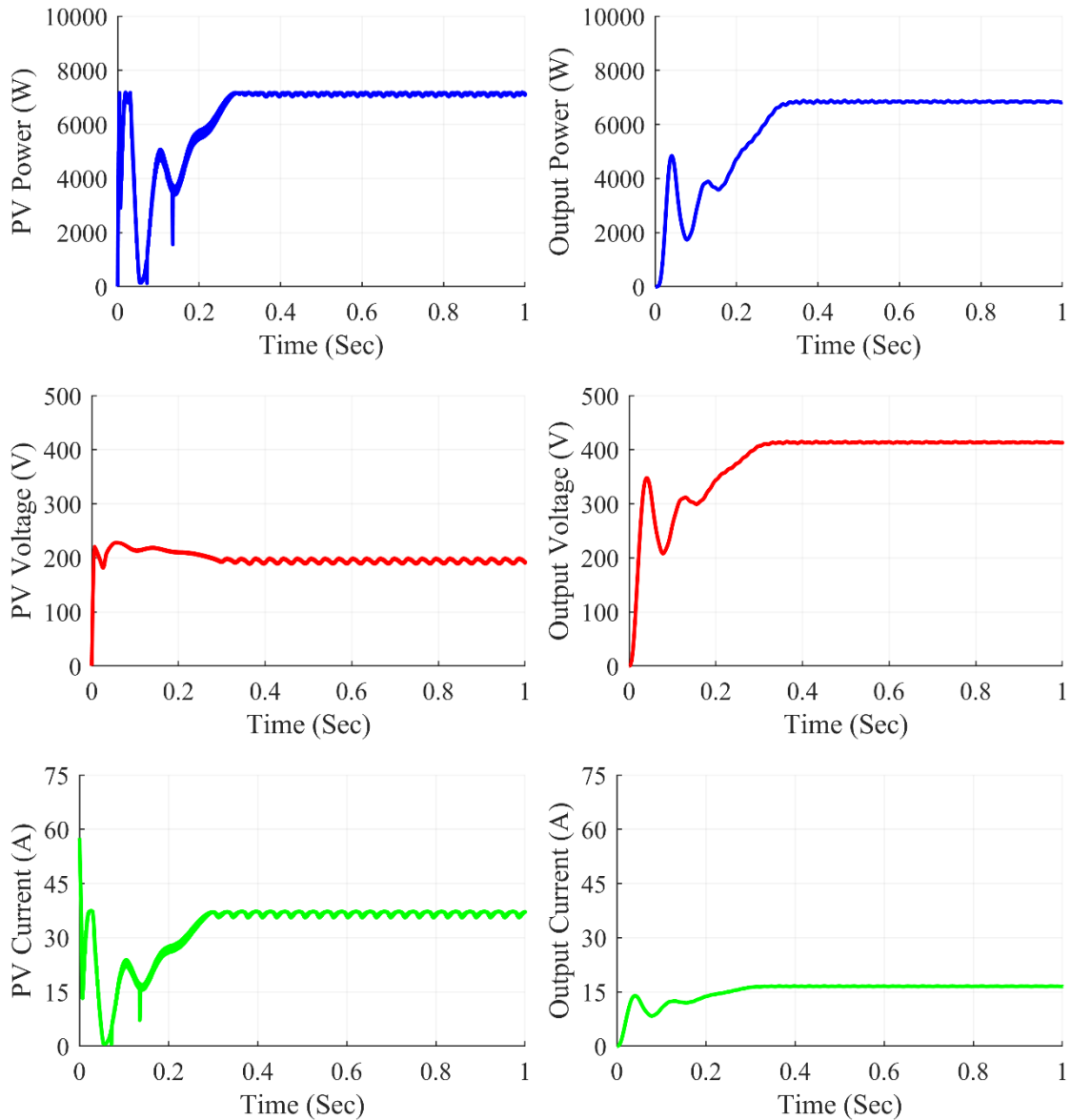


Figure 7.45: Ultra-Lift Luo converter waveforms under center shading condition

The Fig. 7.45 shows Ultra-Lift Luo Converter waveforms under center shading condition. At steady state, we can see that the converter gives average output power of 6824 W, the average output voltage at 413.0 V and the average output current of 16.52 A. The average value of PV power was at 7112 W and the PV current and PV voltage were at 191.6V and 37.11 A respectively.

7.3.7.2 Under corner shading scenario

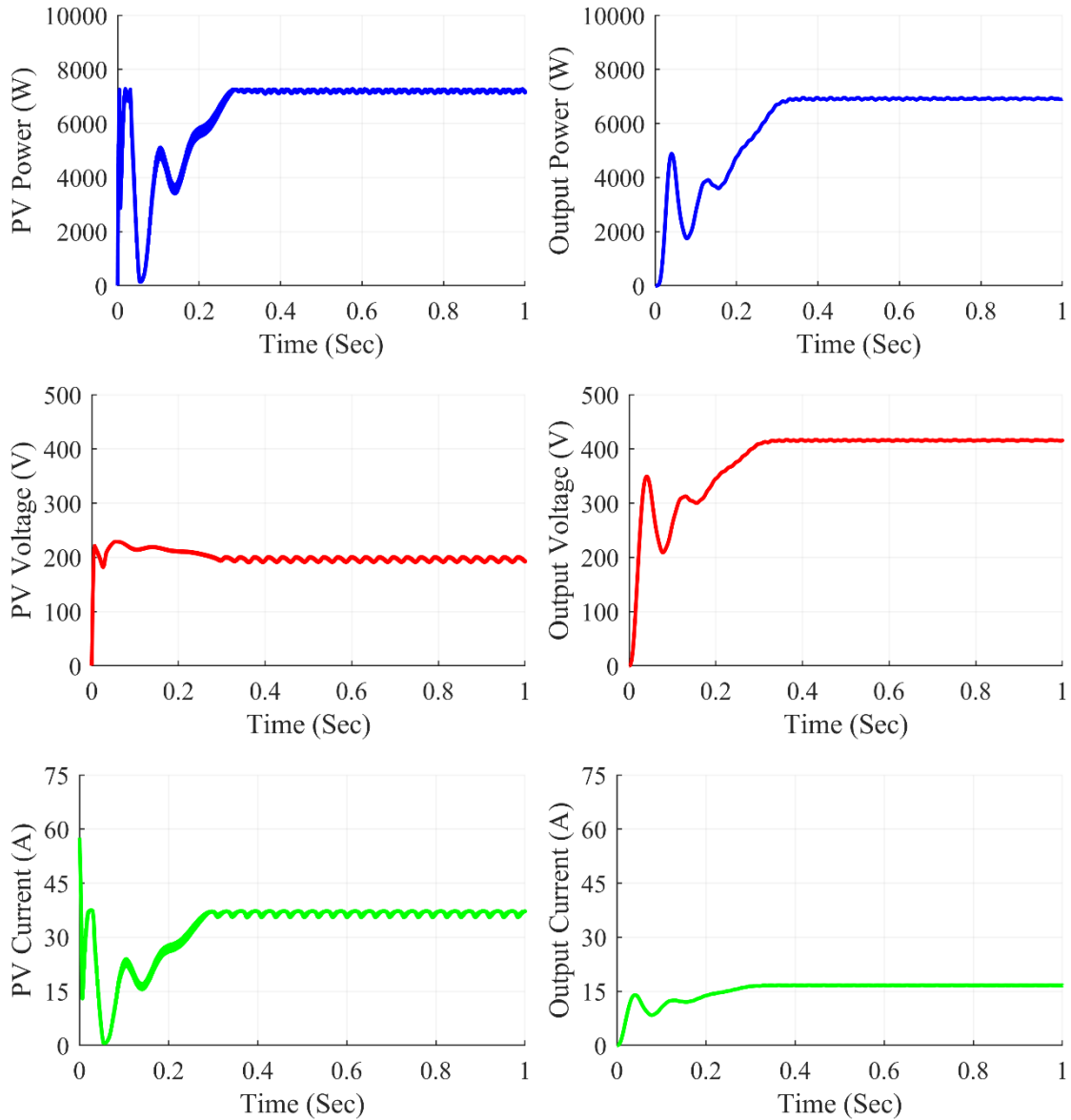


Figure 7.46: Ultra-Lift Luo converter waveforms under corner shading condition

The Fig. 7.46 shows Ultra-Lift Luo Converter waveforms under corner shading condition. At steady state, we can see that the converter gives average output power of 6911 W, the average output voltage at 415.7V and the average output current of 16.63 A. The average value of PV power was at 7164 W and the PV current and PV voltage were at 192/77V and 37.17 A respectively.

7.3.7.3 Under diagonal shading scenario

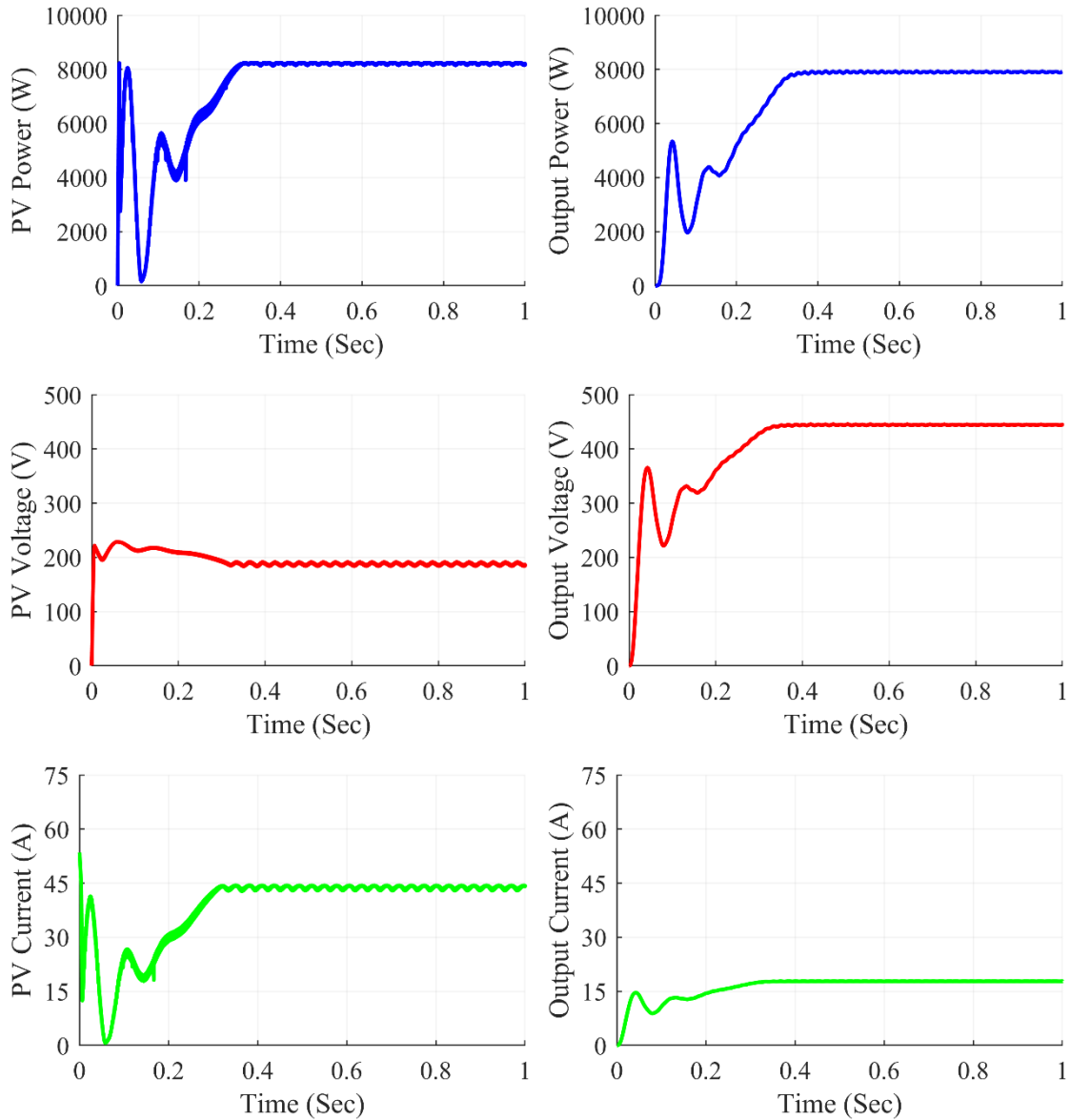


Figure 7.47: Ultra-Lift Luo converter waveforms under diagonal shading condition

The Fig. 7.47 shows Ultra-Lift Luo Converter waveforms under diagonal shading condition. At steady state, we can see that the converter gives average output power of 7912 W, the average output voltage at 444.7 V and the average output current of 17.79 A. The average value of PV power was at 8192 W and the PV current and PV voltage were at 185.3 V and 44.20 A respectively.

7.3.7.4 Under frame shading scenario

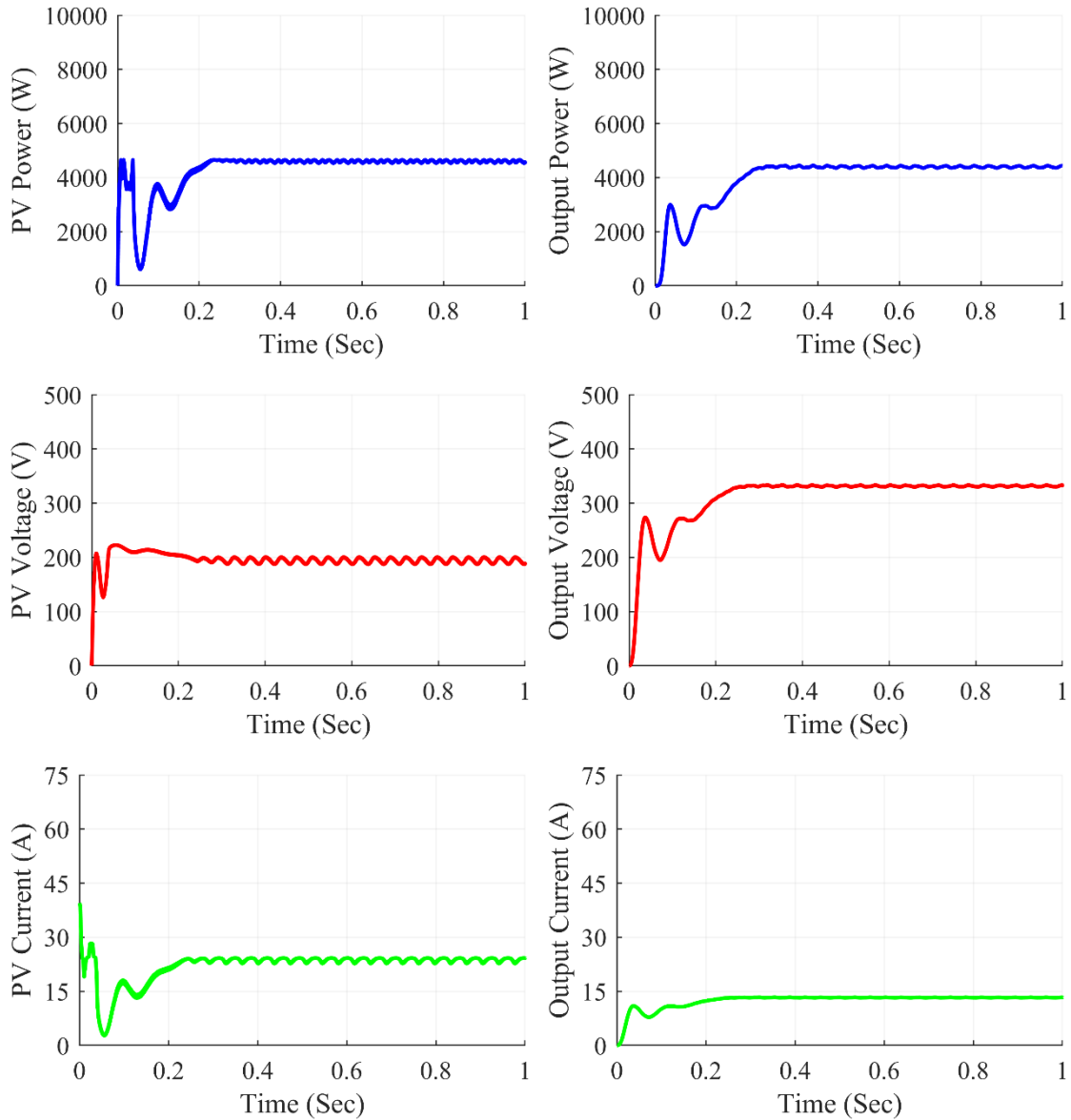


Figure 7.48: Ultra-Lift Luo converter waveforms under frame shading condition

The Fig. 7.48 shows Ultra-Lift Luo Converter waveforms under frame shading condition. At steady state, we can see that the converter gives average output power of 4432 W, the average output voltage at 332.9 V and the average output current of 13.32 A. The average value of PV power was at 4557 W and the PV current and PV voltage were at 188.3 V and 24.20 A respectively.

7.3.7.5 Under random shading scenario

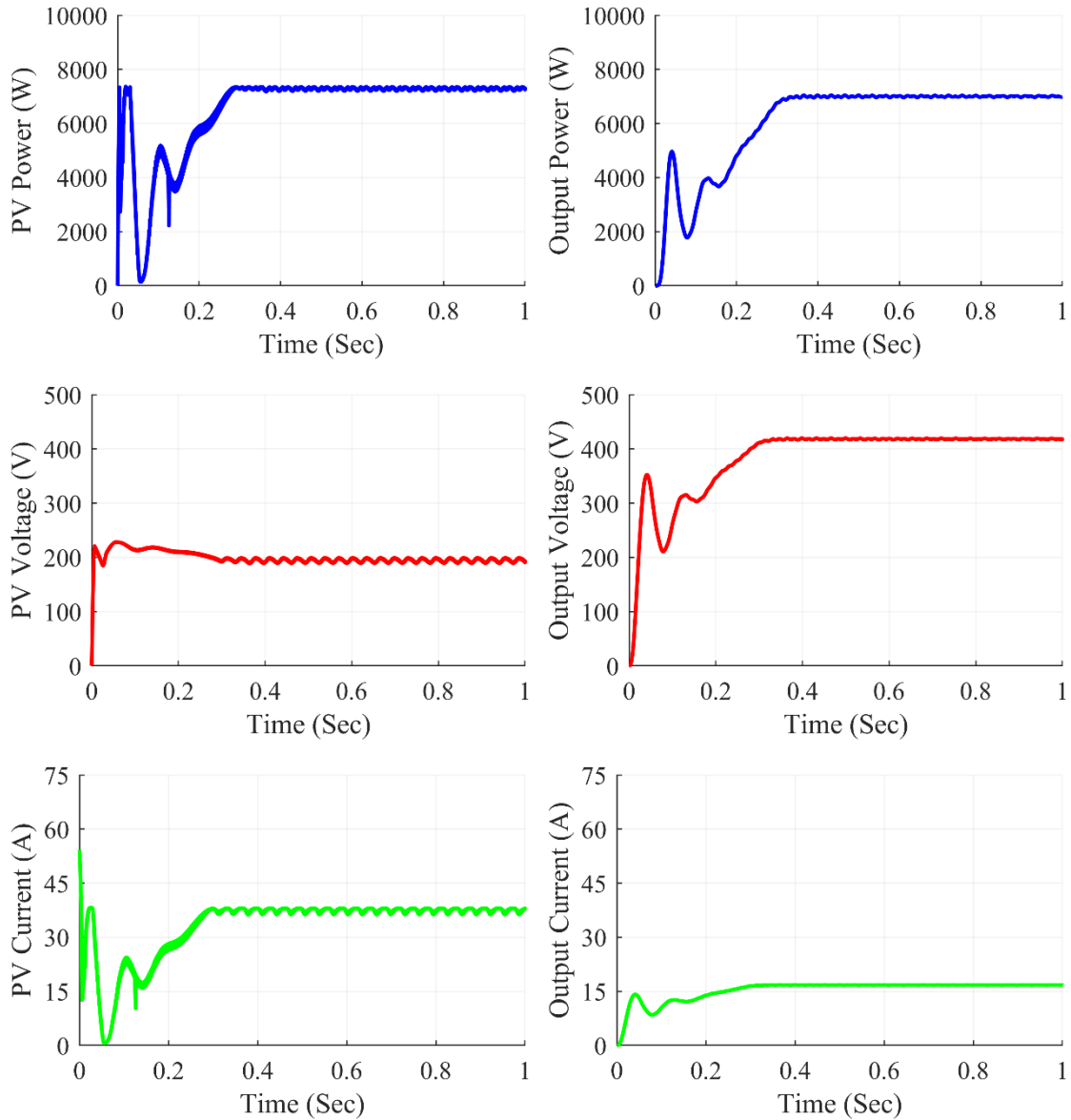


Figure 7.49: Ultra-Lift Luo converter waveforms under random shading condition

The Fig. 7.49 shows Ultra-Lift Luo Converter waveforms under random shading condition. At steady state, we can see that the converter gives average output power of 6982 W, the average output voltage at 417.8V and the average output current of 16.01 A. The average value of PV power was at 7280 W and the PV current and PV voltage were at 192.0 V and 37.92 A respectively.

7.3.7.6 Under right side end shading scenario

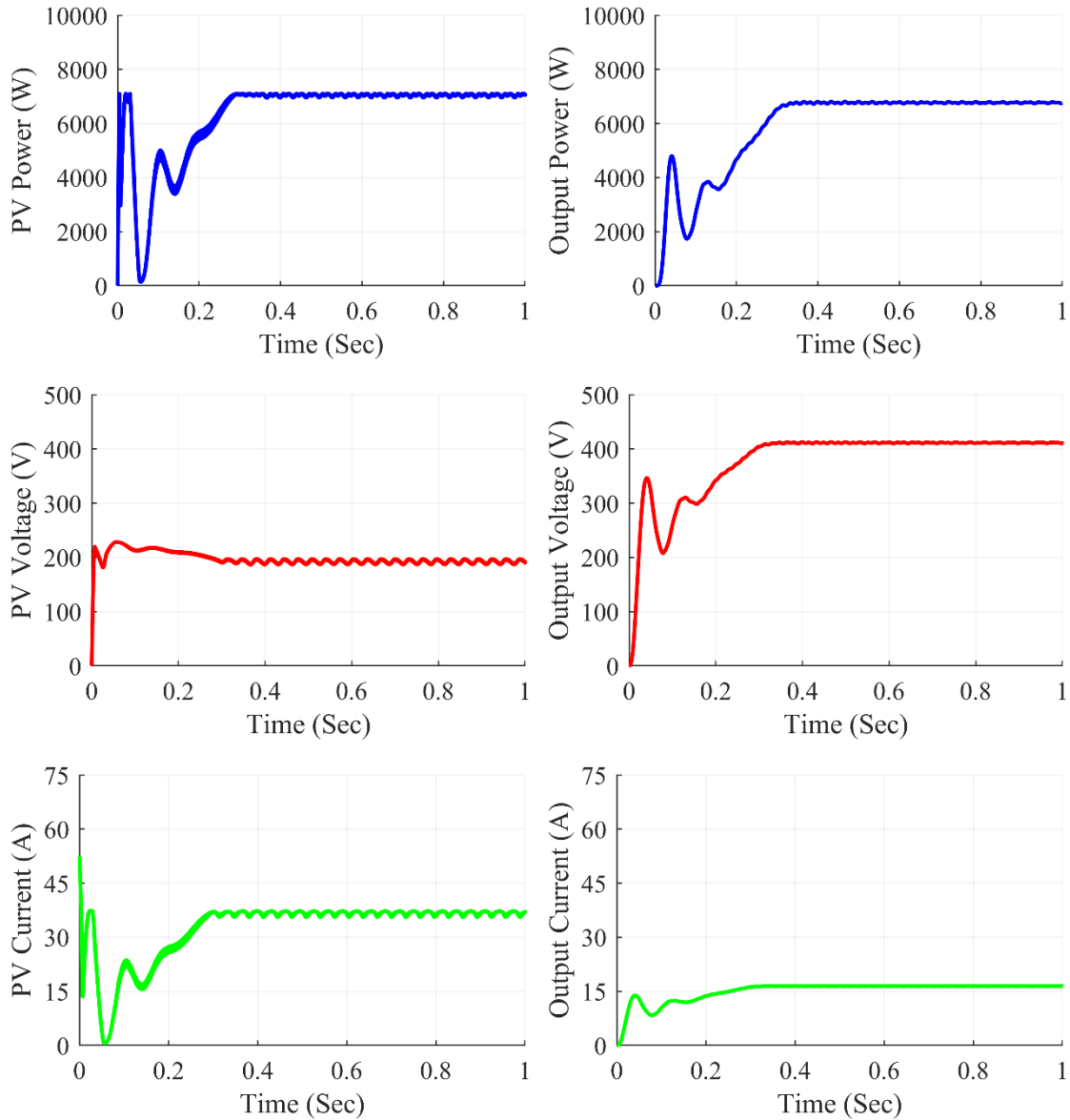


Figure 7.50: Ultra-Lift Luo converter waveforms under right side end shading condition

The Fig. 7.50 shows Ultra-Lift Luo Converter waveforms under right side end shading condition. At steady state, we can see that the converter gives average output power of 6746 W, the average output voltage at 410.7 V and the average output current of 16.43 A. The average value of PV power was at 7069 W and the PV current and PV voltage were at 191.0V and 37.01 A respectively.

7.3.7.7 Under uniform shading scenario

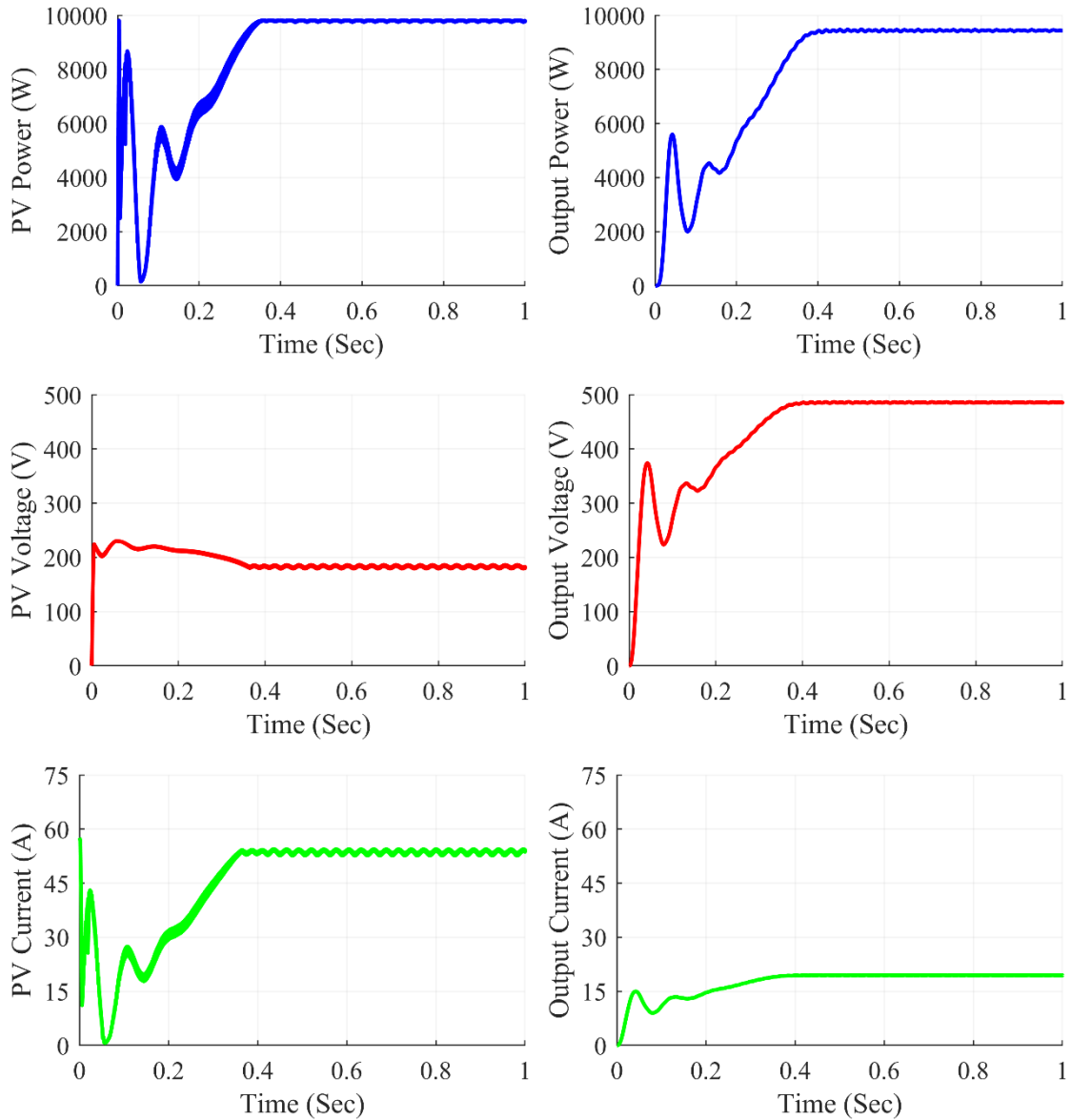


Figure 7.51: Ultra-Lift Luo converter waveforms under uniform shading condition

The Fig. 7.51 shows Ultra-Lift Luo Converter waveforms under uniform shading condition. At steady state, we can see that the converter gives average output power of 9472 W, the average output voltage at 485.5 V and the average output current of 19.42 A. The average value of PV power was at 9787 W and the PV current and PV voltage were at 181.3 V and 53.98 A respectively.

Table 7.7: Ultra-Lift Luo Converter Observations

Shading Conditions	PV Voltage (V_{PV})	PV Current (I_{PV})	PV Power (P_{PV})	Output Voltage (V_{out})	Output Current (I_{out})	Output Power (P_{out})	Duty Cycle (D)
Centre	191.6	37.11	7112	413.0	16.52	6824	0.438
Corner	192.7	37.17	7164	415.7	16.63	6911	0.436
Diagonal	185.3	44.20	8192	444.7	17.79	7912	0.455
Frame	188.3	24.20	4557	332.9	13.32	4432	0.392
Random	192.0	37.92	7280	417.8	16.71	6982	0.440
Right Side	191.0	37.01	7069	410.7	16.43	6746	0.440
Uniform	181.3	53.98	9787	485.5	19.42	9472	0.477

Table 7.7 summarizes the simulation results for the Ultra-Lift Luo converter. Various partial shade scenarios were created on the 7x7 TCT PV array design, feeding power into the Ultra-Lift Luo converter in such a way that maximum power extraction from the PV array was accomplished using the P&O method. The results were fairly accurate, and the desired value was met. From frame shading and uniform shading, the Ultra-Lift Luo converter used duty ratios ranging from 0.392 to 0.477 respectively.

Chapter - 8

CONCLUSION AND FUTURE SCOPE

 Conclusion

 Future Scope

Chapter - 8

8.1 Conclusion

In this thesis, we have presented various Non-Isolated DC-DC Converter topologies for solar PV system operating under various partial shading scenarios. In this regard TCT PV array configurations for power generation and P&O algorithm for maximum power extraction under partial shading conditions have been developed.

We investigated the performance of Total-Cross-Tied (TCT) PV array using Matlab/Simulink for different partial shading scenarios such as center, corner, diagonal, frame, etc. Various parameters affecting the performance of PV array configuration such as mismatching power loss, fill factor, etc. has been compared under PSCs.

For Stand-Alone PV system, we used the conventional non-isolated DC-DC converters such as Boost, Buck-Boost, Cuk, SEPIC and Zeta converter and High Gain non-isolated DC-DC converters such as Positive-Output Super-Lift Luo converter and Ultra-Lift Luo converter. We designed all these converters in Matlab/Simulink for the PV system to extract maximum power from the TCT PV array using P&O MPPT technique under PSCs.

Under partial shading conditions, the Boost converter and Super-Lift Luo converter outperform all other converters. The output power fluctuations and ripple in the output voltage were less noticeable in these converters. These converters achieve the maximum power point faster than other converters. The Luo converter has the lowest duty ratio at the MPP, followed by the boost converter, implying that the switch in these converters will be less stressed.

8.2 Future Scope

The following recommendations for future research are drawn from the work carried out in this thesis:

- More research on the various PV array arrangements, such as bridged-linking, HC, and so on, is required.
- Hybrid PV array configurations such as SP-TCT, BL-TCT, HC-TCT and BL-HC needs to be investigated.
- The performance of the hybrid PV configurations needs to be assessed and compared with the conventional configurations under the same PSCs which are used for conventional configurations.
- The reliability of PV array configurations needs to be analyzed.
- More number of MPPT Techniques need to be developed for fast tracking of the GMPP and fast charging of Electric Vehicle (EV) applications.
- Research on Isolated DC-DC converters should be made to implement in stand-alone PV system for maximum power tracking under partial shading conditions.
- More High gain converters needs to be integrated with new PV array configurations for water pumping applications. The performance of PV array configurations for high gain converters needs to be tested under various PSCs.

REFERENCES

REFERENCES

- [1] D. Feldman, G. Barbose, R. Margolis, T. James, S. Weaver, N. Darghouth, R. Fu, C. Davidson, S. Booth and R. Wiser, “Behind the PV price declines”, *Renewable Energy Focus*, vol. 15, no. 6, pp. 14-15, 2014.
- [2] “Data and Statistics-IRENA Resource”. <https://www.irena.org/Statistics/View-Data-byTopic/Capacity-and-Generation/Technologies>.
- [3] G. Boyle, “Renewable Energy, Power for a sustainable future”, Oxford University Press in association with the Open University, second edition, 2004.
- [4] R. Karki and R. Billinton, “Reliability/cost implications of PV and wind energy utilization in small isolated power systems,” *IEEE Transactions on Energy Conversion*, vol. 16, no. 4, pp. 368-373, 2001.
- [5] B. K. Bose, “Global warming: Energy, environmental pollution, and the impact of power electronics”, *IEEE Ind. Electron. Magazine*, Vol. 4, no. 1, pp. 6-17, Mar. 2010.
- [6] Mekhilef, S.; Safari, A.; Mustaffa, W.; Saidur, R.; Omar, R.; Younis, M. Solar energy in Malaysia: Current state and prospects. *Renew. Sustain. Energy Rev.*, 16, pp.386–396, 2012.
- [7] S. Essakiappan, P. Enjeti, Robert S. Balog, and Shehab Ahmed, “Analysis and mitigation of common mode voltages in photovoltaic power systems”, *Proc. IEEE Energy Conversion Congress and Exposition (ECCE-2011)*, USA, pp. 28-35, 2011.
- [8] International Renewable Energy Agency (IRENA), REthinking Energy 2017: Accelerating the global energy transformation, Vol. 55, pp. 1-130, Jan. 2017.
- [9] S. Rahman, “Green power: what is it and where can we find it?”, *IEEE Power and Energy Magazine*, Vol. 1, no. 1, pp. 30-37, Feb. 2003.
- [10] IEA PVPS Annual Report 2020 Photovoltaic Power Systems Programme, <https://ieapvps.org/wp-content/uploads/2021/04/IEA-PVPS-AR-2020.pdf>.

- [11] <https://iea-pvps.org/snapshot-reports/snapshot-2021/>.
- [12] Renewables 2020 Global Status Report, <https://www.ren21.net/reports/global-statusreport/?gclid=EAIAIQobChMIpoLBtpra9gIVOpNmAh26xgFeEAAYASA>
- [13] G. J. Shushnar et al., "Balance of System costs for a 5 MW photovoltaic generating station," *IEEE Trans. Power Apparatus System*, vol. PAS-104, no.8, pp: 2006-2011, 1985. References Ph.D. Thesis of Mr. Praveen Kumar Bonthagorla Page 159 of 170
- [14] L. F. L. Villa, D. Picault, B. Raison, S. Bacha and A. Labonne, "Maximizing the power output of partially shaded photovoltaic plants through optimization of the interconnections among its modules", *IEEE Journal of Photovoltaics*, vol. 2, no. 2, pp.154 -163, 2012.
- [15] J. A. Gow and C. D. Manning, "Development of a model for photovoltaic arrays suitable for use in simulation studies of solar energy conversion systems", *Proc. 6th Int. Conf. Power Electron. Variable Speed Drives*, pp. 69-74, 1996.
- [16] Massimo Guarnieri, "More-Light on Information [Historical]", *IEEE Industrial Electronics Magazine*, vol.9, no.4, pp.58–61, 2015. doi:10.1109/MIE.2015.2485182.
- [17] G. K. Singh, "Solar power generation by PV (photovoltaic) technology: a review", *Energy*, vol. 53, pp. 1-13, 2013.
- [18] U.S. Department of Energy, "PV Physics", Energy Efficiency and Renewable Energy, Solar Energy Technologies Program, <http://www1.eere.energy.gov/solar>. Retrieved on 17 November 2009.
- [19] M. G. Villalva, J. R. Gazoli, and E. Ruppert Filho, "Comprehensive approach to modeling and simulation of photovoltaic arrays," *IEEE Transactions on Power Electronics*, vol. 24, no. 5, pp. 1198-1208, 2009.
- [20] Aghaei, Mohammadreza, Photovoltaic Solar Energy Conversion Solar PV systems design and monitoring. pp. 117–145, 2020. doi:10.1016/B978-0-12-

819610-6.00005-3. References Ph.D. Thesis of Mr. Praveen Kumar Bonthagorla
Page 160 of 170

- [21] A.Kumar, N. Gupta, V.Gupta, “A Comprehensive Review on Grid-Tied Solar Photovoltaic System”, *Journal of Green Engineering*, Vol 7, no. 1,pp. 213–254, 2017. doi:10.13052/jge1904-4720.71210.
- [22] H. M. Farh and M. Ali Eltamaly, “Maximum power extraction from the photovoltaic system under partial shading conditions,” in *Modern Maximum Power Point Tracking Techniques for Photovoltaic Energy Systems*. Cham, Switzerland: Springer, pp. 107–129, 2020.
- [23] Ji Y-H, Jung D-Y, Kim J-G, Kim J-H, Lee T-W, Won C-Y, “A real maximum power point tracking method for mismatching compensation in PV array under partially shaded conditions”, *IEEE Trans Power Electron*, vol 26,no.4,pp.1001–1009, 2011.
- [24] Silvestre S, ChouderA, “Effects of shadowing on photovoltaic module performance.” *Prog Photovoltaics Res Appl*, vol.16, no.2, pp.141–149,2008.
- [25] Eltamaly, A M “Performance of smart maximum power point tracker under partial shading conditions of photovoltaic systems”. *J Renew Sustain Energy* vol.7, no. 4, pp. 043141.
- [26] E.R.Cadaval, G.Spagnuolo, L.G.Franquelo, C.A.R.Paja, T.Suntio, and W.M.Xiao, “Grid connected photovoltaic generation plants: components and operation,” *IEEE Ind. Electron. Mag.*, Vol. 7, no. 3, pp. 6-20, Sep. 2013.
- [27] S.Kouro, J.I.Leon, D.Vinnikov, and L.G.Franquelo, “Grid-connected photovoltaic systems: An overview of recent research and emerging PV converter technology,” *IEEE Ind. Electron. Mag.*, Vol. 9, no. 1, pp. 47-61, Mar. 2015.
- [28] S. R. Pendem and S. Mikkili, “Hybrid PV array configurations for mitigating the mismatching power loss and number of peaks in the output characteristics under various PSCs,” Proc. of 45th Annual Conference of the *IEEE Industrial Electronics Society (IECON-2019)*, Portugal, pp. 2377-2382, Oct. 14-17, 2019.

- [29] P. K. Bonthagorla and S. Mikkili, "Optimal PV array configuration for extracting maximum power under partial shading conditions by mitigating mismatching power loss," *CSEE Journal Power and Energy Systems*, - Early Access. DOI: 10.17775/CSEJPES. 2019.02730.
- [30] M.F.N.Tajuddin, M.S.Arif, S.M.Ayob, and Z.Salam, "Perturbative methods for maximum power point tracking (MPPT) of photovoltaic (PV) systems: a review," *Int. Jour. Ener. Research.*, Vol. 39, pp. 1153-1178, Feb. 2015. References Ph.D. Thesis of Mr. Praveen Kumar Bonthagorla Page 161 of 170
- [31] B. Subudhi, and R. Pradhan, "A comparative study on maximum power point tracking techniques for photovoltaic power systems", *IEEE Trans. Sustain. Energy.*, Vol. 4, no. 1, pp. 89-98, Jan. 2013.
- [32] B. Bendib, H. Belmili, and F. Krim, "A survey of the most used MPPT methods: Conventional and advanced algorithms applied for photovoltaic systems", *Renew. Sustain. Energy Rev.*, Vol. 45, pp. 637-648, May 2015.
- [33] Z. Salam, J. Ahmed, and B. S. Merugu, "The application of soft computing methods for MPPT of PV system: a technological and status review", *Appl. Energy*, Vol. 107, pp. 135-148, Jul. 2013.
- [34] Tohid Jalilzadeh, Naghi Rostami, Ebrahim Babaei, and Mohammad Maalandish, "NonIsolated Topology for High Step-Up DC-DC Converters," *IEEE Journal of Emerging and Selected Topics in Power Electronics*, - Early Access. DOI: 10.1109/JESTPE.2018.2849096.
- [35] Wuhua Li, and Xiangning He, "Review of non-isolated high-step-up DC/DC converters in photovoltaic grid-connected applications," *IEEE Trans. Ind. Electron.*, Vol. 58, no. 4, pp. 1239-1250, May. 2010.
- [36] M. Al-Soeidat, H. Aljarajreh, H. Khawaldeh, D. D.-C. Lu, and J.G. Zhu, "A Reconfigurable Three-Port DC-DC Converter for Integrated PV Battery System", *IEEE Journal of Emerging and Selected Topics in Power Electronics*, Vol. 8, no. 4, pp. 3423 - 3433, Sep. 2019.

- [37] A. Freitas, F. L. L. Tofoli, E. Mineiro Sa, S. Daher, and F. M. Antunes, “High-voltage gain dc-dc boost converter with coupled inductors for photovoltaic systems”, *IET Power Electron.*, Vol. 8, no. 10, pp. 1885-1892, Jun. 2015.
- [38] Quan Li, and Peter Wolfs, “A review of the single-phase photovoltaic module integrated converter topologies with three different dc link configurations”, *IEEE Trans. Power Electron.*, Vol. 23, no. 3, pp. 1320-1333, May 2008.
- [39] Md. N. H. Khan, M. Forouzesh, Y. P. Siwakoti, Li Li, T. Kerekes, and F. Blaabjerg, “Transformerless Inverter Topologies for Single-Phase Photovoltaic Systems: A Comparative Review”, *IEEE Journal of Emerging and Selected Topics in Power Electronics*, Vol. 8, no. 1, pp. 805-835, Apr. 2015.
- [40] K. K. Gupta, A. Ranjan, P. Bhatnagar, L. K. Sahu and S. Jain, “Multilevel Inverter Topologies with Reduced Device Count: A Review”, *IEEE Trans. Power Electron.*, Vol. 31, no. 1, pp. 135-151, Jan. 2016. References Ph.D. Thesis of Mr. Praveen Kumar Bonthagorla Page 162 of 170
- [41] L. Hassaine, E. OLias, J. Quintero, and V. Salas, “Overview of power inverter topologies and control structures for grid connected photovoltaic systems”, *Renew. Sustain. Energy Rev.*, Vol. 30, pp. 796-807, Feb. 2014.
- [42] Bag, B. Subudhi and P. K. Ray, “A combined reinforcement learning and sliding mode control scheme for grid integration of a PV system”, *CSEE Journal of Power and Energy Systems*, Vol. 5, no. 4, pp. 498-506, Dec. 2019.
- [43] Faa-Jeng Lin, Kuang-Chin Lu, and Ting-Han Ke, “Probabilistic wavelet fuzzy neural network based reactive power control for grid-connected three-phase PV system during grid faults”, *Renew. Energy*, Vol. 92, pp. 437-449, Oct. 2016.
- [44] Pedro M. Almeida, Pedro G. Barbosa, Janaina G. Oliveira, Jorge L. Duarte, and Paulo F. Ribeiro, “Digital proportional multi-resonant current controller for improving gridconnected photovoltaic systems”, *Renew. Energy*, Vol. 76, pp. 662-669, Aug. 2015.

- [45] Jena D, Ramana VV, “Modeling of photovoltaic system for uniform and non-uniform irradiance: a critical review,” *Renewable and Sustainable Energy Reviews*, vol. 52 pp. 400–17, 2015.
- [46] M. Hasan and S. Parida, “An overview of solar photovoltaic panel modeling based on analytical and experimental viewpoint,” *Renew. Sustain. Energy Rev*, vol. 60, pp. 75–83, 2016.
- [47] Duong MQ, Sava GN, Ionescu G, Necula H, Leva S, MussettaM, “Optimal bypass diode configuration for PV arrays under shading influence.”, In: *2017 IEEE international conference on environment and electrical engineering and 2017 IEEE industrial and commercial power systems Europe (EEEIC/I&CPS Europe)*. IEEE, pp 1–5, 2017.
- [48] Bidram A, Davoudi A, Balog RS, “Control and circuit techniques to mitigate partial shading effects in photovoltaic arrays”, *IEEE J Photovoltaics* vol.2, no.4, pp.532–546, 2012.
- [49] Ramaprabha R, Mathur B, “A comprehensive review and analysis of solar photovoltaic array configurations under partial shaded conditions”, *Int J Photoenergy* 2012.
- [50] Wang Y-J, Hsu P-C, “Analysis of partially shaded PV modules using piecewise linear parallel branches model” *World Acad Sci Eng Technol*, vol. 60no.2, pp.783–789, 2009.
- [51] Wang Y-J, Hsu P-C, “An investigation on partial shading of PV modules with different connection configurations of PV cells”, *Energy*, vol. 36, no.5, pp.3069–3078, 2011.
- [52] Kaushika ND, Gautam NK, “Energy yield simulations of interconnected solar PV arrays”, *IEEE Trans Energy Convers* vol.18, no.1, pp. 127–134, 2003.
- [53] B. Subudhi and R. Pradhan, “A Comparative Study on Maximum Power Point Tracking Techniques for Photovoltaic Power Systems,” *IEEE Trans. on Sustain. Energy*, vol. 4, no. 1, pp. 89-98, Jan. 2013, doi: 10.1109/TSTE.2012.2202294.

- [54] R. Ahmad, A. F. Murtaza, and H. A. Sher, Power tracking techniques for efficient operation of photovoltaic array in solar applications A review," *Renew. and Sustain. Energy Rev.*, vol. 101, pp.82-102, Mar. 2019.
- [55] Sholapur, Shridhar et al. "Boost Converter Topology for PV System with Perturb And Observe MPPT Algorithm." *IOSR Journal of Electrical and Electronics Engineering* 9 (2014): 50-56.
- [56] N. Rana, J. Dey and S. Banerjee, "An Improved Buck-Boost Converter Suitable for PV Application," *2020 IEEE Calcutta Conference*, 2020, pp. 273-277.
- [57] Prinkesh Soni, Rakesh Singh Lodhi, Amit Solanki, Ankush Yadav. "Cuk Converter for Photovoltaic Energy System: A Review".
- [58] T. Ajith Bosco Raj, R. Ramesh, J. R. Maglin, M. Vaigundamoorthi, I. William Christopher, C. Gopinath, C. Yaashwanth, "Grid Connected Solar PV System with SEPIC Converter Compared with Parallel Boost Converter Based MPPT", *International Journal of Photoenergy*, vol. 2014, 12 pages, 2014 .
- [59] L. Vignesh, G. Satheesh Kumar, "PV Fed Zeta Converter", *IJERT ICONEEA 2019*.
- [60] A. S. Tekade, R. Juneja, M. Kurwale and P. Debre, "Design of Positive Output Super-Lift Luo Boost Converter for Solar Inverter," *2016 International Conference on Energy Efficient Technologies for Sustainability (ICEETS)*, 2016, pp. 153-156.